Ferromagnetomechanics

Daniel Peter
Daniel Bulte

A thesis submitted in fulfillment of the requirements
for the degree of Doctor of Philosophy.

Electrical Engineering (Launceston)
School of Engineering
The University of Tasmania

March, 2001

Abstract

The effect of applied external stress on the magnetic properties of ferromagnetic materials has been recognised as one of the most important ferromagnetic phenomena for over a century. Research into the field has been driven by investigations of non-destructive testing, degaussing, and maritime applications.

A comprehensive investigation of the magnetomechanical behaviour of mild steel under static biaxial stresses was undertaken with the intention of adapting and improving techniques of obtaining magnetic and strain data, producing accurate data for analysis, and developing insights into a tentative alternative theory of stress and magnetism.

A method of obtaining Initial Magnetisation Curves is presented which equates them with Normal Magnetisation Curves. A conceptual mechanism by which applied stress and magnetism interact is introduced in order to explain coincident points and kinks on hysteresis loops obtained at different, static biaxial stresses. Finally the set of biaxial strain and magnetisation data is presented for a mild steel cruciform specimen.

Declaration

This thesis contains no material which has been accepted for a degree or diploma by the University or any other institution, except by way of background information and duly acknowledged in the Thesis, and to the best of the Candidate's knowledge and belief no material previously published or written by another person except where due acknowledgement is made in the text of the Thesis.

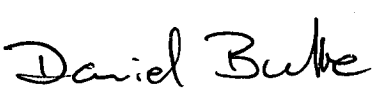

Daniel Bulte

Daniel Bulte

Acknowledgments

My sincerest thanks are extended to the following people:

- Richard Langman, for his fantastic supervision and support, and also for putting up with my odd working hours and fear of alarm clocks.
- The School of Engineering, both in Launceston and Hobart, for the opportunity to work and study in such a friendly environment.
- The Australian Defence Science and Technology Organisation, and particularly Tony Christopoulos and Jim Smelt for funding this project and looking after me so well.
- Rob Wrigley, Drew Honeychurch, Ros Lindsey, Steve Avery, Judy Bonsey, Glenn Mayhew, Jean Weeding, and Bernard Chenery for building, fixing, finding, and organising just about everything I needed for 3 & 1/2 years.
- Adam Redman, Dean Chatwin, Mike Lee, and Trevor Innes, for making Launceston such a fun place to be.
- Stuart and Rita Corney, for listening to me, feeding me, entertaining me, and being great friends.
- My father, and my brother Graeme for all of their support.
- Lastly and most of all to Elanor, for staying with me through changing cities and being the joy of my life.

The most exciting phrase to hear in science, the one that heralds new discoveries, is not "Eureka!" (I found it!), but "that's funny..."

Isaac Asimov

Research is what I'm doing when I don't know what I'm doing.

Werner von Braun

(Magnets) are good for children's toys and for holding notes to refrigerators, but how many chapters can you get out of that?

from: Driving Force by James Livingstone

Contents

Chapter 1

Preface

1.1 The Stress Associated With Magnetics

Magnetism is an effect which has been recognised for thousands of years. It has been a source of interest to science longer than almost any other field. It is often one of the first examples of scientific phenomena to which we are introduced as children. Magnetism plays a greater role in society today than at any other time, now that more information is stored magnetically than by most other conventional methods.

It is somehow ironic that one of the fundamental effects associated with magnetism has yet to have a sound theory developed regarding its source and nature, this effect being the magnetomechanical effect. The effect of stress on magnetism, and its apparent inverse effect of magnetostriction are covered in most basic magnetics texts. As early as 1892 it was noted by Ewing [25], "No part of our subject is more interesting than that which deals with the effects of mechanical stress in altering the susceptibility, the retentiveness, and other qualities of the three magnetic metals".

Investigations into the nature of the relationship between applied external stress and magnetic properties over the past century have served to develop and refine our understanding of the field. From Ewing's treatment [25] [26] to Becker and Döring's work in 1939, progress in the general understanding of magnetics

led to huge advances as domain theory and quantum mechanical explanations of magnetism produced theories upon which almost all future work would be based. Bozorth's development of a domain theory of the effect of stress [10] was one of the greatest steps forward in the field.

More recent research by the likes of Langman [47], Birss [60], Sablik [61], and Jiles and Atherton [40] has produced ever more refined theories and formulae to explain stress-magnetism relationships. One of the inescapable features of magnetism however, is the fact that sample history, and order of treatment can cause huge discrepancies in the effects observed. Static fields and cycled stresses produce results which are almost incomparable with those produced from static stresses and cycled fields.

Even the appropriate form in which to present the data may be disputed: should one use hysteresis loops, normal magnetisation curves, initial magnetisation curves, anhysteretic curves, or different presentations still for static fields and cycled stresses? Data obtained or presented by different methods are notoriously difficult to compare.

This thesis deals with the design and development of equipment, software, and techniques with which to obtain large quantities of highly accurate magnetic-stress data. The data is in the form of initial magnetisation curves and hysteresis loops obtained at constant applied biaxial stresses. Stresses were both compressive and tensile in nature, up to a maximum of 120 MPa.

The structure of the thesis is as follows. Chapter 2 contains the foundations of the approach taken, an outline of the motivations behind the research as a whole, and some of the critical choices made along the way. Chapter 3 is a review of some of the most important work done both theoretically and experimentally in the field, with emphasis given to those works upon which this research is based, and problem areas which we have attempted to avoid, or deal with.

Chapter 4 details the investigations involved in deciding how to obtain and present the data in this thesis. Some long-held views about magnetics are challenged, and a hypothesis is presented to support our choice of Initial Curves

rather than Normal Curves. Chapter 5 outlines the essential pieces of hardware and equipment used in the experimental side of the research. Chapter 6 gives a brief explanation of the important procedures and functions of the Dante software system which was developed to control the applied fields and data acquisition. Chapter 7 presents a sample of the results obtained experimentally. Only a few results are presented here which show the important features seen in the data, and as an example of the formats chosen.

Chapter 8 is considered to be the most important chapter of the thesis as it details the analysis of the data obtained, and outlines the thought processes which led to the development of a hypothesis which will hopefully form the kernel of a fully comprehensive theory of the magnetomechanical effect. Chapter 9 is the conclusion which deals with the most important issues raised in the thesis, and suggests future research to further extend the understanding of the magnetic-stress relationship.

Appendix A outlines some of the technical difficulties which needed to be overcome during the course of this investigation. Appendix B contains the complete set of data obtained experimentally during this research.

Chapter 2

Introduction

2.1 The Project

A research project to investigate the magnetic properties of high-strength steels under conditions of biaxial stress was funded by the Australian Defence Science and Technology Organisation. The research for this thesis was designed to run in parallel with this project with the two investigations complementing each other. At the beginning of the project the Belle-Wrigley stressing rig (see Chapter 5) already existed, but had not been extensively used, thus little of the other necessary equipment was available. The first stage of the project was therefore the design, construction and development of the equipment, electronics, and software which would be required. Over one and a half years of work was required to construct all of the equipment detailed in Chapter 5, and to write and debug the Dante software outlined in Chapter 6. Integrating all of the equipment, the computers, the software, and the laws of physics was an extremely time-consuming task, and many rewrites and rebuilds were required along the way (see Appendix A).

Once methods of obtaining the magnetic and stress data were decided upon, based on limitations of the equipment, and unavoidable features of the materials (eddy currents etc.), the second stage of the research could begin. However, the scope of the research had to be reduced due to time limitations, and the

range of different materials to be studied had to be greatly decreased. It was decided to concentrate the bulk of the research on the behaviour of mild steel as it is probably the most commonly used structural steel, and is therefore of most interest industrially.

2.2 General Survey

Magnetism has been known to science for thousands of years, but, as with many branches of science, it has only been in the last 200 years that any real progress has been made towards understanding it. From the work of Coulomb and Oersted in the 18th and 19th centuries in developing a classical understanding of magnetic effects, to the extensive work done by Ewing at the turn of the 20th century, our knowledge of magnetic phenomena in all of its forms has blossomed. Ferromagnetism, paramagnetism, diamagnetism, magnetostriction, and a host of other effects were discovered and analysed; yet it was the development of quantum mechanics which really launched modern magnetics. The Bohr atomic model and development of the concept of the Bohr magneton spearheaded a quantum revolution in magnetics, for it is with the knowledge of electron spins, magnetic moments, and Hamiltonians that we now define magnetism. What follows is a brief introduction to some of the important basics of magnetism, with preference given to those areas pertaining to the magnetomechanical effect. Unless otherwise specified SI units are used.

Almost all materials acquire a magnetic moment in the presence of a magnetic field [64]. The magnitude of this moment, per unit volume, is called the magnetisation of the medium. The magnetisation has the same units and characteristics as the magnetic induction, and may be regarded as adding to the value of the flux density which would have been present if the region occupied by the magnetised medium were replaced by a vacuum. Thus, the total flux density B in a medium may be written as

$$B = \mu_0(H + M) = \mu_0 H + I, \tag{2.1}$$

where μ_0 is the permeability of free space, H is the applied field strength, and I is the intensity of magnetisation given in Tesla, thus $I = \mu_0 M$[38]. Alternatively the magnetisation can be said to depend on B_0, and thus can be written

$$M = \chi B_0 = \chi \mu_0 H, \tag{2.2}$$

where χ is the magnetic susceptibility of the medium.

Materials may be broadly classified by the sign and magnitude of their susceptibilities into three categories[64]. (i) The majority of solids are diamagnetic, for which χ is negative and quite small. Equation (2.1) thus implies that M is negative so that a diamagnetic material reduces the flux density when it is placed in a field. (ii) When χ is small and positive the substance is called paramagnetic and is characterised by χ being inversely proportional to temperature. (iii) Ferromagnetic materials have large, positive values of χ, and also show spontaneous magnetisation so that B is finite and non-zero in the absence of a field, and is equal to M.

This gives a good explanation of what may be observed when materials are placed in magnetic fields; however, it provides no clues as to *why* they behave in these ways. The short answer is: electrons spin. In fact electrons rotate in more than one way when they are part of atomic or molecular structures since they orbit about a nucleus while simultaneously spinning on their own axes. On a small scale the electron circulates very rapidly and thereby creates a strong circular current of the order of 40 amps. This gives the particle a distinct magnetic-dipole moment $e\hbar/2mc \approx 10^{-19} A.cm^2$. This is the Bohr magneton, μ_B.

In addition to the classical dipole-dipole interactions present in bulk substances[38], there exists an interaction between spins which has no analogue in classical or electrical considerations; this is the exchange interaction. The latter is a consequence of the fact that the spin must be considered as an extra degree of freedom and must be labeled separately. The total wave function of electrons must be antisymmetrical in the space and spin co-ordinates of the particles, i.e. $f(x_1, x_2) = -f(x_2, x_1)$. Thus if the co-ordinates of two particles are interchanged, the wave function must change sign [21].

One of the consequences of this condition is the Pauli principle. If two electrons with parallel spins were in the same orbit, then an exchange would have no effect. Therefore such a state cannot exist. If the spins were antiparallel, then an interchange would flip the spins, and there would be no conflict with the antisymmetry rule.

A further consequence of the antisymmetry rule is that two electrons with parallel spins cannot simultaneously occupy the same location (such as an orbit). This seems obvious; however, the result of this condition is less subtle than one might expect. Because of their Coulomb repulsion, two electrons will naturally repel each other, but this antisymmetry effect keeps them even further apart. As a result of this it is to be expected that the Coulomb interaction (e^2/r_{12}) (where e is the electron charge, and r_{12} is the separation), and therefore the total energy, will be lower when the spins are parallel than when they are antiparallel. This effect plays a role in determining the electron configuration for the higher orbits. Electrons in the higher orbitals will occupy as many different orbitals as possible, while aligning their spins as much as the Pauli principle will allow in order to minimise their total energy.

Similar effects can play a role when two electrons belong to neighbouring atoms, causing a coupling between the spins, which is thus referred to as spin-spin coupling. It is this coupling which brings about magnetic "ordering". If the electron spins are parallel they cannot simultaneously occupy the regions of overlap of the two neighbouring orbits, and their Coulomb energy is correspondingly reduced.

The end result of these effects is that the energy of the whole system is lower if the atomic spins are all parallel (the atomic spin being the net electron spins of each atom). Thus, each iron atom has a magnetic moment of $2\mu_B$, and neighbouring spins are coupled parallel as an indirect consequence of the Pauli principle.

The exchange of two electrons between atoms is governed by a spin-dependent energy which takes the form

$$E_{ij} = -2J_{ij}S_i \cdot S_j, \tag{2.3}$$

where S_i and S_j are the dimensionless spin vectors of the neighbouring metal ions i and j respectively. The difference in energy between the parallel and antiparallel spin configuration is

$$E_{\uparrow\uparrow} - E_{\uparrow\downarrow} = -2JS(2S+1). \tag{2.4}$$

Therefore, for a simple ferromagnet Weiss field theory [71] would give the Curie temperature T_C as

$$kT_C = \frac{2}{3}zJS(S+1) \approx \frac{z}{6}|E_{\uparrow\uparrow} - E_{\uparrow\downarrow}|, \tag{2.5}$$

where z is the number of neighbours interacting with each ion.

It is possible to compare the exchange interaction with the interaction of $\mathbf{S}_i$ with a magnetic field $\mathbf{H}$, in which case

$$E = -2\mu_B \mathbf{H} \cdot \mathbf{S}_i. \tag{2.6}$$

This shows that the exchange interaction is formally equivalent to the interaction of $\mathbf{S}_i$ with a magnetic field,

$$H_W = \sum_j \frac{J_{ij}}{\mu_B} S_j, \tag{2.7}$$

which is called the Weiss, or molecular field. This is, of course, not a real field which can be measured, but is simply an interaction between the atomic moments. If the magnetisation is considered to be uniform, S_j can be approximated by $M_s/2N\mu_B$, where N is the number of atoms per cubic centimetre of type j. The Weiss field is thus written

$$H_W = WM, \tag{2.8}$$

where

$$W = \frac{zJ}{2N\mu_B^2}.$$

The magnetic moment of an ion is not solely due to the spins of electrons for all elements. In rare-earth elements, for example, the spin and orbit add together so that $J = L+S$. The interaction between $\mathbf{L}$ and $\mathbf{S}$ is described by the spin-orbit energy

$$H_{\text{sp}} = \beta \mathbf{L} \cdot \mathbf{S}. \tag{2.9}$$

The interaction is relativistic in nature. The electron circles around the nucleus, but to an observer on the electron it appears that the nucleus orbits it. According to the theory of relativity, both frames of reference will have equivalent physical consequences. Therefore, the virtual current produced by the nucleus gives a magnetic field at the electron which tends to align its spin perpendicular to the plane of the orbit.

In a crystal the outer orbits of the electrons are considerably perturbed by the surrounding ions. This results in the disappearance (or quenching) of the orbital angular momentum, denoted by L. In quenching its L the electron has lost the ability to lower its energy by means of the spin-orbit interaction. There is however, the possibility of regaining a fraction of this energy β by partially unquenching the orbit. This energy depends on the orientation of $\mathbf{S}$ with respect to the plane of the orbit. Because of the electrostatic interaction, the orbital plane is fixed with respect to the crystal axes, so that the energy actually depends on the orientation of $\mathbf{S}$ with respect to these axes. This results in magnetocrystalline anisotropy.

Another important magnetic property of solids is magnetostriction. When a substance is exposed to a magnetic field, its dimensions change. This generally results in a change of shape, but not volume. Magnetostriction occurs in all pure substances [23], however, even in ferromagnetic substances the effect is very small. At saturation the change in length is typically of the order of $10^{-5}l$, where l is the unmagnetised length (in weakly magnetic substances the effect is markedly smaller). The magnetostriction λ is defined by

$$\lambda = \frac{\Delta l}{l}. \tag{2.10}$$

The value of of λ measured at saturation is called the saturation magnetostriction λ_s. The value of λ_s can be positive, negative, or even zero in some materials.

As the volume of a specimen tends to remain constant between the demagnetised state and saturation there is a transverse magnetostriction λ_t which is approximately one-half of the longitudinal λ but of opposite sign.

Magnetostriction is due mainly to spin-orbit coupling just as magnetocrystalline anisotropy is. Magnetostrictive strains are small due to the fact that the orbital magnetic moments are almost entirely quenched and therefore not very susceptible to rotation by an applied field.

2.3 Domains

Thus far a primarily subatomic approach has been taken in the discussion of magnetic effects. One of the key features of magnetic theory is the bulk material concept of domains. An implication of the Weiss field theory [71] is that all ferromagnetic substances below their Curie temperatures should be spontaneously magnetised even in zero applied field. It was quite obvious however, that in bulk specimens this was not the case. This led Weiss to suggest that ferromagnetic crystals are always magnetically saturated throughout small regions below their Curie temperature. Hence, when a crystal is in a demagnetised state, the directions of magnetisation of these regions are randomly oriented so that the resultant magnetisation along any direction of the specimen is zero. He called these crystal regions "domains". The effect therefore, of an applied field, is not to induce magnetisation at an atomic level, but rather to alter the domain structure so that the net magnetisation of the substance parallel to the applied field becomes non-zero. This is achieved by increasing the size and/or number of domains with magnetisation vectors in (or close to) the direction of the applied field [26].

Experimental evidence of this hypothesis was soon after provided by Barkhausen, who observed that changes in the magnetisation of a ferromagnetic substance occurs by a series of discontinuous jumps, no matter how smoothly the applied field is increased, indicating discontinuities in the domain structure.

It was subsequently shown by Landau and Lifshitz [43] that the subdivision of a specimen into domains results in a considerable reduction in the magnetostatic energy from that of the saturated state. The effect of an applied magnetic field H_a on a domain magnetised to an intensity M_s in a direction making an angle

θ with the field direction is to exert on it a couple equal to $M_s H \sin\theta$ per unit volume. This couple tends to rotate the magnetisation into the field direction. This makes a contribution to the total energy of the system of

$$E_M = -M_s H \cos\theta, \tag{2.11}$$

where H is the field strength actually acting on the domain. This is considerably less than the applied field H_a due to the demagnetising factor of the specimen. When no external field is applied the magnetostatic energy of the specimen is deemed to be the work required to assemble all the constituent dipoles, and is given by

$$E_M = -\frac{1}{2} M_s H_D \cos\theta, \tag{2.12}$$

where H_D is the demagnetising field of the specimen. H_D is in general a non-uniform field and its form is determined by the shape of the specimen (it is uniform only for a saturated prolate ellipsoid). This makes it very difficult to accurately determine the demagnetising fields of rectangular and more complex shaped specimens.

The formation of domains also results in the formation of boundaries between adjacent domains. However, the change in the direction of magnetisation does not occur abruptly from one atomic site to the next, because a sudden change across a single atomic plane would result in an extremely high exchange energy (from equation (2.3)) as was first shown by Bloch [9]. Therefore, the change in magnetisation direction must occur gradually over a number of atomic sites; the region of this change is called the domain wall.

The width of a domain wall is determined by a number of factors. Within the wall, adjacent spins are not parallel, which causes an increase in the exchange energy. This would tend to make the wall as wide as possible so each transition would be as small as possible over the total change (which is determined by the angle between the easy directions being traversed). However, the spins within the wall do not lie in easy directions [19], and thus an anisotropy energy is associated with the wall which is proportional to its width. These two energy considerations

compete with each other and the magnetostatic energy to produce walls of finite width. In iron and steel which have [100] easy directions, 90° and 180° walls are formed. Nickel, which has [111] easy directions, has 180°, 71°, and 109° walls. A result of these considerations is that there is an energy which may be attributed to each unit area of wall which forms part of the total energy of the ferromagnetic substance.

The magnetisation process is generally considered to be the motion of domain walls across domain regions, thereby flipping the spin directions on the atomic sites within the domain being encroached upon. As was noted earlier, this motion is observed to be discontinuous by means of Barkhausen jumps. Wall motion can be hindered by imperfections in the crystal lattice. Inclusions, dislocations, and residual stresses can cause the wall motion to become discontinuous. The wall can "catch" on these imperfections (also known as pinning sites), and on grain boundaries, which can cause the walls to bend, slow down, or suddenly snap across a region as a pinning site is overcome. This effect is believed to be partially responsible for magnetic hysteresis.

Because of these hinderances some domain wall motion is considered to be irreversible, as a result of which energy is lost to the system. Thus when an applied field is removed, the domain walls do not return to their original positions, and a remanent magnetisation of the substance is the result in most ferromagnetic materials. In order to reduce the magnetisation, a field must be applied in the opposite direction to force the domain walls over the hinderances to leave the specimen in a state of zero induced magnetisation. This field is referred to as the coercive field.

At very high fields all domain walls will have moved as far as is possible, leaving all spins aligned with those easy axes which are closest to the direction of the applied field. Thereafter, further increases in the induction can only occur by overcoming the anisotropy energy and rotating the spins away from the easy directions towards the applied field. This effect is reversible as the spins will return to the easy axes when the field is once again reduced.

2.4 Summary

When considered together, all of these concepts form the very basics of magnetism and ferromagnetism. Magnetism has many varied incarnations. The effects and interactions of spinning and rotating charges are limited only by the conditions under which they may be found, and as these are near limitless, new and amazing effects of magnetism will continue to be discovered. From the discovery of lodestones which caused slivers of iron to point north, to the revelation that sunspots are regions of huge magnetic fields spewing matter from deep within the sun, to medical imaging using nuclear magnetic resonance, magnetism has surprised, amazed, and intrigued humans.

In the following chapter just one aspect of magnetics will be reviewed, that being the effect of externally applied stress on the magnetic properties of ferromagnetic materials, known as the magnetomechanical effect. This is only one of the multitude of magnetic effects, and this introduction and the following review has paid extra attention to the areas which are important to developing an understanding of the magnetomechanical effect as it has been studied in this research.

For a more balanced introduction to magnetics, the reader is referred to almost any of the fine texts in the bibliography at the end of this thesis, in particular those by Jiles [38] and Cullity [23].

Chapter 3

The History of Magnetomechanics

3.1 Overview

The existence of the magnetomechanical effect has been known for over a century, and many detailed investigations have been made by the pre-eminent researchers in the field of magnetics. Magnetomechanics is often discussed intimately in terms of its relationship to magnetostriction, but the two topics will be covered separately here.

The stress-dependence of the magnetic properties of ferromagnetic materials is of such an extent that it ranks alongside field strength and temperature as the primary factors determining magnetic changes [10]. In some materials a tension of 10 kg.mm^{-2} will increase the permeability in low fields by a factor of 100; in others the permeability is decreased by tension, whilst in others the permeability is increased in low fields, and decreased in higher fields. In all materials the saturation induction is unaffected by a stress within the elastic limit, and it is affected by stresses large enough to produce plastic flow only when a change of phase or state of atomic ordering occurs in the material [10].

There are numerous different methods of observing and investigating the relationship between stress and magnetism, and even more ways of presenting the

subsequent data. Stresses may be either tensile or compressive, uniaxial or bi-axial, constant or cycled. In typical magnetics style every different method will produce different results due to the extreme sensitivity of magnetisation to the history of the sample, and thus are dificult to compare. The results will also differ depending on whether high or low fields are considered (ie. Rayleigh region or saturation), and whether low, near elastic limit, or plastic strains are applied.

Many of the texts which cover the magnetomechanical effect go into great detail in presenting specific results obtained on Permalloy or silicon iron under exotic conditions as some remarkable features may be observed by altering stresses or fields mid-cycle to produce very asymmetrical results. However, the benefits of discussing those results in this thesis are very limited, as such materials were not investigated. Instead only very simple magnetisation-stress combinations for mild steel have been considered.

As the works considered in this chapter span nearly a century the standards, formats and units used changed dramatically over this period. Wherever possible equations have been left in the forms as found in the original works. This decision was made in order to facilitate the referral to the original works. Every attempt has been made to clearly define the terms and symbols used, however, as a result the definitions found in this chapter are most often only valid in the section in which they are found, and the definitions of symbols in the rest of the thesis take precidence in all other sections. Any errors or mistakes in the original works have been faithfully reproduced.

3.2 Bozorth

Theoretical explanations of the magnetomechanical effect also abound, albeit rather simplistic or empirical ones in the main. Bozorth [10] gives a very good description of what he calls the Domain Theory of Effect of Stress. He proposes that when the changes in stress and magnetostriction are small and reversible, there is a thermodynamic relation between the change of induction B, with stress

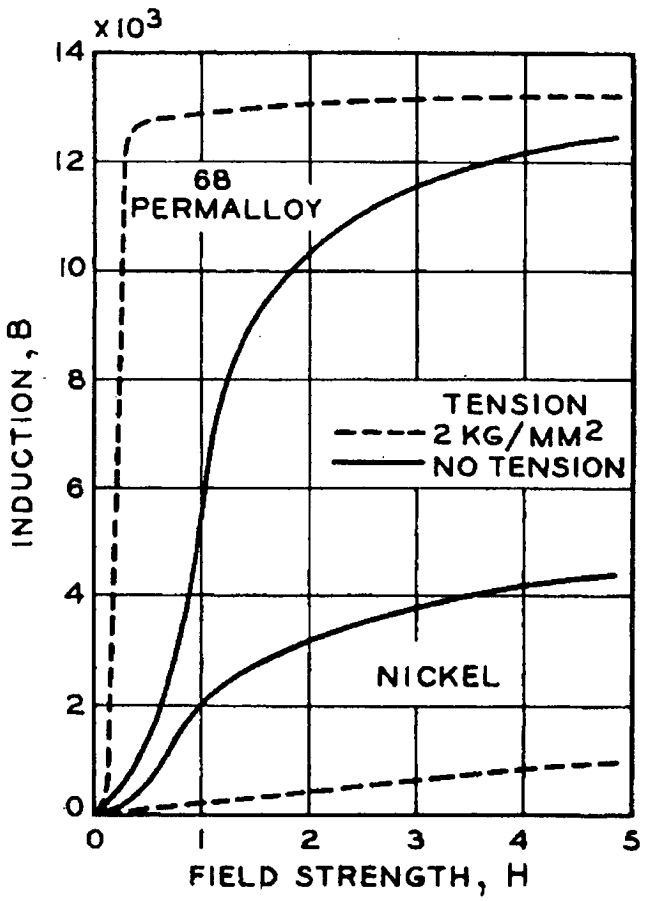

Figure 3.1: Effect of tension on the magnetisation curves of 68 Permalloy and Nickel [10].

(tension) σ, and the length l, as affected by magnetising field strength H. The relationship is described in the cgs system by

$$\frac{1}{l_0}\left(\frac{\partial l}{\partial H}\right)_\sigma = \frac{1}{4\pi}\left(\frac{\partial B}{\partial \sigma}\right)_H . \tag{3.1}$$

Bozorth dealt almost exclusively with tensile, uniaxial stresses. This is a limiting factor when considering his work; however, the contributions made by him merit attention nonetheless. He contends that the dependence of magnetisation on stress may also be described in terms of the energy associated with the stress and the direction of spontaneous magnetisation I_s in a domain. Suppose the

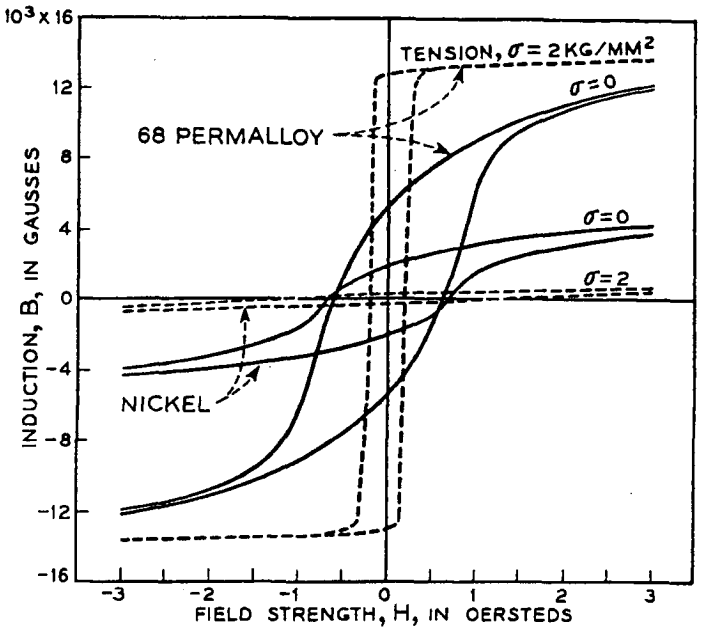

Figure 3.2: Effect of tension on the hysteresis loops of 68 Permalloy and Nickel [10].

magnetic strain energy density for the polycrystalline case is given by

$$E_\sigma = \frac{3}{2}\lambda_s \sigma \sin^2\theta, \tag{3.2}$$

where λ_s is the magnetostrictive expansion at saturation, and σ the angle between the saturation magnetisation I_s and the tension σ. This expression shows that when λ_s and σ are positive the energy is a minimum for $\sigma = 0$, and therefore that the domains are stable when I_s is parallel to σ. Consequently I for such a material is generally increased by tension. When $\lambda_s\sigma$ is negative the domains will tend to be orientated with I_s perpendicular to the axis of tension, and magnetisation will be decreased by tension.

Bozorth's book contains an enormous volume of data. A few of the graphs which are relevent to this research are reproduced here in order to show some of the shapes which were produced by the application of different stresses. Both hysteresis loops and normal magnetisation curves are shown for nickel, iron, and 68 Permalloy under a range of different stress and field conditions in Figures (3.1), (3.2), (3.3), (3.4), (3.5), and (3.6).

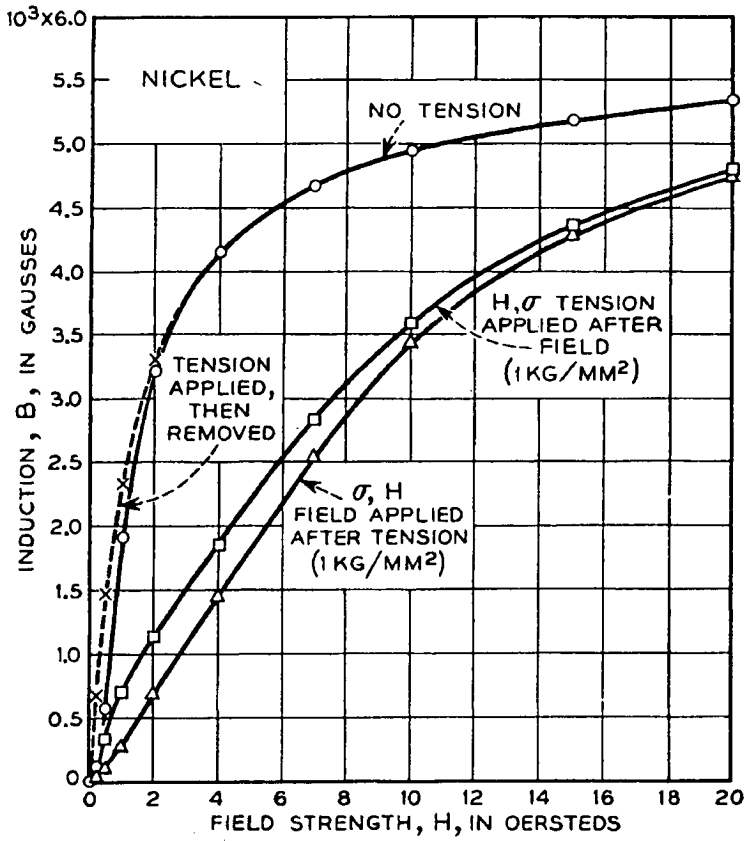

Figure 3.3: Effects of applying stress and field in different orders, in nickel [10].

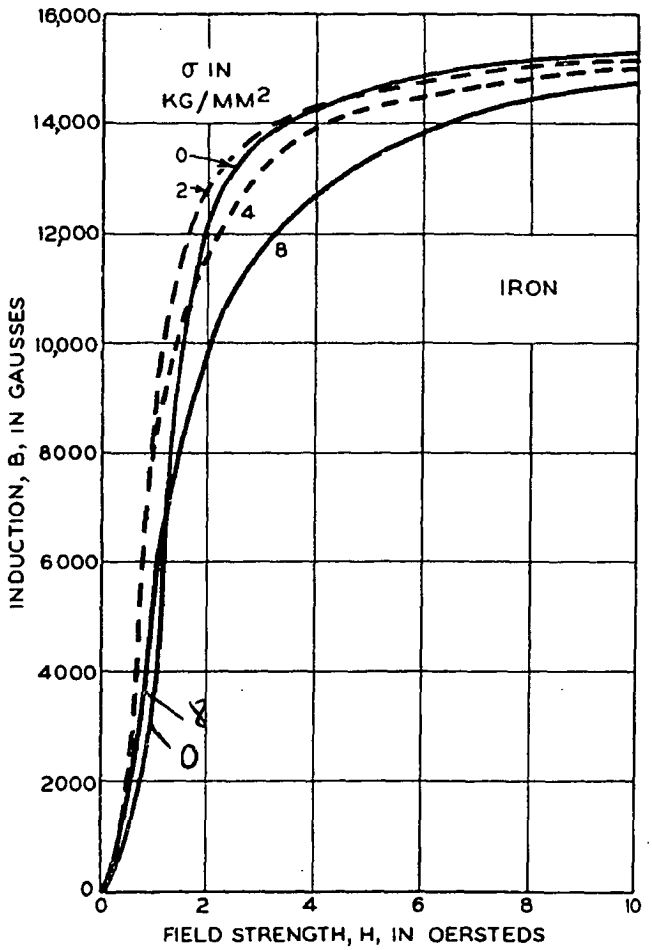

Figure 3.4: Magnetisation curves of iron subject to various tensions [10].

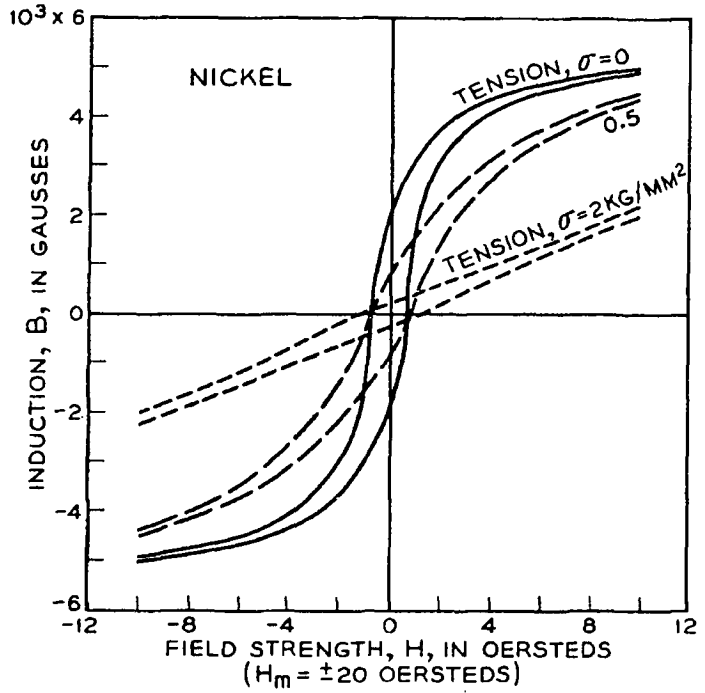

Figure 3.5: Effect of tension on the hysteresis loop of nickel [10].

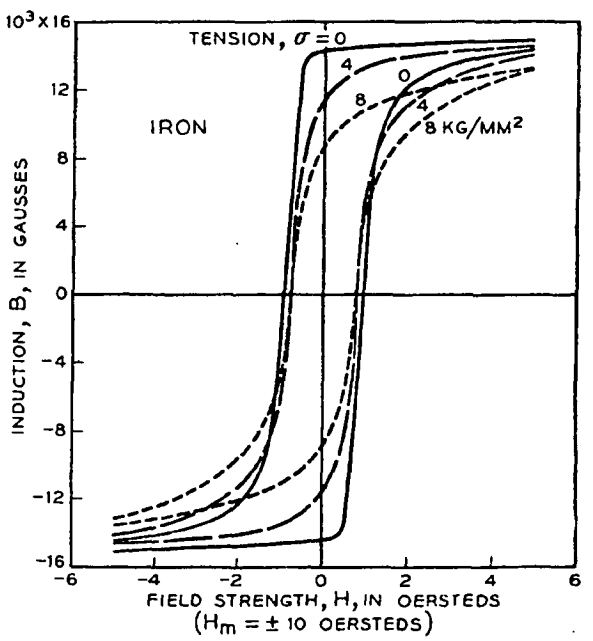

Figure 3.6: Hysteresis loops of iron under tension [10].

3.3 Brown

An important, mostly theoretical, paper published in the same era as Bozorth's book was the 'Irreversible Magnetic Effects of Stress' by W. F. Brown [12]. His treatment starts with Rayleigh's law as the analytical description of small hysteresis loops [4]. The extension of the description to cases in which the independent variable is stress rather than magnetising force comes from assuming that Rayleigh's law applies to the elementary process of domain wall displacement to which the macroscopic magnetisation changes are due. It is then possible to generalise the theory to include effects of stress.

For the validity of the theory it is not necessary that Rayleigh's law hold for a single domain wall, provided it holds on the average for a group of many similar walls. Brown assumed that the individual process was a discontinuous irreversible jump, but that the jumps of different walls occur at different values of magnetising force or stress. A derivation of Rayleigh's law (in the generalised form assumed) therefore requires a statistical study of the behaviour of domain walls such as that given by Néel [51].

In this treatment an iron crystal is considered in which the internal stresses are not too high, and so each domain is (in the demagnetised state) magnetised to saturation along one of the "directions of easy magnetisation" i.e. the $\langle 100 \rangle$ directions. Application of a magnetising force or stress causes displacements of the walls separating adjacent domains, so that the more favourably magnetised domain grows at the expense of its neighbour. In the case of a magnetising force, the more favourably magnetised domain is the one whose magnetising vector is closer to the magnetising force. In the case of a tension, the more favourably magnetised domain is the one whose magnetisation vector is closer in direction to the tension. Thus 90° walls, eg. between [100] magnetisation and [001], can be displaced either by magnetising force or by tension, but 180° walls, eg. between [100] and $[\bar{1}00]$, are unaffected by tension. Furthermore, the 90° walls themselves may be grouped into two classes: those for which tension and positive magnetising

force produce displacements of the same sign, and those for which they produce displacements of opposite signs.

Magnetising force and tension are thermodynamically equivalent to a hydrostatic pressure within each domain, acting on its domain walls. This pressure is

$$p = HI_s \cos(I, H) + \frac{3}{2} T\lambda_{100} \cos^2(I, H), \tag{3.3}$$

for the case of magnetising force H and tension T along the same direction. Here I_s is the saturation magnetisation, and λ_{100} is the saturation magnetostriction for a crystal magnetised along [100]. Subtraction of the pressures on opposite sides of a wall gives the net pressure on the wall.

By considering the pressures applied to each of the possible 3-dimensional wall configurations and their resulting motions, formulae were derived to describe the changes in magnetisation produced when an initially demagnetised specimen is subjected to the following treatment sequence: (i) the magnetising force is increased to a value H; (ii) a tension T is applied; (iii) the tension is removed.

Upon carrying out the details of the calculation and combining the contributions of all types of wall, the following formulae for the irreversible magnetisation I_{ir} of a single crystal were obtained; the reversible part is simply $\chi_0 H$, where χ_0 is the initial susceptibility.

(i) H applied:

$$I_{ir} = I_s^3 H^2 (2\beta_1 \phi_1 + \beta_2 \phi_2), \tag{3.4}$$

with

$$\begin{aligned} \phi_1 &= 2(n^3 + 3nm^2 + n^3 + 3nl^2 + m^3 + 3ml^2), \\ \phi_2 &= 8(n^3 + m^3 + l^3), \end{aligned}$$

where (l, m, n) are the direction cosines of the field direction with respect to the (x, y, z) axes, and the constant β has one value β_1 for all wall types which undergo displacements under positive magnetising force and tension, and another value β_2 for all wall types which are not affected by tension.

(ii) T applied; ΔI_{ir} measured from the state with H at its final value and T zero:

$$\Delta I_{ir} = \beta_1(3I_s^2\lambda_{100}HT\psi_1 + (9/8)I_s\lambda_{100}^2T^2\psi_2), \tag{3.5}$$

with

$$\begin{aligned}\psi_1 &= 4(n^4 - l^4),\\ \psi_2 &= 2[n(n^2 - m^2)^2 + n(n^2 - l^2)^2 + m(m^2 - l^2)^2].\end{aligned}$$

(iii) T removed; ΔI_{ir} measured from the state at the end of step (ii):

$$\Delta I_{ir} = 0. \tag{3.6}$$

The removal of tension causes no change of macroscopic magnetisation because the displacement of walls produces equal and opposite changes of magnetisation.

The variation of magnetisation with tension during step (ii) is given, for the polycrystalline specimen, by

$$\Delta I = \gamma_1 HT + \gamma_2 T^2, \tag{3.7}$$

where

$$\begin{aligned}\gamma_1 &= 3\beta_1 I_s^2\lambda_{100}\langle\psi_1\rangle,\\ \gamma_2 &= (9/8)\beta_1 I_s {\lambda_{100}}^2\langle\psi_2\rangle.\end{aligned}$$

The theoretical model leads not only to a definite (if limited) formula for the variation of magnetisation with tension, but to definite values of the constants in the formula, and to evaluate them one needs only a set of purely magnetic data on the particular specimen, i.e. the variation of normal permeability with small magnetising force.

The validity of equation 3.7 is conditional on the tension not exceeding a certain critical value beyond which assumptions made during its derivation become invalid. The implications of Brown's theory are shown in Figure (3.7). As can be seen, the predicted magnetic response of a material is independent of the sign of the applied stress (i.e. the behaviour is the same for both compression and tension).

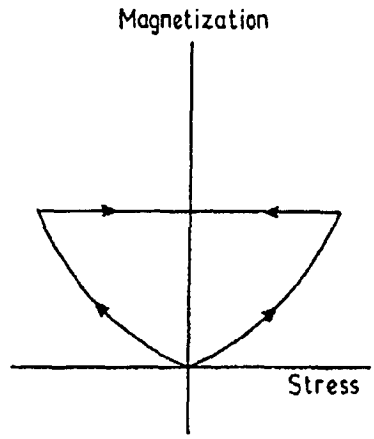

Figure 3.7: Prediction of magnetisation-stress curves according to Brown's theory [12].

With such confidence and enthusiasm one could be forgiven for believing that a complete explanation of magnetomechanics could not be far away. Unfortunately, subsequent work by Craik and Wood [22], showed that this theory did not fit for compression, and thus is fundamentally lacking in some way.

3.4 Lee

In an extremely comprehensive work by Lee just a few years later, 'Magnetostriction and Magnetomechanical Effects' [50], the greater magnitude of the task at hand is glimpsed.

He suggests that since the strain in a ferromagnetic crystal is determined partly by the direction of the spontaneous magnetisation, it is to be expected that if such a crystal is strained by an external force, this additional strain will in general alter the direction of the spontaneous magnetisation. It will hence be shown that the effect of a simple compression or tension is to introduce an additional term to the anisotropy energy, superimposed on the normal crystal energy E_k.

If a uniform tension of magnitude σ is applied to a crystal, a term usually known as the magnetoelastic energy is added to the crystal energy. The values of

$alpha_i$, the direction cosines of the domain magnetisation vector with respect to the orthogonal axes, required to make the total energy a minimum thus depend in a complicated manner on the magnitude and signs of K_1, λ_{100}, λ_{111}, and σ. It may be noted that the energy depends on $\lambda_{100}\sigma$ and $\lambda_{111}\sigma$ so that a substance with positive magnetostriction constants, subject to tension, behaves exactly as one whose magnetostrictive constants are negative, and submitted to compression. The effect of stress therefore, is to create new energy minima for the domain vectors in addition to those given by the crystal anisotropy.

Further development using this approach reached a hurdle at this point as the general case which has been presented is extremely complicated for arbitrary values of the constants, and therefore no general solution was put forth. It was necessary therefore to consider only approximate solutions in the two cases when the crystal energy is much greater than or much less than the magnetoelastic energy.

The simplest case occurs when the crystal energy is the dominant term. It is then reasonable to assume that the domain vectors remain in one or other of the easy directions caused by the crystal energy alone; that is, that the magnetoelastic energy merely makes some of the energy minima of the crystal energy deeper than others. There are then two cases to be considered:

(1) $K_1 > 0$, easy direction [100]. In this case, two of the $alpha_i$ are zero for each domain. If $\lambda_{100}\sigma$ is positive, then a minimum occurs when each domain vector lies parallel or antiparallel to that easy direction making the smallest angle with the direction of σ. If $\lambda_{100}\sigma$ is negative, then it will have an algebraic minimum when the vectors make the largest possible angle with σ, still remaining in an easy direction.

(2) $K_1 < 0$, easy direction [111]. In this case $alpha_i^2 = \frac{1}{3}$, and so the term involving λ_{100} is constant, the magnetoelastic energy being determined solely by the term in λ_{111}. Here again this has an algebraic minimum or maximum when each domain vector lies parallel or antiparallel to the easy direction making the least or greatest angle with σ, as $\lambda_{111}\sigma$ is accordingly positive or negative.

In each case, provided the magnetoelastic energy is smaller than the crystal energy, the effect of a stress σ is to make the easy axis lying nearest σ the deepest or shallowest minimum as $\lambda_e\sigma$ is positive or negative accordingly, where λ_e is the magnetostriction constant in the easy direction.

When K_1 is small it is permissible to neglect the crystal energy and so the domain vector orientation is determined by the magnetoelastic energy alone. In the case in which λ_{100} is much greater or less than λ_{111}, the energy will be a minimum under tension when the vectors lie parallel and antiparallel to the direction of greatest algebraic magnetostriction making the smallest angle with σ. The opposite is true for compression.

When λ_{100} and λ_{111} are equal the magnetoelastic energy reduces to the form

$$E_\sigma = -\frac{3}{2}\lambda_s\sigma\cos^2\phi, \tag{3.8}$$

in which ϕ is the angle between I_s and σ. This statement, together with the assumption that $K_1 = 0$, is the one most often used to analyse the behaviour of ferromagnetic substances under stress. If $\lambda_s\sigma$ is positive the domain vectors align themselves parallel and antiparallel to the stress axis, and the material eventually behaves like a uniaxial crystal. The magnetisation-field curve becomes rectangular and the saturation magnetostriction becomes zero. If $\lambda_s\sigma$ is negative, the stress axis becomes a difficult one and the domain vectors orientate themselves in the plane perpendicular to this.

The total energy of the system in the presence of a magnetic field is

$$E = -I_sH\cos\phi - \frac{3}{2}\lambda_s\sigma\cos^2\phi. \tag{3.9}$$

For equilibrium $\partial E/\partial\phi = 0$, whence

$$I = \frac{I_s^2}{3\lambda_s\sigma}H \quad \text{and} \quad \frac{dl}{l} = \frac{3}{2}\lambda_s\frac{I^2}{I_s^2},$$

so that the magnetic susceptibility is constant and the magnetisation curve degenerates into a straight line.

3.5 Chikazumi

A number of important concepts are dealt with in the excellent book 'Physics of Magnetism' by Chikazumi [20]. In discussing magnetism and stress Chikazumi considers a hollow cylinder, if the cylinder is twisted, the effective tension makes an angle of 45° from the axis, so that the magnetisation lines up in a helical way. If an AC magnetic field is applied parallel to the axis, it induces the magnetisation change along the helical line, which can only be detected by a secondary coil wound lengthways around the cylinder wall. In the absence of torsion, the magnetisation changes along the axis of the cylinder, and no signal is induced in the secondary coil. Thus, the AC signal picked up by the secondary coil is a good measure of the torsional force.

In principal, the magnetisation caused by the tension σ can be determined by minimising the sum of the magnetostrictive energy and the potential energy of domain magnetisations. This, however, can be solved from a thermodynamical relation, provided that the deformation is known as a function of the applied field. If the internal energy is a function of magnetisation I and the elongation $\partial l/l$, the equilibrium condition gives

$$\frac{\partial E}{\partial I} = H, \tag{3.10}$$

and

$$\frac{\partial E}{\partial(\partial l/l)} = \sigma. \tag{3.11}$$

Since

$$\frac{\partial^2 E}{\partial(\partial l/l)\partial I} = \frac{\partial^2 E}{\partial I \partial(\partial l/l)}, \tag{3.12}$$

we have

$$\frac{\partial H}{\partial(\partial l/l)} = \frac{\partial \sigma}{\partial I}. \tag{3.13}$$

It can therefore be shown, that for rotation magnetisation

$$\Delta I = \frac{3\lambda I_s}{2K_u} \sin^2\theta_0 \cos\theta_0 \Delta\sigma, \tag{3.14}$$

and so for the 90° wall displacement

$$\Delta I = \frac{3\sqrt{2}\lambda_{100} I_s S}{\alpha} \sin\theta_0 \cos^2\theta_0 \Delta\sigma. \tag{3.15}$$

For polycrystalline material we have

$$\Delta I = \frac{3\lambda I_s}{8K_u}\Delta\sigma, \tag{3.16}$$

for rotation magnetisation, and

$$\Delta I = \frac{3\sqrt{2}\pi\lambda_{100} I_s S}{16\alpha}\Delta\sigma, \tag{3.17}$$

for displacement of 90° walls, where S is the total area of 180° wall per unit area, and α is the second derivative of the wall energy.

It should be noted that equation (3.12) is valid only when the energy is a unique function of I and $\partial l/l$. In the presence of 180° walls the magnetostrictive energy is not a unique function of magnetisation I, and (3.12) is no longer valid. This is the reason why the magnetisation is insensitive to the applied stress in the demagnetised state.

At this point a concept not yet discussed in this review is introduced: the phenomenon that the applied stress causes a deformation via the change in domain magnetisation in addition to the elastic deformation. This phenomenon is called the ΔE effect, because the effective Young's modulus is changed by the additional deformation. For rotation magnetisation,

$$\Delta I = -I_s \sin\theta_0 \Delta\theta, \tag{3.18}$$

and it may be shown that

$$\begin{aligned} \Delta\left(\frac{\partial l}{l}\right) &= -3\lambda \sin\theta_0 \cos\theta_0 \Delta\theta, \\ &= \frac{3\lambda}{I_s}\cos\theta_0 \Delta I, \\ &= \frac{9\lambda^2}{2K_u}\sin^2\theta_0 \cos^2\theta_0 \Delta\sigma. \end{aligned} \tag{3.19}$$

For polycrystalline materials

$$\overline{\sin^2\theta_0 \cos^2\theta_0} = 2/15,$$

so that

$$\Delta\left(\frac{\partial l}{l}\right) = \frac{3la^2}{5K_u}\Delta\sigma. \tag{3.20}$$

Since this gives the additional elongation,

$$\frac{3\lambda^2}{5K_u} = \frac{1}{E_{\text{mag}}} - \frac{1}{E_0} \simeq -\frac{\Delta E}{E_0^2},$$

or

$$\frac{\Delta E}{E} = -\frac{3\lambda^2}{5K_u}E_0. \tag{3.21}$$

If $K_u = \frac{3}{2}\lambda\sigma_i$, $\Delta E/E$ becomes

$$\frac{\Delta E}{E} = -\frac{2\lambda}{5\sigma_i}E_0. \tag{3.22}$$

For 90° walls, by using $\Delta I = \sqrt{2}I_s \cos\theta_0 Ss$, we can show

$$\begin{aligned}\Delta\left(\frac{\partial l}{l}\right) &= 3\lambda_{100}\sin\theta_0\cos\theta_0 Ss,\\ &= \frac{3\lambda_{100}}{\sqrt{2}I_s}\sin\theta_0\Delta I,\\ &= \frac{9\lambda_{100}^2 S}{\alpha}\sin^2\theta_0\cos^2\theta_0\Delta\sigma.\end{aligned} \tag{3.23}$$

For polycrystalline materials (3.23) becomes

$$\Delta\left(\frac{\partial l}{l}\right) = \frac{6\lambda_{100}^2 S}{5\alpha}\Delta\sigma, \tag{3.24}$$

from which we have

$$\frac{\Delta E}{E} = -\frac{6\lambda_{100}^2 S}{5\alpha}E_0. \tag{3.25}$$

If α is governed by $\lambda\sigma_i$, $\Delta E/E$ becomes

$$\frac{\Delta E}{E} = -\frac{12\lambda_{100}}{5\pi\sigma_i}E_0, \tag{3.26}$$

which gives a value almost equal to that in (3.22). Thus the contribution of 90° walls is almost equal to that of rotation magnetisation for highly stressed materials. These results show that $\Delta E/E$ is proportional to λ.

Chikazumi also used a number of very simple models to theoretically predict the shapes of hysteresis loops. The quality of the models increases, predictably,

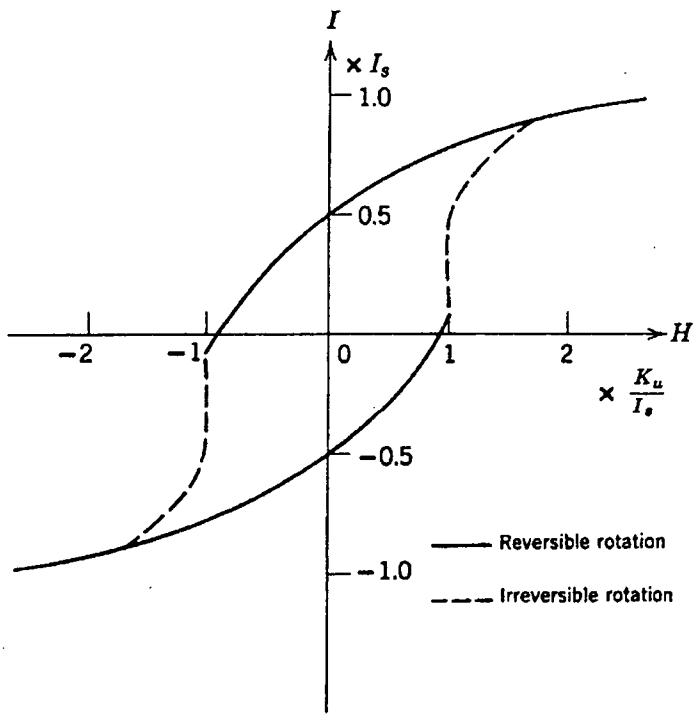

Figure 3.8: Magnetisation curve of the aggregate of single domain fine particles with uniaxial anisotropy [20].

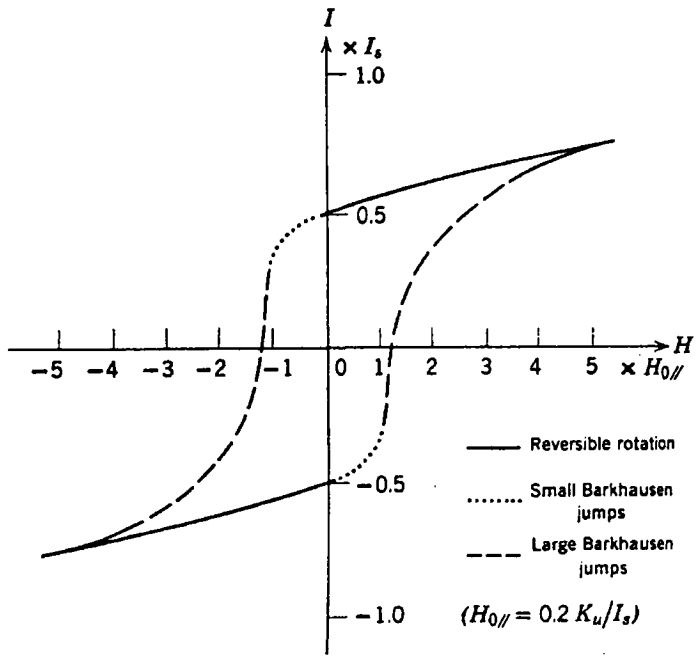

Figure 3.9: Magnetisation curve of the aggregate of fine uniaxial particles with a multidomain structure [20].

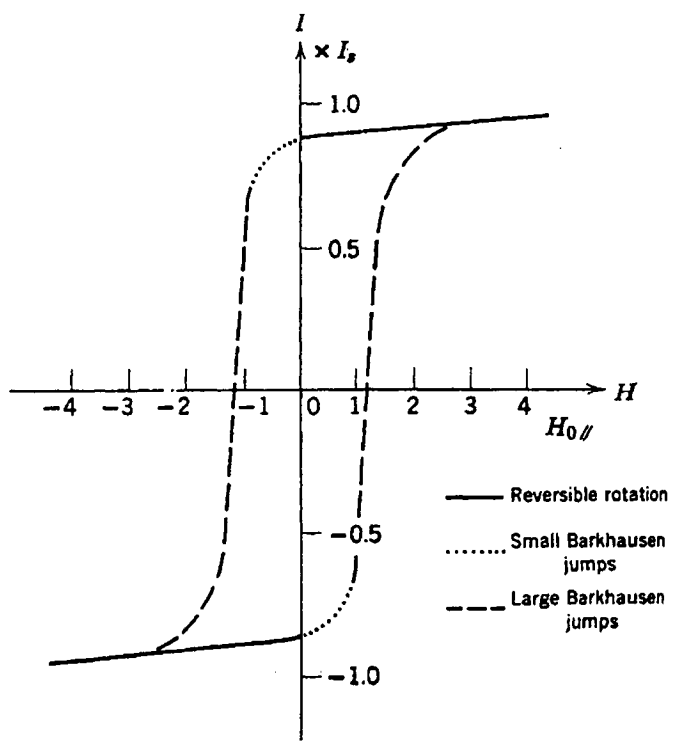

Figure 3.10: Magnetisation curve of a cubic substance ($K_1 > 0$) [20].

with the complexity of the model. The models divide the hysteresis loops into regions where one particular magnetisation mechanism dominates over the others. The models are shown in Figures (3.8), (3.9), and (3.10). The model presented in Figure (3.10) is of most relevance to this thesis in its segregation of magnetisation mechanisms as it closely resembles some of the features found in the model discussed in Chapter 8.

3.6 Cullity

One of the most readable texts available on magnetics is 'Introduction to Magnetic Materials' by Cullity [23]. An introduction and overview is given for almost every area of magnetism yet the reader is gently led into each new concept. His treatment of the effect of stress on magnetisation is an excellent example of this.

A peculiar property of iron, Villari reversal, is explained very well. The magnetostriction of polycrystalline iron is positive at low fields, then zero, then negative at higher fields. This results in the magnetic behaviour of iron under stress being rather complicated. At low fields tension raises the B, H curve and at higher fields lowers it; the crossover of the tension curve with the zero stress curve at a particular field strength, which depends on the stress and on the preferred orientation, is called the Villari reversal. Compression has a reverse, and larger effect, lowering B at low fields and raising it at large fields. The Villari reversal occurs at about 1.6 kA/m in pure iron.

The magnetomechanical effect can be most simply described by the following example. If a material has positive λ, it will elongate when magnetised; applied tensile stress, which tends to elongate it, will therefore increase the magnetisation, and applied compressive stress will decrease it. Thus, in Figure (3.11), if a field H_1 produces a magnetisation of A at zero stress, then application of a stress $+\sigma_1$ will raise the magnetisation to B at constant field. The magnetisation in the remanent state at zero stress is C, and the same stress $+\sigma_1$ will increase this to D. But a stress applied to a demagnetised specimen will not produce any

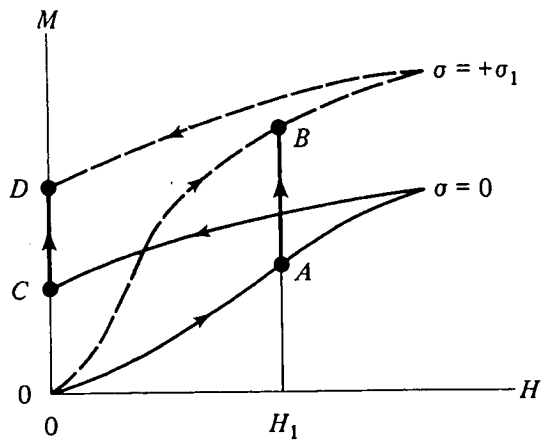

Figure 3.11: Effect of tension on the magnetisation of a material with positive magnetostriction (schematic), *from Cullity* [23].

magnetisation, as shown by the intersection of the full line and dashed curves at the origin.

If the crystal anisotropy is weak the direction of I_s in the absence of a field will be controlled largely by stress, and, in a polycrystalline specimen with no preferred orientation, equation (3.8) will apply. Let Figure (3.12a) represent a small portion of the specimen, comprising four domains. The application of a small tensile stress to the demagnetised specimen, as in (3.12b), will cause domain walls to move in such a way as to decrease the volume of domains magnetised at right angles to the stress axis, because such domains have a high magnetoelastic energy. These domains are completely eliminated by some higher value of the stress, as in (3.12c), and E_{me} is now a minimum. The domain structure is now identical with that of a uniaxial crystal. Only a small applied field is now required to saturate the specimen, because the transition from Figure (3.12c) to (3.12d) can be accomplished solely by the relatively easy process of 180° wall motion.

Two points emerge from this examination of magnetisation under stress:

1. In the demagnetised state, stress alone can cause domain wall motion. This motion must be such as to ensure zero net magnetisation for the whole specimen.

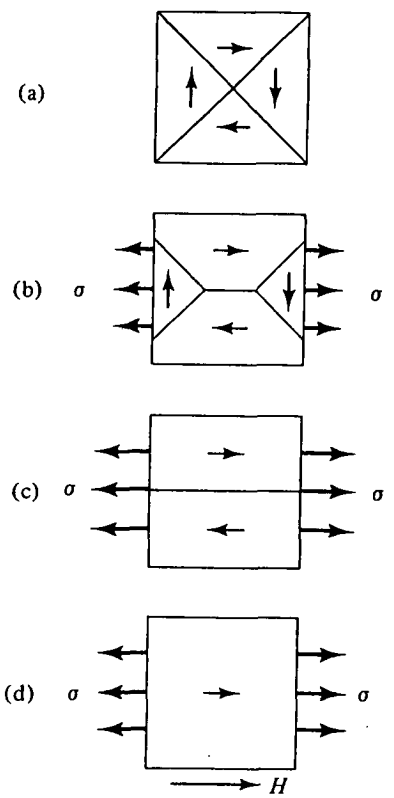

Figure 3.12: Magnetisation of a material with positive magnetostriction under tensile stress (schematic), *from Cullity* [23].

2. Stress alone can create an easy axis of magnetisation. Therefore, when stress is present, stress anisotropy must be considered, along with any other anisotropies that may exist. The stress anisotropy energy, which is a magnetoelastic energy is given by

$$E_{\text{me}} = K_\sigma \sin^2 \theta, \tag{3.27}$$

where the stress anisotropy constant K_σ is given by $\frac{3}{2}\lambda_s \sigma$.

3.7 Birss

A major paper detailing the magnetomechanical effect was written by Birss [8] in 1970. It is a thorough treatment covering aspects of the magnetisation process, interanl stresses, Rayleigh's laws and effects of externally applied stresses, among other topics. The work of Birss is substantially different to the effects considered in the bulk of this thesis as the fields applied were restricted to the Rayleigh region, however the paper is a significant work in the field and deals with some important issues. However, it is important to note that due to the realtively low applied fields considered, the mechanism of domain vector rotation as a means of magnetisation is ignored.

After a detailed review of general magnetics, the influence of stress on the magnetisation process is dealt with. Stress induced changes are considered in terms of domain wall pressures, the energy gradient, dE_w/dx, called "l'opposition", and large-scale changes in the equilibrium domain configuration. The domain wall pressure considerations are a review of work done by Brugel and Rimet [14][13] which extended the work done by Brown [12] on 90° and 180° walls. The influence of stress on "l'opposition" is considered in terms of the application of tension diminishing the gradient of the internal stresses in the material. As wall motion is hindered by inclusions and internal stresses it may be considered that a reduction in these could result in wall motions which "would have occurred" had these hindrances not been present. magnetically hard materials which are characterised by a large number of such hinderances will naturally display this

effect the most strongly. The effect on "l'opposition" was considered in isolation by considering changes caused by temperature, so changes in wall pressures were not present.

The effect of large-scale chnages in overall domain structure caused by stress on magnetisation processes is then considered. The principle concept is the notion that the overall equilibrium domain configuration is determined by a balance between the rates of change of surface and volume terms of the domains. It is suggested that when a stress is applied, E_σ can make a contribution to the volume terms and thus the application of sufficient stress may alter which domain pattern has the lowest energy. It is noted that although these three effects are discussed seperately, they are in fact intimately interrelated and may be considered as limiting extremes of the one effect. Thus the rest of the paper is concerned with limiting conditions under which effects of stress may be considered. The asymmetry of behaviour under positive and negative stresses is also dealt with.

3.8 Langman

In more recent times a new generation of names have come to the fore in the field of stress effects in magnetism, and many advances have been made which deepen the understanding of the area, as well as discovering new concepts and applications.

The first works to be reviewed in this area are those of Richard Langman. The paper 'The Effects of Stress on the Magnetization of Mild Steel at Moderate Field Strengths' [47] is of particular relevance to this work as many of the methods employed are similar to those used in this research.

Magnetisation properties were considered both parallel to, and perpendicular to, uniaxially applied stresses under hysteretic and anhysteretic conditions. The peak flux densities for a given field were then compared for different applied stresses. Predictions of the rearrangement of domains due to the effects of stress were then made.

Consider a 2-dimensional representation of polycrystalline iron which has been subjected to a sufficient field H for all domains to be pointing in the nearest easy direction to H. This will mean that the range of directions is $\pm 45°$ from H. For convenience this is called the kneepoint of the magnetisation curve.

There are five magnetic energy components that affect the domain magnetisation pattern: i) magnetostatic; ii) magnetoelastic; iii) domain wall; iv) crystal anisotropy; and v) demagnetising.

Assuming that the material is magnetised to the kneepoint, the domain walls have moved to their limits and can be ignored. Crystal anisotropy can be ignored because the field is not high enough to rotate the moments away from the easy axes. Demagnetising energy is present but is assumed constant. Thus magnetostatic and magnetoelastic components remain.

1) Magnetostatic energy

$$E_{ms} = -M_s H \cos\theta \quad \mathrm{J/m^3}, \tag{3.28}$$

where θ is the angle between the intrinsic magnetisation M_s and the applied field H.

2) Magnetoelastic energy

$$\begin{aligned} E_{me} &= -1.5\lambda_{100}\sigma(\alpha_1^2\gamma_1^2 + \alpha_2^2\gamma_2^2 + \alpha_3^2\gamma_3^2) \\ &\quad -3\lambda_{100}\sigma(\alpha_1\alpha_2\gamma_1\gamma_2 + \alpha_2\alpha_3\gamma_2\gamma_3 + \alpha_3\alpha_1\gamma_3\gamma_1) \quad \mathrm{J/m^3}, \end{aligned} \tag{3.29}$$

where $\alpha_1, \alpha_2, \alpha_3$ are the direction cosines of M_s, and $\gamma_1, \gamma_2, \gamma_3$ are the direction cosines of σ.

Suppose a domain is initially (for zero stress) along the $+x$ crystal axis, at an angle θ to the field H. If a tensile stress is applied perpendicular to H, then, depending on the relative combined values of the two energy components (magnetostatic and magnetoelastic), the domain magnetisation might change to any of the other three easy directions. The $\pm x$ and $\pm y$ axes are all easy directions of magnetisation, the same as the crystal axes. The energies of the four directions are

$$+x: \quad -M_s H \cos\theta - 1.5\lambda_{100}\sigma \sin^2\theta,$$

$$+y: \quad -M_s H \sin\theta - 1.5\lambda_{100}\sigma \cos^2\theta,$$

$$-x: \quad -M_s H \cos\theta - 1.5\lambda_{100}\sigma \sin^2\theta,$$

$$-y: \quad -M_s H \sin\theta - 1.5\lambda_{100}\sigma \cos^2\theta.$$

The second term is always negative (λ_{100} is positive), and for $0° < \theta < 45°$, the energies of the $+y$ and $-x$ directions will always be more positive than the other two directions. Since the domain direction will be such that energy is kept at a minimum, only the $+x$ and $-y$ directions need to be considered for $0° < \theta < 45°$. By symmetry, for $-45° < \theta < 0°$ only the $+x$ and $+y$ directions need to be considered. Hence, domains may only lie within 90° of the direction of the applied H.

The domain pointing along the $+x$ axis in the absence of stress may change to point along the $-y$ axis, if when the stress is applied, the energy is thereby lowered. The stresses at which the domain switches occur are called threshold stresses. Suppose that a fraction f of these domains is along the $+x$ axis, and a fraction $(1-f)$ is along the $-y$ axis; f takes the value 1 or 0. The total energy is;

$$E_t = f[-M_s H \cos\theta - 1.5\lambda_{100}\sigma \sin^2\theta] + (1-f)[-M_s H \sin\theta - 1.5\lambda_{100}\sigma \cos^2\theta]. \tag{3.30}$$

Writing $M_s H = K$ and $1.5\lambda_{100}\sigma = K'$, and rearranging terms gives

$$E_t = f[K' \cos 2\theta - K\cos\theta + K\sin\theta] - [K'\cos^2\theta + K\sin\theta]. \tag{3.31}$$

The second brackets are independent of f and can be ignored. For minimum E_t, $f[K'\cos 2\theta - K\cos\theta + K\sin\theta]$ must be a minimum. If $K(\cos\theta - \sin\theta) > K'\cos 2\theta$ the minimum is for $f = 1$; otherwise it occurs for $f = 0$.

Compression K' in the magnetoelastic energy is negative and subsequently:
1) for compression parallel to the field the range of threshold stress is the same as for tension perpendicular to the field; and
2) because compression perpendicular to the field does not affect the domain orientations, it is like tension parallel to the field.

The investigation did not extend to the 3-dimensional case as the errors introduced by the assumptions made became unmanageable. A number of other factors also limited most of the work to an "ideal case", however two important points were covered in the theory which were in good agreement with experimental results. These being:

1) tension parallel to the field has very little effect on flux density, whereas tension perpendicular to the field considerably reduces the flux density; and

2) there is symmetry between parallel tensions and perpendicular compression, and vice versa.

A later work [49] dealt with magnetic properties of mild steel under conditions of biaxial stress and thus is even more relevant here.

The results presented show that for uniaxial stresses with stress and magnetisation parallel to each other tension had little effect on the peak flux density B but that compression reduced B considerably. The coercive field H_c was slightly increased by compression at the higher applied fields but was slightly decreased by it at the lower applied fields. Tension had very little effect on H_c at any of the applied fields. Compression caused the B-versus-H loops to change from a sigmoid shape to a lentil shape.

For applied equal biaxial stresses the results showed that for B, B_r, and μ_r, compression caused more of a decrease than tension. The effects on H_c were smaller and appeared to be almost identical for tension and compression; the trend was that increasing stress of either sign increased H_c slightly at the higher applied fields but decreased it at the lower fields.

A proposal is then made to explain domain directions for minimum energy for equal biaxial stresses.

Suppose the applied field is zero so that equation (3.28) gives $E_{ms} = 0$. In Figure (3.13a) assume that M_s lies along crystal axes and that closure domains are formed by 90° walls. If uniaxial tensile stress σ_x is applied, domains 1 and 3 have a magnetoelastic energy of $E_{me} = -1.5\lambda_{100}\sigma$. Domains 2 and 4 have $E_{me} = 0$ because $\gamma = 0$. In Figure (3.13b), which shows domains in the z

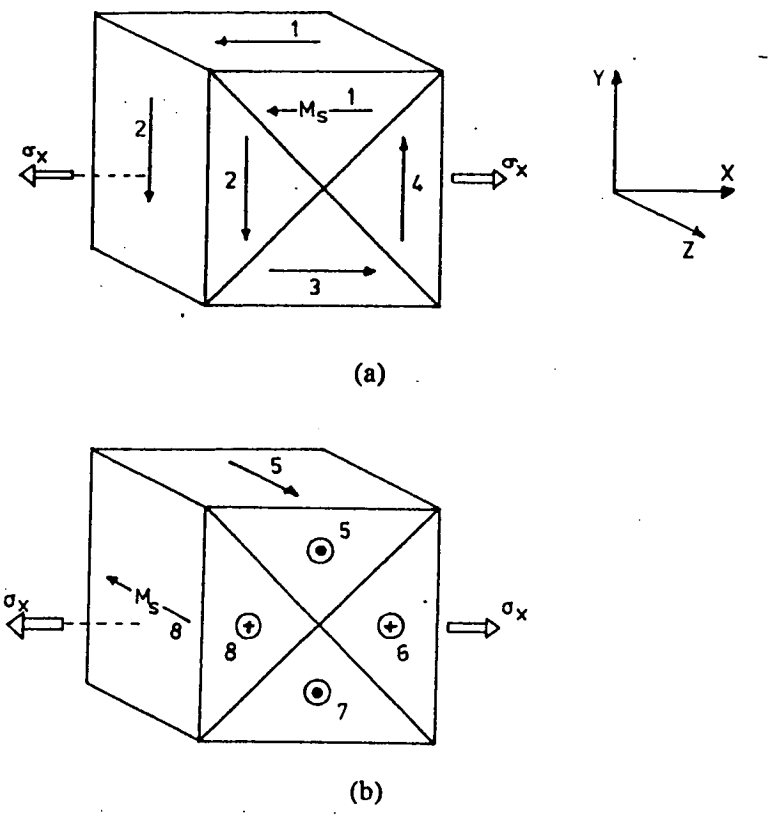

Figure 3.13: Stress and domain directions [49].

direction, $E_{me} = 0$ for all domains. Thus, in an attempt to make the total E_{me} as small (negative) as possible, domains 1 and 3 will grow at the expense of the others. On the other hand, if the stress is only along the y axis, domains 2 and 4 will grow.

If we now have equal biaxial tensile stresses $\sigma_x = \sigma_y$, $E_{me} = -1.5\lambda_{100}\sigma$ for domains 5, 6, 7, and 8. Thus domains 1-4 are favoured (equally) by equal tensile stresses, and domains 5-8 are not. If the stresses σ_x and σ_y are equal and compressive, $E_{me} = 1.5|\sigma|\lambda_{100}$ for domains 1-4 and zero for domains 5-8. Thus the latter domains give a lower energy and are favoured.

With reference to the cruciform specimen of steel used for the B-versus-H measurements, the z direction is perpendicular to the surface. The domain directions of Figure (3.13b) will be favoured by biaxial compression in the plane of the steel, provided adequate closure domains can form at the ends, as in Figure (3.13 a). Any domains in the z direction will have to be switched (by the applied field) to the x direction before any increase in the bulk magnetisation in the x direction occurs. This will in general require more energy than if the domains were already in the x and y directions (as a result of biaxial tension). Thus lower permeability would be expected.

This argument ignores wall energies (these are relatively low compared with E_{me} and E_{ms}), but on a qualitative level it does suggest a reason why the steel magnetises rather more easily for biaxial tension than for biaxial compression.

A sample of some of the biaxial-stress results obtained by Langman are shown in Figures (3.14), (3.15), and (3.16). As can be seen, the changes induced in the sizes and shapes of the hysteresis loops are very dramatic at these applied fields and stresses. It can also be seen that the effects of compression parallel to the applied field is very similar to tension perpendicular to the field (with appropriate scaling due to the different strain effects). The maximum applied fields are quite low in these results compared to those used in this thesis, but the general effects of stress are essentially the same as those obtained by Langman.

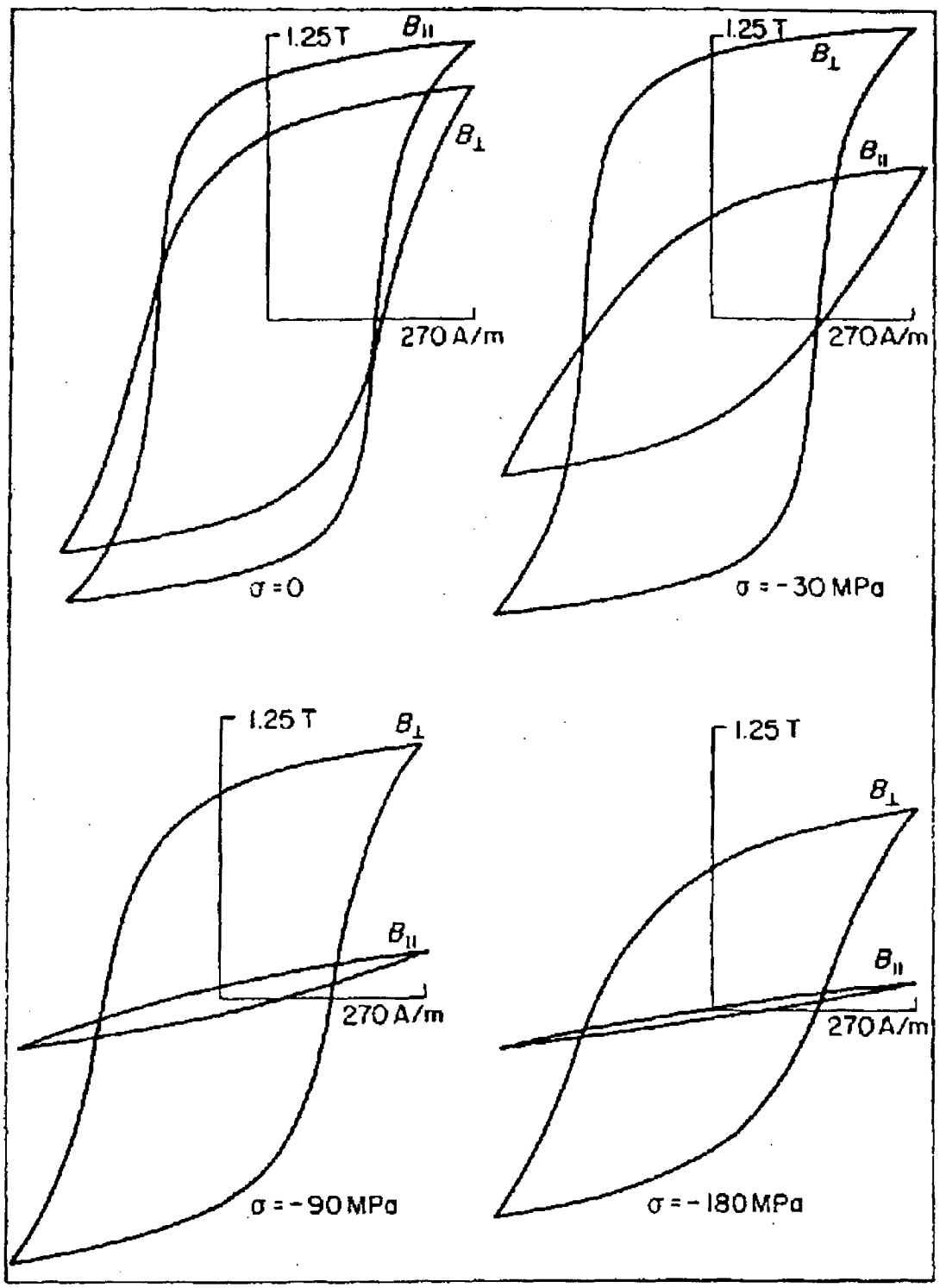

Figure 3.14: Bvs$H$ loops for annealed mild steel, in compression. $B_{||}$ is loop measured parallel to stress, $B_{\perp}$ is loop measured normal to stress [46].

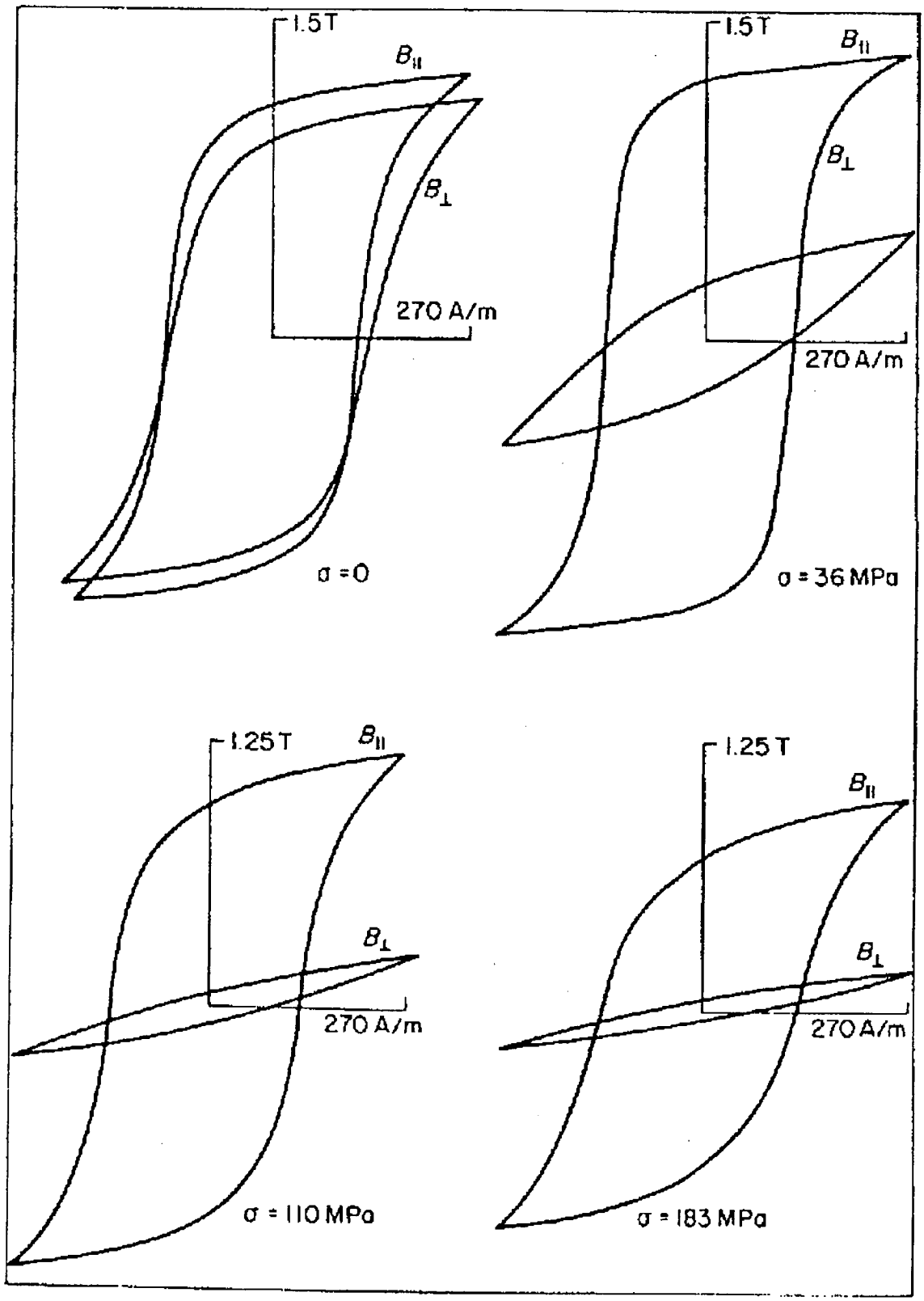

Figure 3.15: Bvs$H$ loops for annealed mild steel, in tension. $B_{||}$ is loop measured parallel to stress, $B_{\perp}$ is loop measured normal to stress [46].

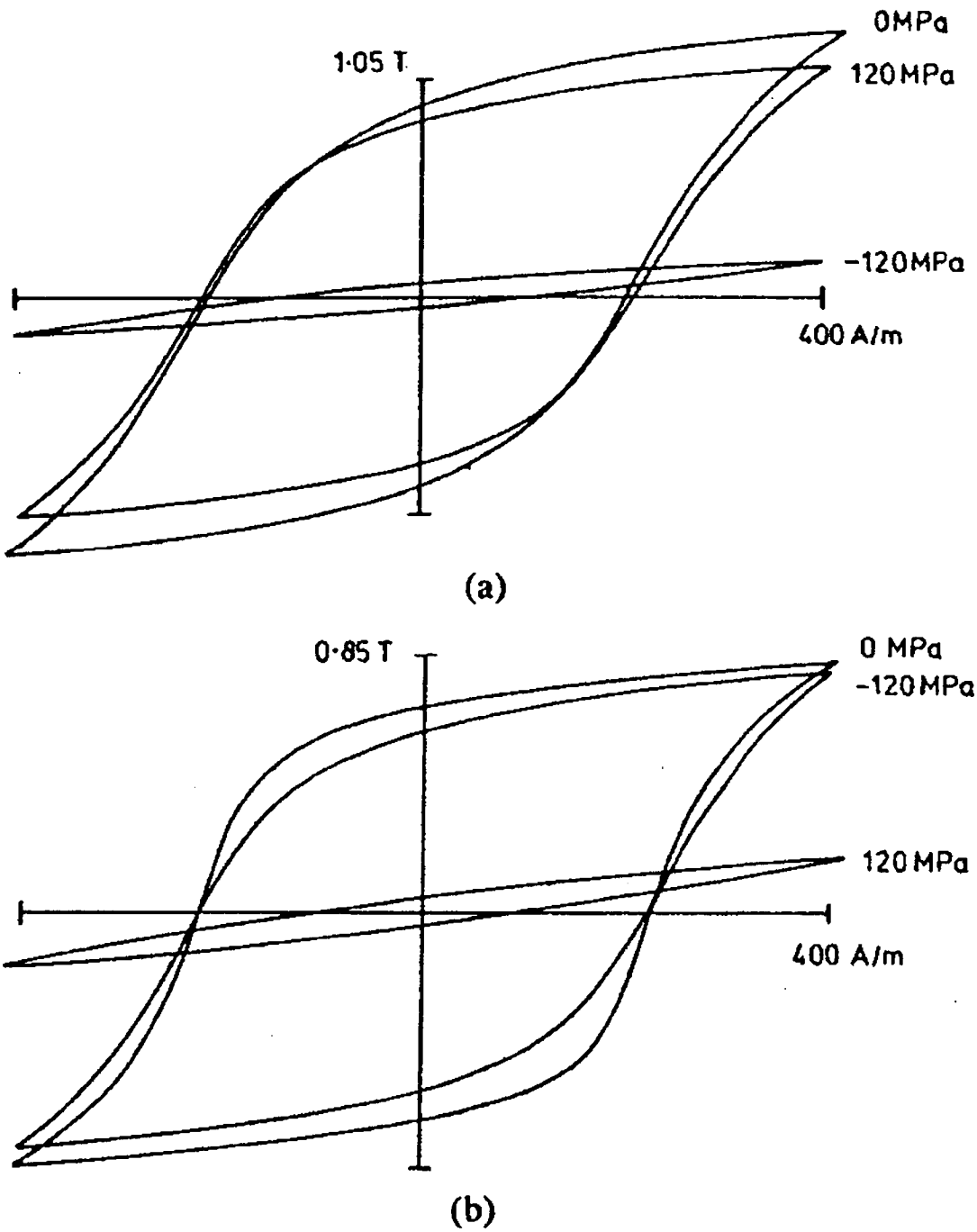

Figure 3.16: Sample hysteresis loops for for mild steel. Stress was held constant while the field was cycled. $B_{||}$ is flux density for field parallel to stress. $B_{\perp}$ is for field perpendicular to stress. (a) $B_{||}$, (b) $B_{\perp}$ [47].

3.9 Robertson

One of the priciple researchers in the field of magnetisation and stress effects in naval applications is Robertson [56] [57] [58] whose work has also directly affected the development of the Collis Class submarine. In his 1990 paper "A review of investigations of the magnetisation of steel due to the application of stress" [56] a thorough treatment of the concept is presented. Emphasis is placed on experimental results and theoretical models are not considered in any detail.

The work begins with a clear and extensive definition of terms and symbols used, and then presents an introduction to simple magnetic processes. Methods of determining the anhysteretic curve are briefly considered followed by a short list of *popular* mathematical models which explain simple magnetic processes proposed by Rayleigh [10], Jiles and Atherton [41], and Preisach and Néel [54][51].

The role played by magnetostriction on the interaction of stress and magnetic properties is considered next. Primarily the longitudinal, or Joule, magnetostriction given by

$$\lambda = \frac{d - d_0}{d_0}, \tag{3.32}$$

where d_0 is the initial length of the specimen, is investigated for a number of different ferromagnetic materials under various conditions. Saturation magnetostrictions for most ferromagnetic materials are of the order of 20 x 10^{-6}.

The magnetisation curve of a ferromagnet may be considered in three stages. Initially the dominant magnetisation process is domain wall motion, which is associated with positive magnetostriction for iron and steel. At higher applied fields, near the knee of the initial magnetisation curve, domain rotation becomes the dominant process of magnetisation. This is associated with negative magnetostriction. Finally, at very high fields the magnetisation and the Joule magnetostriction saturate, resulting in a small volume magnetostriction effect. Applied stress may cause large changes in the observed magnetostriction because it also affects domain orientation.

Factors which increase the magnetic hardness of steels tend to reduce λ or

make it more negative. Domain wall motion gives rise to positive λ but rotation causes negative λ. Increasing the magnetic hardness has a greater effect on wall motion than in restricting domain rotation.

A discussion of the physical basis of the interaction between stress and magnetisation is then embarked upon. According to equilibrium thermodynamics, tensile stress applied to a material with positive and steadily increasing magnetostriction increases the magnetisation in the direction of the stress. Compression decreases the magnetisation under the same conditions.

Cycling applied stress tends to move the magnetisation towards the anhysteretic curve in much the same way as field cycling does. Whether the material reaches a point on the anhysteretic due to stress cycling depends on the amplitude of the stress in comparison with the coercivity and the number of cycles applied. Fluctuating stresses and field both assist the motion of domain walls past obstacles in the microstructure.

Experimental results on the effect of stress fluctuations are considered in the remainder of the paper. The parallel effects of field and stress cycling are emphasised. The results of several experimental investigations were replotted to show the effect of stress superimposed on the normal and anhysteretic magnetisation curves for the materials considered. Changes in magnetisation due to processes involving stress fluctuations are considered in terms of reversible and irreversible components.

The experimental results considered were separated into subsections depending on the order and methods of treatment. Demagnetisation followed by application of a steady field, then a steady stress; and demagnetisation followed by the application of a steady stress, then a steady field were considered first. This was an appropriate place to begin as most of the early experimental work was carried out in this manner. In general it was concluded that static tensile applied stress increases the magnetisation in weak H fields but decreases magnetisation in strong fields. Compressive stress may increase or decrease the magnetisation depending on the magnitudes of the stress and the applied field.

A great deal of work is then reviewed in the section dealing with the application of a static field and then cycling the applied stress (the application, then removal of stresses, either tensile or compressive). For materials with positive magnetostriction the process of demagnetisation followed by application of a field and then a static tensile stress causes a continuous increase in magnetisation as stress is increased. Subsequent removal of the stress causes some reduction in magnetisation, but the final state still has much greater magnetisation than that induced by the field alone. The irreversible change is noted to be towards the anhysteretic.

For compressive stresses, the process leads to an initial positive change in B as stress is increased, followed by a negative change at higher stress due to the domination of the reversible component. Removal of the stress returns the magnetisation to a level similar to, but belwo, that caused by the tensile process with the same stress magnitude. For materials with negative magnetostriction, the roles of tension and compression are reversed.

A detailed analysis of the results produced by a number of researchers is included and the reader is referred to the paper [56] for these. In general it was found that the cyclic application of stresses tended to shift the magnetisation towards the anhysteretic; however, there are some circumstances under which this simple rule no longer holds. One must also consider the fact that the application of stress also changes the position of the anhysteretic curve itself. Another important result was the importance of the slope of the magnetostriction curve

$$\Lambda' = \left(\frac{\partial \lambda}{\partial H}\right)_{\sigma}, \tag{3.33}$$

in determining the magnetisation change due to stress cycling. In the case of field cycling the differential permeability is the relevant factor.

Brief mention is made of the few investigations into biaxial effects, and some basic results are reproduced. A simple phenomenological model is presented which summarises to a first order approximation the effects determined in the body of the paper. Finally, some effects of material properties are considered and reults from some of the more *exotic* materials are mentioned.

In the conclusion it was noted that understanding of the magnetomechanical effect at the fundamental level is rather limited. However, from a phenomenological point of view the understanding is sufficient to allow a quantitive prediction of the behaviour of a material to be made, based on knowledge of the magnetostriction curve and basic magnetic properties such as the normal induction curve and major hysteresis loop.

3.10 Jiles and Atherton

As well as the large amount of experimental work which has been done to produce data for analysis, a great deal of very important work has been done theoretically in attempts to formulate hypotheses and create models which explain and predict the effects of applied stress on the magnetisation of real materials.

Possibly the most important advance in the field of ferromagnetics was Jiles and Atherton's development of an equation to describe hysteresis [39] [40] [36]. The equation describes both the initial magnetisation curve and hysteresis loops of ferromagnetic materials, and was derived theoretically based on a mean field approximation. The equation is an adaptation of those produced by Langevin [44], and Weiss [71] where the force which restrains the domain wall motions is provided by the pinning of the walls at defect sites.

The Weiss mean field equation is

$$M = M_s \left[\coth\left(\frac{\mu_0 m(H+\alpha M)}{kT}\right) - \frac{kT}{\mu_0 m(H+\alpha M)} \right], \tag{3.34}$$

where α is a dimensionless term representing the strength of the coupling of the individual magnetic moments of the magnetisation M.

When one considers the pinning of domain walls as a restraining force which inhibits changes in magnetisation the aggregate effect behaves similarly to a frictional force. Let the density of pinning sites be n per unit volume and the average pinning energy per site be E_p. Then the total energy lost against pinning per

unit volume swept out by domain walls will be nE_p, and hence,

$$\frac{dE_{\text{loss}}}{dx} = nE_pA, \tag{3.35}$$

where A is the area of a particular domain wall and x is the distance through which it is moved. The change in magnetisation is proportional to the volume swept out by the moving domain wall, $dM = A \cdot dx$, and therefore,

$$\frac{dE_{\text{loss}}}{dM} = \kappa, \tag{3.36}$$

where κ $(= nE_p)$ is a constant.

Under an applied field H the domain walls are acted upon by a force which tends to move them in such a way that the bulk magnetisation approaches its anhysteretic value. In the absence of pinning this energy is reversible and so

$$\int M dB_e = \int f\left(\frac{M + \lambda H}{a}\right) dB_e, \tag{3.37}$$

where $f(x)$ is the Langevin function and the parameters λ and a are such that, $\lambda/a = \mu_0 m/kT$ and $1/a = \alpha\mu_0 m/kT$ from equation (3.34).

If there is any hysteresis loss then

$$\int f\left(\frac{M + \lambda H}{a}\right) dB_e = \int M \cdot dB_e + \int \kappa dM, \tag{3.38}$$

and differentiating with resepct to B_e gives the basic differential equation of the model

$$M = f\left(\frac{M + \lambda H}{a}\right) - \kappa\frac{dM}{dB_e}. \tag{3.39}$$

Subsequently the theory was expanded to include the magnetomechanical effect [40]. In this work the theory and application of equation (3.39) was dealt with in much greater detail. It was shown that the parameter κ varies with M and H. The exact form of the κ dependence must be determined empirically in each case. In the sample considered it was found that

$$\kappa = \kappa_0\left[1 + \frac{\kappa_1}{\kappa_0}\exp\left(-\frac{H_{\max}}{1500}\right)\right]\left\{1 - \left(\frac{M_{\max}}{M_s}\right)^2\left[1 - \left(\frac{H}{H_{\max}}\right)^2\right]\right\}, \tag{3.40}$$

where $\kappa_0 = 3250$ and $\kappa_1 = 2000$.

It was proposed that the influence of stress on magnetisation may be understood in terms of the dependence of the coefficients a and α from equation (3.39) upon stress and the effect of stress on domain wall pinning.

The determining factor to consider is whether the dominant mechanism behind the change in magnetisation is domain wall motion or not. The effect of an applied stress is to cause some of the domain walls to break away from their pinning sites and consequently they will move in such a way as to cause the magnetisation to approach the anhysteretic value. In the low field region, domain wall motion is the dominant mechanism and under these conditions experimental results have indicated that the change of magnetisation has the same direction independent of the sign of stress. These results are in accordance with the theory which predicts that the application of a stress cycle will cause the magnetisation to move from the initial magnetisation condition towards the anhysteretic curve as this represents the global thermodynamic equilibrium state.

It was concluded that the application of stress causes the pinning energy to vary and in some cases this results in the domain walls breaking away from their pinning sites. When this occurs the walls are subject to the magnetic potential of the ideal crystal and hence move towards the anhysteretic equilibrium until they encounter further defect sites and are pinned again.

A paper published by Jiles in 1995 [37] went even further to provide an explanation of the magnetomechanical effect. Entitled 'Theory of the Magnetomechanical Effect', the work is very comprehensive and the reader is referred to the original text as any abridged review cannot do the paper justice. In short, however, the publication describes a model that explains the apparently disparate range of experimental observations of the magnetomechanical effect. The equations derived in previous works [39], [40] were expanded to include a quantitative description of stress-dependent magnetostriction and anhysteretic magnetisation curves, and the mechanism by which the change in elastic energy supplied to the material causes a reduction in the displacement of the magnetisation from the anhysteretic magnetisation.

The principal equation derived is

$$\frac{dM}{dW} = \frac{1}{\xi}(M_{\text{an}} - M) + c\frac{dM_{\text{an}}}{dW}, \tag{3.41}$$

where W is the elastic energy per unit volume supplied to the material by the changing applied stress given by $W = \sigma^2/(2E)$, where E is the relevant elastic modulus. ξ is a coefficient with dimensions of energy per unit volume, which relates the derivative of irreversible magnetisation with respect to elastic energy to the displacement of the irreversible magnetisation from the anhysteretic magnetisation M_{an}. The coefficient c describes the flexibility of the magnetic domain walls.

Equation (3.41)gives the reduction in the displacement of the magnetisation from the anhysteretic as well as the asymmetry in response to tension or compression, which occurs as a result of the stress dependence of the anhysteretic magnetisation.

3.11 Sablik

A considerable amount of work has also been done by Sablik and others (including Jiles) [6] [61] [40] to extend the scope of the Jiles-Atherton theory to predict stress effects in ferromagnetic hysteresis. In 'Model for the Effect of Tensile and Compressive Stress on Ferromagnetic Hysteresis' [6], three different models are presented and their attributes compared with each other in their successes at modelling observed behavior. The models attained some success, albeit limited, with one model performing better at low fields, and another at higher fields.

Subsequent work by Sablik [61] expanded the models even further to include biaxial stress. A model is considered whereby biaxial stress effects are reduced to an effective net uniaxial stress which is then used in collaboration with the Schneider model [62] [63] to produce theoretical curves for comparison with the experimental data obtained. Data with equal biaxial stresses produced by Langman were also considered in light of the model.

The resulting model, although somewhat limited in scope when compared with the Jiles-Atherton theory, has the advantage of compensating for the Ewing-Villari effect at positive stresses. Basically this means that positive effective stress increases remanence slowly to a Villari maximum while negative effective stress monotonically decreases remanence.

In addition, a biaxial stress-rig and cruciform specimens comparable in concept to those used in this investigation were used, and thus the results of this work are of considerable importance to this review. Sablik's paper also provides an excellent review of investigations, both experimental and theoretical, into the effects of biaxial stress on magnetisation.

3.12 Squire and Pearson

A great deal of research into magnetoelastic effets has been performed by Squire over the last decade. Much of this work has been with amorphous wires and ribbons, and therefore does not lend itself to analogies with the work undertaken in this research. However, very recent work with Pearson and others [52] studying stress effects of magnetisation is comparable and thus warrants consideration.

Study into field and stress dependence of the irreversible magnetisation changes in iron [52] was aimed at extending work done by Pravdin [69], and comparing and contrasting his results and theirs with the Jiles-Atherton theory. Applied stresses were uniaxial on a 99.99% pure iron rod. The results were interpreted in terms of domain wall pressures; considering pressures caused by applied stress, applied field, and wall pinning. The results of this work showed that the maximum change in irreversible magnetisation at low stresses did not occur at the maximum difference between the anhysteretic magnetisation and the initial magnetisation, as predicted by the Jiles-Atherton theory. Rather, at low tensile stresses the peak in ΔM_{irr} is closer to the peak in $(\partial\lambda/dH)$, as suggested by Pravdin.

Further investigations are underway to extend the data available for the analysis to biaxial stresses as well, however, at the time of writing only limited access

to these results was available [35]. The equipment used to obtain this biaxial data is subtley different from that used in this research, and so the specifications are presented here for comparison.

Instead of cruciform specimens, a circular disk with a 40mm diameter is used, and Helmholtz coils replace the twin U-core yoke system. The flux sensing coils which require holes in the sample have been discarded, and in their place a theoretical calculation of the magnetisation is determined using

$$M = \frac{H_{\text{app}} - H_{\text{int}}}{D}, \tag{3.42}$$

where H_{app} is the applied field, H_{int} is the internal field measured by a Hall probe adjacent to the surface of the specimen, and D is the demagnetising factor. A strain gauge attached underneath the sample measures the planar strain components at the centre of the sample, from which the stress components σ_x, σ_y are derived. The stresses were applied using electromagnetic actuators and lever systems.

The author hopes that the results of further investigations using the equipment described above may be compared with those presented in this thesis as each of the different methods have their own benefits and pitfalls.

3.13 Computers

Possibly the greatest advance in the field of experimental magnetics has been the introduction of computer controlled data acquisition and field application, which has allowed vast amounts of very accurate data to be obtained quickly and easily.

One of the first comprehensive systems designed for use with stress and magnetisation experiments is described in [24]. One of the driving factors behind the developement of this system was the drift of the integrating voltmeter, a problem which had plagued magnetics for decades. This problem may be almost completely overcome using computers. A great simplification of the process of demagnetising is also achievable.

The computer controlled both the applied uniaxial stress using a stepper motor, and the magnetic field by the current supplied to the coil of an electromagnet. The flux and field data were still obtained using more traditional methods, i.e., a flux meter, a Hall probe, and a voltmeter, the outputs of which were displayed on an X-Y plotter. The strains were measured by strain gauges in much the same manner as that which was employed in this work (see Chapter 5).

The demagnetisation of the sample was handled in a very precise manner, ensuring that symmetrical loops were attained at each step before reducing the field maximum. The computer control allowed anhysteretic curves, initial magnetisation curves, and hysteresis loops to be obtained. Thus from the shapes of different hysteresis loops and the general equation for hysteresis derived by Jiles and Atherton, the stress dependence of the various parameters describing hysteresis were found.

The effects of applying a stress cycle of predetermined amplitude to the sample at different points around a hysteresis loop was also investigated. It was found that the general principle governing these changes was that when a stress of either sign (i.e., compression or tension) was applied to a ferromagnetic steel sample in an applied field H, the magnetisation always changed in such a way that it approached the anhysteretic magnetisation at the given field strength.

This paper was published in 1984 and in the intervening years the advancements made in computing and software power and flexibility has, of course, been phenomenal. Today it would be almost unthinkable to attempt data acquisition of this nature without the aid of a computer and associated hardware. However, the origins of these methods is as important to present investigations as the past work on developing theory and research methods.

Chapter 4

Acquiring the Data

4.1 Data Presentation

For every method of obtaining magnetic data there is a multitude of different ways of presenting it. A decision had to be made as to which methods of obtaining magnetic-stress data would be employed, and subsequently which methods of presenting said data would be used. The traditional forms of magnetics data presentation are the hysteresis loop and the normal magnetisation curve. More complex methods like the anhysteretic curve take much longer to obtain and require very good equipment to maintain accuracy. The research being performed for the Defence Science and Technology Organisation required the production of normal magnetisation curves, so equipment was designed to produce the simple normal curves and hysteresis loops. These methods are also possibly the easiest to interpret as they are so familiar.

For accurate data at low fields (< 100 A/m) an appropriate demagnetising process was also required for the 6–8mm thick samples which were being used in the research. The best test of a demagnetising method is to take positive and negative inital curves, each after demagnetising, and comparing their absolute values. If the curves are the same, the demagnetising technique works. During the investigation of the natures of the normal magnetising curve and the initial magnetising curve, however, certain discrepancies were noticed.

The precise nature of the relationship between the normal and initial induction curves has been plagued by a degree of uncertainty in magnetics texts for over 100 years. There is a general, although certainly not unanimous acceptance that the curves produced by each of the methods are concurrent. However, there seems to be little discussion as to whether this is an obvious and natural conclusion, or sheer coincidence. [10] [68]

It seems somewhat incongruous that in magnetics a data set may be obtained by two fundamentally different methods when the magnetic history of a sample is so critical to determining the flux density produced by an applied field. It is very unlikely that the evolution of the domain structure of a ferromagnetic material experiencing the cyclicly applied fields of the normal method would bear any resemblance to that experienced by the same material in a simple, increasing uni-polar field. Yet the most authoritative texts in the field equate the two with little or no explanation [10].

4.2 The Initial and Normal Curves

In his book 'Introduction to Magnetic Materials' [23], Cullity states quite unambiguously "The curve of B vs H from the demagnetized state to saturation is called the initial, virgin, or normal induction curve." This emphatic statement over simplifies the complexities of the curves as the different titles do indeed infer subtle yet important differences in the means by which the curves are obtained. Bozorth is far more specific about the terms in his book 'Ferromagnetism' [10]. Quoting directly from chapter one; "The normal permeability, often referred to simply as the permeability, is $\mu = B/H$, measured when the specimen is in the 'cyclic magnetic state'. Under these conditions the material responds equally when the field is applied in either of the two opposite directions. Before such a measurement the specimen is ordinarily demagnetized by applying an alternating field with amplitude high enough to cause the induction to approach saturation, then slowly reducing the amplitude to zero. The material may be demagnetized

also by heating the material above the Curie point and cooling in zero field; in this case the magnetization curve is referred to as the "virgin" curve. In either case the curve represents the values of B (or $B - H$ or I) and H measured as H is increased from zero, or it is (preferably) the locus of the tips of hysteresis loops taken with increasing amplitudes of H, the field having been reversed several times at each amplitude."

An even more detailed comparison is given by Golding in 'Electrical Measurements and Measuring Instruments' [28]. He refers to the production of the normal curve as the "Method of Reversals" and the initial curve by the "Step-by-Step Method". In the descriptions he goes into great detail of the appropriate use of a ballistic galvanometer and stresses that in order to achieve a "reproducible cyclic magnetic state" the applied field must be reversed at least twenty times. In the Step-by-Step method the corresponding B value for each applied H is found as the sum of all previous galvanometer throws. It is stressed that with this method care must be taken when switching between the tappings on the potential divider to increase the field, as errors in B will be cumulative. No definite indication is given as to whether either of the methods provides superior results; however, he implies that the Method of Reversals is the more commonly used.

Another detailed description of the two methods is given by Ewing in 'Magnetic Induction in Iron and Other Metals' [25]. The procedures outlined appear to be very similar but there are a number of critical differences in the techniques described by Ewing to those described by Golding. Quoting from Ewing: "To test the permeability and to determine the form of the magnetisation curve, one or other of two plans may be followed: (1) By Steps. A weak current may be applied and the throw noted, then the resistance at B_1 may be suddenly reduced, and the additional throw noted, and so on, each throw measuring the magnetic effect of a sudden increase in the magnetising current. The whole magnetism acquired at any stage is then to be estimated by summing up the throws. The same process evidently allows us to trace the individual and cumulative effects of successive diminutions in the strength of the magnetising current, and thus to trace the

magnetisation curve throughout any step-by-step process of applying, removing, or reversing magnetising force. This is its advantage: on the other hand, it has the practical drawback that if an error happens to be made in measuring the throw at any step it is carried forward and effects all the subsequent values of the magnetisation. (2) By Reversals. Another plan is to suddenly reverse the current in the primary coil. Half the throw is then taken as measuring the actual magnetisation. Breaking the current also allows the permanent magnetism to be calculated by showing the amount that disappears in the withdrawal of the magnetic force. As to the effect of each reversal, care must be taken that the currents are progressively increased, and even then the assumption that half of that effect measures the total magnetism is not quite accurate, especially in the case of hard iron or steel, which is less ready to be magnetised by a force of one sign after a force of the opposite sign has been applied than if the opposite force had not acted. In soft iron the curve of magnetisation as determined by this process of reversals is not materially different from the curve determined by the process of steps."

The Step-by-Step method outlined is essentially the same, however, the Reversals method differs markedly for it does not mention the "reproducible cyclic magnetic state", which Golding so emphasised, at all. On the contrary, Ewing warns that the very act of cycling the field positive to negative is in itself a possibe source of errors. It is arguable that Ewing's Reversals method does not actually produce a normal induction curve. The American Society for Testing Materials standard A340 [1] defines normal induction as "B- the maximum induction, in a magnetic material that is in a symmetrically cyclically magnetized condition." The normal induction curve is defined as "a curve of a previously demagnetized specimen depicting the relation between normal induction and corresponding ascending values of magnetic field strength. This curve starts at the origin of the B and H axes."

A very comprehensive study of the Reversals method, and of demagnetising, was reported by Burrows [15]. His conclusions for both are important and still

Table 4.1: A sample of Burrows' results

H=	1	3	4	5	7	10
1st reversal	190	1900	4200	6800	9980	12460
B_{max}	192	2010	4300	6930	10080	12520
cycles for max. B	4	7	8	9	9	5
B_{final}*	190	1930	4150	6790	9990	12470
$B_{max} - B_{final}$	2	80	150	140	90	50
$\frac{B_{max}-B_{final}}{B_{final}}$	0.01	0.04	0.04	0.02	0.01	0.00

relevant. In fact, it would seem that his careful measurements, although done before 1907, are the basis for most subsequent discussions and "recipes" for the success of the Reversals method and for correct demagnetising. Burrows' method was to apply successive reversals of the same magnetising current to the specimen, and to measure the change in flux density for each reversal. He did this for several different field strengths, and for four materials (transformer iron, low carbon steel, high carbon steel, and an iron ring - compositions of the materials were not stated). Table (4.1) shows his results for low carbon steel. Units of B are gauss and units of H are oersted.

B_{final} is the value after 600 cycles are completed, and cycles for max. B is the number of cycles completed at the point where the largest B value (B_{max}) was recorded. Similar effects occured for the other materials tested. In general, the largest percentage difference between B_{max} and B_{final} is around the steepest part of the Bvs.H curve. Burrows concludes "No marked difference in the manner in which the various specimens approach the cyclic state can be noticed. Any irregularities that occur in the curve indicating the manner of approach are found during the first few cycles, and are due probably to a small residual polarisation which is large enough to modify the first reversal but is soon wiped out by continued reversals. Such irregularities might be expected in accordance with the theory of molecular magnets. In view of the proceeding experiments it seems quite proper to fix the final maximum value of the apparent induction as the *definition* of the true normal induction. The initial and maximum values are

rejected because of their uncertainty and the fact that they can not be verified by repetition without another demagnetisation."

These results show that the SCM condition is not exactly reached until after several hundreds of reversals, which is at odds with the usual "recipe" that a few reversals (up to twenty) are sufficient. Of course, it is important to keep the size of the change in induction with the number of reversals in perspective: it is only between zero and 3 %, whereas the errors to be expected with "precision" permeameter measurements are $\pm 1\%$ in B and $\pm 3\%$ in H [1].

Burrows' contribution to the art of demagnetising is also significant.[a] Important concepts presented by Burrows are the upper and lower limits of the demagnetising force.

(i) Upper limit of demagnetising force.

"It is well at the outset to determine something of the nature of the polarisation (remanent flux density) effects which are to be removed by the process of demagnetisation. To this end several specimens of iron were examined after having been exposed to different magnetic treatments. The iron was first demagnetised as well as might be and its apparent induction determined for a series of values of the magnetising force. Then the iron was subjected to a strong magnetising force of 100 units (gauss) after which the induction was redetermined. This polarising force was applied and removed several times, but it was not reversed in this first comparison." The results of this experiment for low carbon steel are shown in Figure (4.1). Figure (4.1) shows that there is some difference between the induction curve (a), which is obtained by reversals after correct demagnetising, and curve (b), which had the 100 oersted (polarising) field applied before the reversals. The difference is shown by curve (c), to a B scale magnified 10 times.

When the applied field was greater than 10 oersted, there was no difference, i.e. the polarisation effect does not influence the results. Burrows called this 10

[a]Some of these measurements are reported by Spooner [66], whose book may be more readily available than Burrows' paper [15].

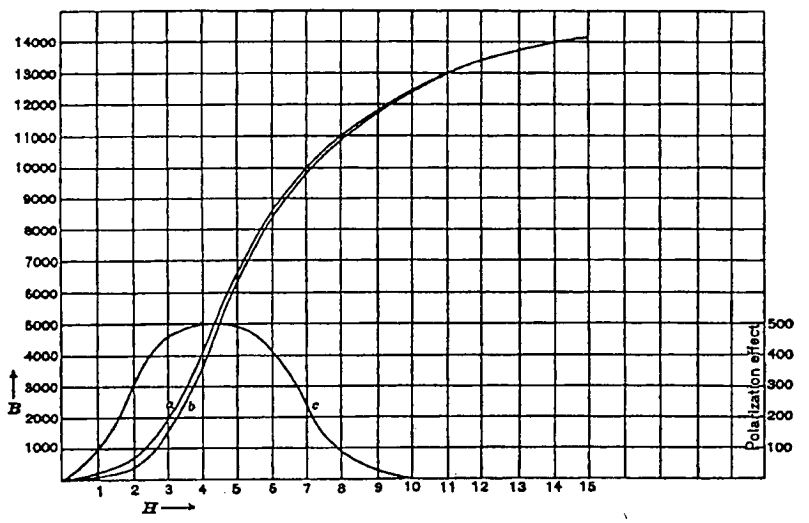

Figure 4.1: Burrows' results showing characteristics of low carbon steel[15].

oersted the critical demagnetising force for the low carbon steel (force ≡ field). The other materials showed similar overall effects for different critical demagnetising forces.

(ii) Lower limit of demagnetising force.

The low carbon steel was polarised initially as before. Then the demagnetising was carried out from a point well above the critical demagnetising force down to a certain minimum value. Finally, the cyclic apparent induction (i.e. by reversals) was measured for a particular applied field. These operations were repeated modifying only the final minimum value of the demagnetising force. The ranges of applied force can be seen in the first row of Table (4.2), for example the demagnetising forces corresponding to $H = 1$ were 15–0.2 oersted, then 15–2.5 oersted, then 15–5 oersted. The whole operation was then repeated for a higher value of field for the reversals (second row in the table), and so on. The B values for the 15 to 0.2 oersted limits are for the correct demagnetising. Burrows summarises his measurements on all four materials in the following paragraph.

"If the demagnetisation is carried from the critical demagnetising force down to a certain point, the demagnetisation is complete for all values above the final demagnetising force. For magnetising forces below this final value of demagnet-

Table 4.2: Showing the apparent induction of low carbon steel as influenced by the lower limit of the demagnetising force.

Limits of demagnetising force	15-0.2	15-2.5	15-3	15-5	No demag-netisation
Time interval	75	73	167	156	
Number of cycles	83	80	200	180	
H	*B*	*B*	*B*	*B*	*B*
1	190	185	175	152	90
2	680	680	668	566	370
3	1930	1930	1930	1795	1460
4	4150	4150	4150	4150	3470
5	6790	6790	6790	6790	6300
6	9140	9140	9140	9140	8670
7	9990	9990	9990	9990	9740
8	11070	11070	11070	11070	10950
9	11880	11880	11880	11880	11820
10	12470	12470	12470	12470	12460
15	14170	14170	14170	14170	14170

isation the demagnetisation is incomplete, and the incompleteness is greater the greater the interval between the final demagnetising force and the magnetising force used to produce the induction desired."

Burrows next dealt with the frequency of demagnetisation reversals, looking at the effectiveness of demagnetising frequencies from 900 Hz down to 1 Hz. He concluded that a frequency of 1 cycle per second was acceptably low enough to avoid imperfect demagnetisation due to eddy currents. Linked to this was a study of the rate of decrease of demagnetising force. It turned out that about 100 reversals, such that the incremental decrease in induction each reversal was constant, achieved the best demagnetisation. Note that unequal steps of decrease of magnetising force are needed to give equal steps in the decrease of induction.

Burrows summarises his findings thus. "In view of evidence offered in the preceding pages the following rule may be outlined as the best (ballistic) method of procedure in magnetic testing:

The magnetic system, consisting of the test pieces and the connecting yokes, should be mounted with its plane perpendicular to the earth's field. If necessary

the system should be protected from mechanical vibrations by means of a pad of felt, or something equivalent. If an accuracy of 1 per cent in the steep part of the B-H curve is desired the temperature should be kept at some standard temperature (e.g., 20° C.) constant to 1° or 2° C. It is not feasible to apply a temperature coefficient correction on account of the difficulty in getting its value."

"The demagnetisation should be accomplished by a current reversal at the rate of approximately one cycle per second, while gradually diminished in such a way that the rate of decrease of the induction is as nearly as may be uniform. An ammeter in circuit and a rough estimate of the shape of the $B-H$ curve will enable one to regulate the rate of decrease of current with sufficient exactness. The initial demagnetising current should be sufficient to carry the induction beyond the knee of the B-H curve, and the final current should be not greater than the smallest magnetising current to be used.

The full demagnetisation may be accomplished in about ninety seconds.

Now apply the lowest magnetising force desired and reverse at the same speed as in the demagnetising. At intervals get a ballistic deflection. Continue this until two deflections about twenty-five reversals apart show only a negligible difference (several hundred reversals may be required in the steep part of the B-H curve, while half a dozen are sufficient in the upper portions). This final deflection is the normal induction.

Without demagnetising again, apply the next larger magnetising force and reverse as before. Continue in this way till all the required points on the curve have been obtained."

Section 8-procedure, of ASTM standard A341 [1], is obviously close to what Burrows recommends. [16]

Turning to the two best known models of hysteresis, (namely the Rayleigh equations and the more general Jiles and Atherton equations) for help only shows that Initial $\equiv$ Normal. This is inherent to the models. Both models predict the shape of the B vs H curve starting from the origin (i.e. the demagnetised state with $B = H = 0$) to some values ($H'B'$). If H is reversed to $-H'$, the models

Table 4.3: Cross-Sections of Samples

Specimen	Cross-Section
Mild Steel	40.1mm x 6.0mm
Silicon-Iron	30.0mm x 13.0mm
Alloy Steel D36	29.2mm x 3.3mm

predict the corresponding flux density to be $-B'$. Of course the shape of the curve from $(H'B')$ to $(-H' - B')$ differs from the initial curve.

4.3 Experimental Work

Field and flux density data was obtained using the hardware described in Chapter 5. The Normal and Initial curves presented here for mild steel and alloy steel (D36) were obtained from rectangular cross-section bar samples in the laminated silicon-iron permeameter. The curves for silicon-iron were taken from a laminated ring with rectangular cross-section which was uniformly wrapped with toroidal solenoids acting as the magnetising and search coils. The field was measured as a direct function of the current in the magnetising coil. The cross-sections of the specimens tested are shown in Table 4.3.

4.4 Demagnetising

The first step in obtaining magnetic data of this type is to precisely demagnetise the sample under investigation. It is generally accepted that ferromagnetic materials may be demagnetised by subjecting them to a series of reversals of a diminishing field. It must be stressed however, that details of this procedure are critical if it is to be successful. The crucial factors are: the initial field maximum, the frequency at which the field strength is cycled, and the size of the decrement of the maximum field value used each cycle.

It was found that although these topics had been considered in a number of

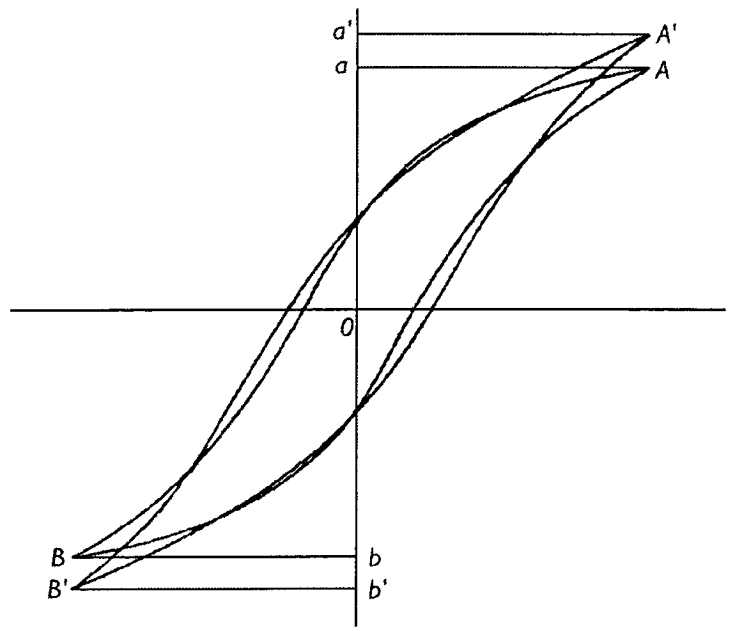

Figure 4.2: Burrows' ideal curve to illustrate the effect of magnetic viscosity on the apparent induction[15].

the papers reviewed in Section 4.2, they needed to be determined in relation to each other *for every particular specimen* as both the composition and the form of the sample affected their values. The initial field maximum which produced the best results was found to be just above the knee (as proposed by Burrows). The optimal cycling frequency was determined by the cross-sectional area and composition of the sample, as eddy currents were found to play a major role in enabling or preventing accurate demagnetising.

Burrows states that a demagnetising frequency of 1 Hz, together with starting at an appropriately high value of field, will be adequate to demagnetise a steel bar. However, he also mentions the phenomenon of magnetic viscosity ([15] pg 261). Referring to Figure (4.2), "Suppose the iron has been subjected to forces of $+H$ and $-H$ alternately at the rate of one reversal per second. Then it will trace a hysteresis loop having its vertices at two symmetrical points as A and B. If, however, the reversals are interrupted when the iron is at point A, the steady

application of the force will cause the induction to creep from A to A'. After this creeping has ceased a reversal of the magnetising force will bring the state point down to B. A further pause will again show a creeping from B to B', which is symmetric with A'. In some of the irons measured it has amounted to as much as 1%"

This can be explained by our measurements. A steel ring with a cross-sectional diameter of 20mm and a major diameter of 150mm was magnetised with a triangular waveform magnetising current of frequency 0.1 Hz. Figure (4.3) shows the magnetising current waveform and the waveform of the voltage induced in the flux coil. The shaded portion is where the magnetising voltage starts to change slope, but the flux voltage is of the same sign. This lasted approximately 0.2-0.4 seconds. The BH loop which resulted from this continuous cycling of magnetising current is shown in Figure (4.4). We propose that the B values corresponding to a, a', b, and b' coincide in Figures (4.2) and (4.4). When a round steel bar is magnetised by a solenoid coil, the flux in the bar when there is alternating current in the coil is less than the flux would be were there direct current, due to eddy currents that are induced in the bar by the AC. The ratio of flux for AC to that for DC is given by [45]

$$\frac{\Phi_{ac}}{\Phi_{dc}} = 1 - 0.0208(a/d)^4, \tag{4.1}$$

for values of a/d not substantially greater than 3. In this equation a is the radius of the bar, d is depth of penetration; defined by $d = \sqrt{\rho/\mu\omega}$, where $\rho =$ electrical resistivity, $\mu =$ magnetic permeability, and $\omega =$ angular frequency of magnetising current. The permeability will of course depend on the flux density, and so this is an approximation, but the formula will provide values of the order of magnitude of the decrease in flux to be expected. This equation was used to calculate appropriate cycling rates for demagnetising and producing results.

For the steel ring considered earlier, $a = 10$mm and $d = 7$mm at 0.1 Hz. The magnetising waveform used was triangular, whereas the formula is for a sinusoidal waveform, but the error is negligible. Thus $\Phi_{ac}/\Phi_{dc} = 0.91$, or a 9% decrease. At a frequency of 0.05 Hz, $a/d = 1.0$, and there would only be 2% less flux in the ring.

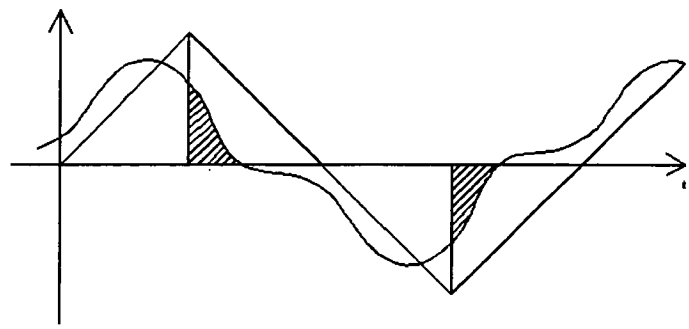

Figure 4.3: Schematic waveforms of the magnetising current (triangular) and the voltage induced in the flux coil.

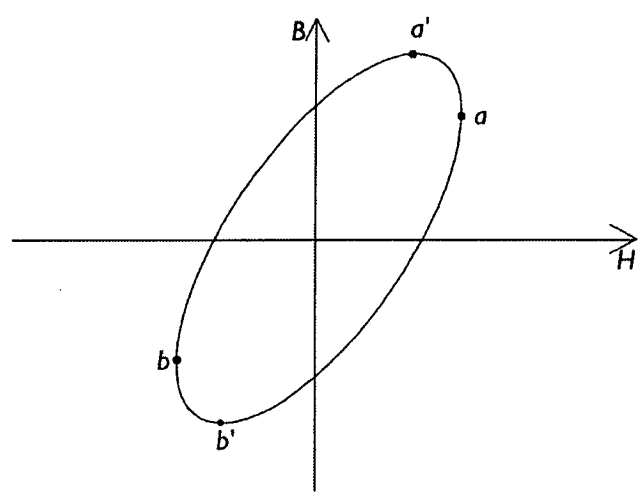

Figure 4.4: Schematic of a BH loop showing the effects of eddy currents on the measured flux density.

The BH loop for 0.1 Hz is shown in Figure (4.2). Burrows worked with a low carbon steel rod with a diameter of 0.578 inches, resistivity of $13.4\text{x}10^{-8}\Omega m^{-1}$ and maximum permeability of 1800. At the frequency he was working, 1Hz, the depth of penetration was $d = 3\text{mm}$. Thus $a/d = 2.44$, and $\Phi_{ac}/\Phi_{dc} = 0.26$, therefore there is a strong likelihood that the steel would not be correctly demagnetised, and that the creeping of B over time from point A to A' is a result of the eddy currents dying out during the pause interval. The actual situation is of course more involved than shown here, but the numbers presented are correct to within a few tens of percent, and would explain the magnetic viscosity or creep effects that he reported.

Another effect of eddy currents in the specimen on the shape of the BH loop was discussed by Snoek [65]. In this case he considers that the transient eddy currents initially prevent the full demagnetising effect occuring in the finite length specimen, and so the B value was actually *larger* than the final value, the opposite of what occurs in the cases we are considering.

The optimal increment for reducing the maximum field each cycle was found to be approximately 1% of the initial maximum, i.e. 100 cycles to reduce to zero, in agreement with Burrows [15]. However, the rate of cycling used was 0.05Hz, substantially lower than the 1Hz recommended by Burrows. To ensure that eddy currents were not a problem a "clipped" triangular waveform was used, where the field was "paused" for 2 seconds at the apex of each ramp. This method was used to demagnetise the specimens on each occasion prior to the data sets presented here being obtained. This is discussed in greater detail in Chapter 6.

4.4.1 The U-cores

In a long rod or large flat plate a U-core arrangement will, when used to demagnetise a region, only demagnetise the area between the two contact regions (or poles). This is because the flux is directed along the shortest route between the poles, it will spread out to fill a slightly larger area than exactly that which is between the poles to minimise energy conditions but will be basically restricted

to a smallish area.

In a set up like the Belle-Wrigley rig however the situation is different. Due to the rig design and the fact it is made primarily from mild steel there are now two independent paths from one pole to the other, one being the short route across the middle of the sample, the other being via the rig itself and the outer regions of the cruciform sample. The flux density through this path will naturally be less than that directly between the poles of the U-cores but flux will nevertheless flow through these areas. A partial demagnetisation of the outer sections of the cruciform and the rig will result.

The ultimate test of whether any remanant magnetisation in these areas has any effect on the magnetisation of the central region of the cruciform is the initial curve test. If the sample is run through a demagnetisation process as described and a positive initial magnetisation curve obtained, then the sample demagnetised again and a negative initial magnetisation curve obtained, the two curves will only coincide exactly if the region being considered (i.e. the center of the cruciform) is perfectly demagnetised. Any magnetisation of the other materials in contact with the sample or other areas of the sample itself, is either zero or not affecting the central region or the two curves would not coincide.

The flux density in the rig and outer arms would not reach sufficient values to completely demagnetise them, but the process is enough to remove any magnetisation which is large enough to affect the data obtained from the center of the cruciform.

4.5 Obtaining the curves

Normal and Initial curves were obtained from three different specimens for comparison. The materials chosen were: a mild steel bar; an alloy steel bar (D36); and a laminated silicon-iron ring. In the production of the Normal curves a clipped triangular waveform was once again employed to magnetise the samples with the field pausing for 2 seconds at the end of each ramp before continuing.

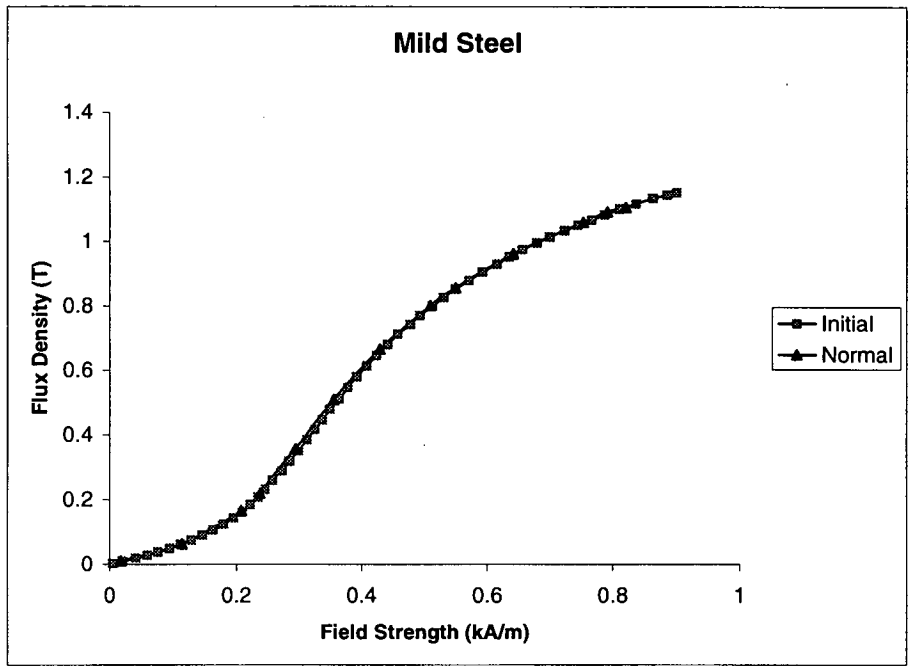

Figure 4.5: Normal and Initial curves for Mild Steel.

The Normal curves were the mean of the curves produced by the positive loop tips, and the absolute values of the negative loop tips. The Initial curves were obtained with a single ramp at a cycling frequency of 0.01Hz, and were the mean curves of the positive field Initial curve, and the absolute values of the negative field Initial curve (see Chapter 7). The curves obtained are shown in Figures (4.5), (4.6), and (4.7).

Conventional wisdom dictates that the flux density reached upon the first application of a particular field is not the "true" value [59], [15]. Thus to obtain a Normal magnetisation curve the field must be reversed or cycled several times about each field value before the corresponding flux density values are recorded. However, with the methods of applying fields used during this investigation, this cycling was found to be redundant. Therefore the Normal curves presented here were obtained from a waveform with a peak value which was increased every half cycle. As a result of this there was no $-H$ point corresponding to any $+H$ point; however, the data points obtained lie on the same curve. The positive curve and

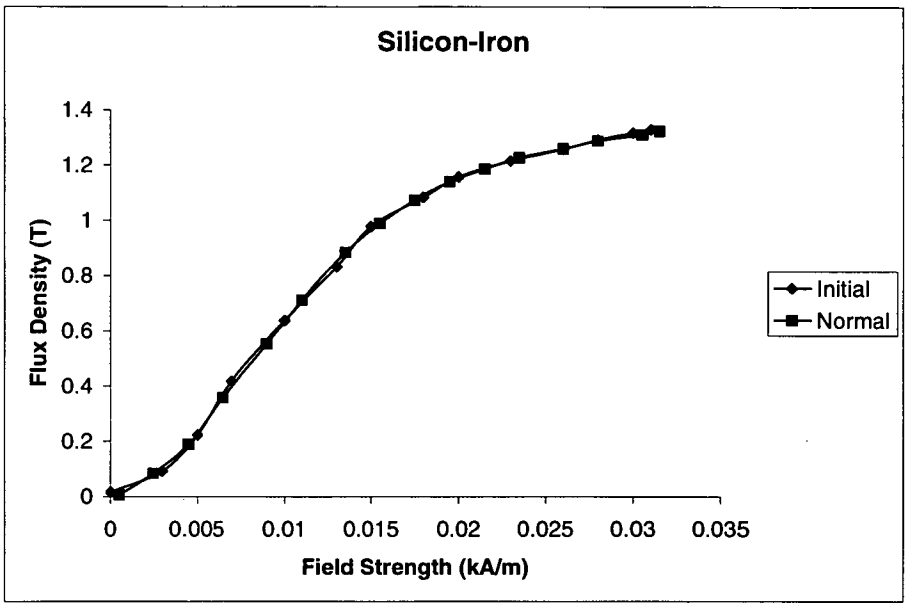

Figure 4.6: Normal and Initial curves for Silicon-Iron.

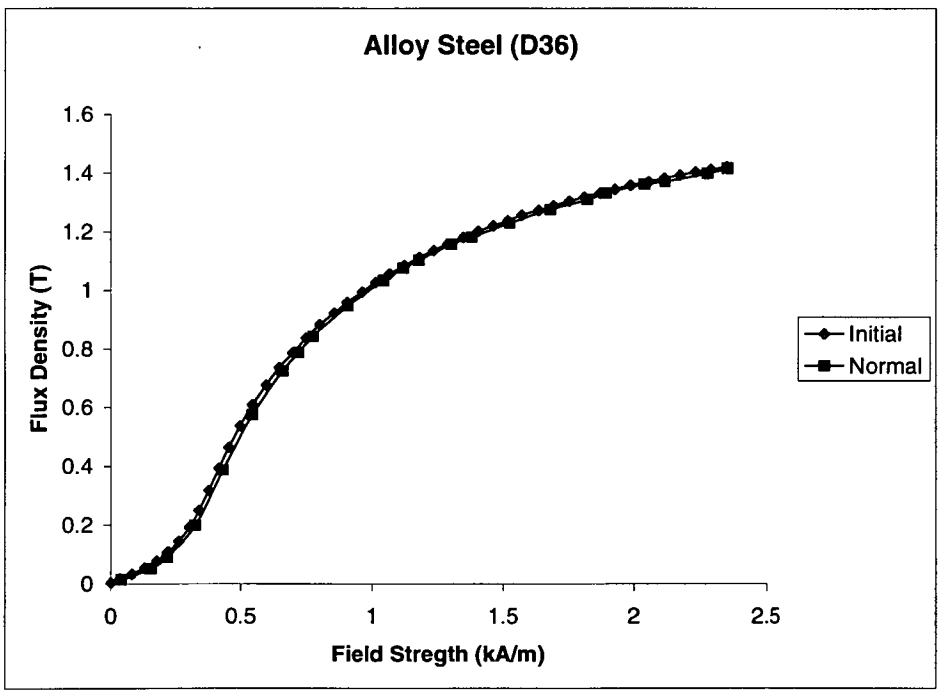

Figure 4.7: Normal and Initial curves for Alloy Steel.

absolute values of the negative curve were averaged in order to compensate for any offsets on the inputs which would cause erroneous results. This was particularly important for the Flux Density values as any offset on the Analogue to Digital input would be integrated, so even small values could greatly alter the results.

4.5.1 Errors

The greatest potential area for errors was the flux density readings due to the integration of the voltage signal. Offsets on the input were accounted for by taking 100 samples at zero flux which were then averaged to give a baseline value which was then subtracted from subsequent data obtained from that channel during that sampling sequence. However, the resolution of the PC30 boards is only 5 millivolts. The maximum error this is capable of producing over a 25 second sampling cycle is 1.8 % of the maximum flux density.

The next most significant source of errors is from anomalous voltage spikes produced in the electrically noisy environment. These however, were of very short duration, and therefore amounted to less than 0.01 % error. Thus the total error for the results presented here is 1.8 % of the maximum flux density.

4.6 Comparing the methods

The graphs presented show very clearly that the curves produced by the Normal and Initial methods are concurrent when produced under the appropriate conditions. The maximum separation of the Normal and Initial curves in the reults shown is $\pm 1.2\%$. This in itself does not seem such a controversial outcome; however, the ramifications of this are greater than may at first be apparent. The result implies that the flux density reached upon the first application of a given field strength is in fact the true flux density to be associated with this field. This implies that the concept of a "reproducible cyclic magnetic state" becomes superfluous, because the specimen reaches such a state on the initial application of the field. Reversing the field "several times" (anywhere between 3 and 100

times depending on the reference) would appear to be unnecessary if the field is correctly applied.

Chapter 5

Hardware

5.1 The Cube

In order to take very low field readings it is necesary to create an environment to work in which has zero net field. This requires the exclusion of the local geomagnetic field from a volume large enough to contain the sample under investigation, and any equipment to which it is physically connected. Due to the size of the Belle-Wrigley rig the volume required was approximately $1m^3$. The zero-field volume was produced by a structure which for obvious reasons was dubbed "The Cube". The cube was a wooden frame of side length 2.4m which was the suport structure for 9 coils of wire which were divided into groups of three and oriented to produce homogeneous fields in the x, y, and z axes.

A 3-coil group was chosen over the more traditional Helmholtz pair as it provided a greater volume of uniform field as well as easier access to the centre of the volume. The configuration of the 3 coil group was optimised using a 2D model created in the finite element analysis software Vector Fields Opera 2D using cylindrical coordinates, and using references [29], [55], [27], [18]. The optimal configuration was attained using a ratio of 1:0.6:1 amp-turns with axial separation of coil centres equal to the radius of the coils. Each coil system was then set up along each of the x, y, and z axes. The central coil of each system was suspended in a hoop of PVC conduit, whereas the outer coils were attached

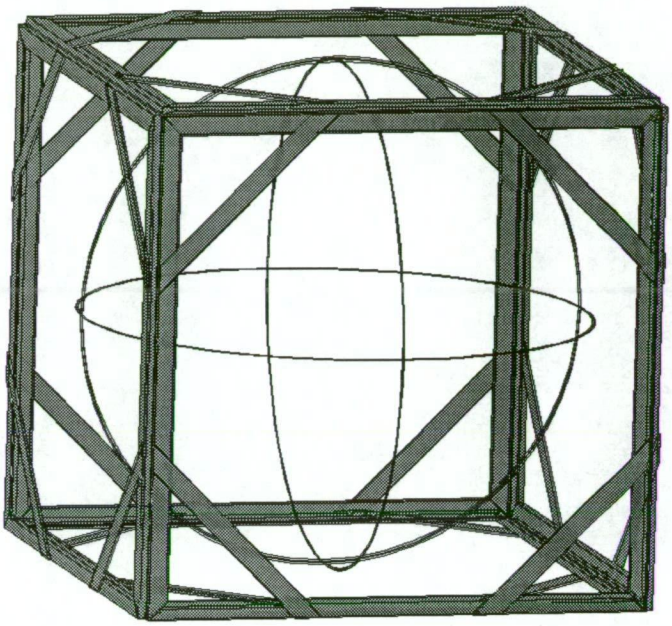

Figure 5.1: The Cube

Table 5.1: Cube Specifications

Axis	Local Geomagnetic Field	No. of Turns	Current
X	8.62 A/m	13; 8; 13	1 amp
Y	10.06 A/m	15; 9; 15	1 amp
Z	40.25 A/m	15; 9; 15	4 amps

to each side of the wooden cube (see Figure (5.1)).

A analysis of the field produced by each coil set is shown in Figure (5.2). As can be seen, the geomagnetic field is excluded to within 1% in a $1m^3$ volume in the centre of the cube.

Due to the location of the research (Hobart, Tasmania) the local geomagnetic field has a declination of approximately 70° from the horizontal, and thus the vertical coil set provided the largest contribution to cancelling the field. The values of the local field in the x, y, and z axes were measured with a magnetometer, and the results are shown in Table (5.1) along with the amp turns produced by each coil system.

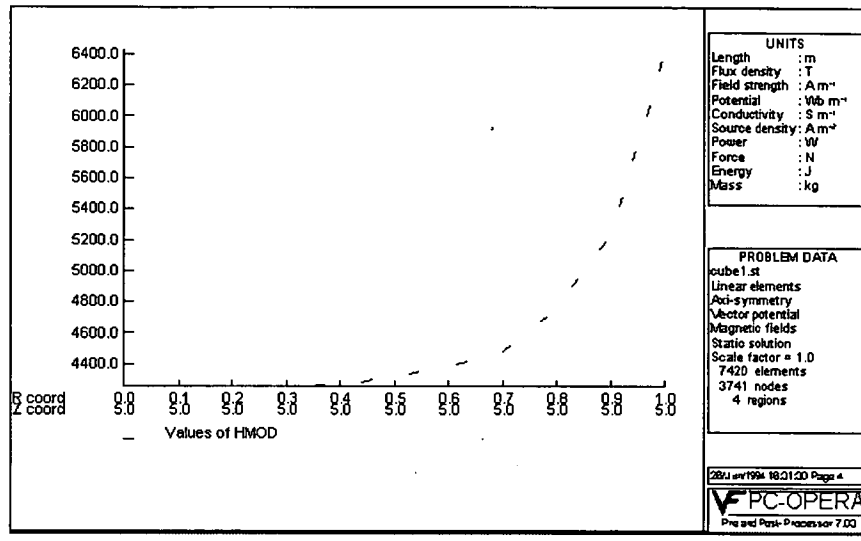

Figure 5.2: Opera2D analysis of the change in field 1m radially out from center of the Cube.

The entire cube structure was made from non-magnetic materials. The cube sides were wooden, and joined using brass screws, the PVC hoops containing the inner coils were supported by wooden beams and fine cord. Magnetic objects and materials were kept as far from the cube as practical in order to keep the natural geomagnetic field in the region as homogeneous as possible. The Belle-Wrigley rig itself was supported by a wooden stand to raise it into the centre of the cube so that it was almost entirely inside of the one cubic metre of lowest field. The x and y coil groups were wound from 0.6mm diameter cotton wrapped copper wire, the z coil group was wound from 0.8mm diameter cotton wrapped wire. Each set of 3 coils (x, y, and z) was wired in series, and connected to a separate power supply.

5.2 The Belle-Wrigley Rig

The Belle-Wrigley Rig is a purpose-built piece of equipment which employs a vertical lever system to apply either tensile or compressive stresses in two perpendicular horizontal directions simultaneously to a cruciform specimen. The rig

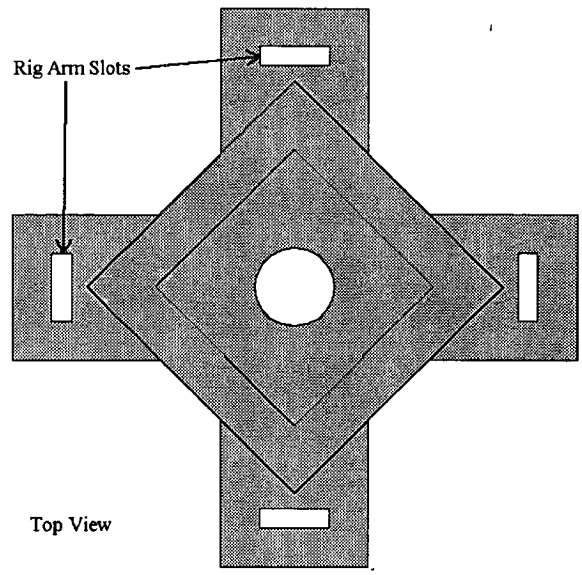

Figure 5.3: Rig Base.

consists of a base-frame (Figure (5.3)) which supports four lever-arms (Figure (5.4)) mounted vertically. Each arm has a movable jaw with which to clamp the specimen. Opposing arms are linked via a heavy threaded rod at the top; large nuts (with turning bars) on this rod push the tops of the arms either closer together, or further apart. The arms pivot in the base-frame and thereby apply the stresses through the jaw-clamps to the cruciform specimen.

The jaw-clamps are free to rotate in the vertical plane so that, as the stress-arms lean away from the vertical, the jaws remain horizontal (Figure (5.4)). To ensure the specimen does not bend or twist when stressed, a series of "halo-screws" (Figure (5.5)) are employed. The halo is a square frame which is mounted directly above the specimen in the xy plane which has four bolts passing through it vertically, one in the middle of each side. These bolts may be screwed directly onto the head of each jaw-clamp. A second series of bolts mirror these passing up through the base-frame to the underside of each jaw-clamp. Together these eight halo-screws can adjust the relative vertical positions of the four jaw-clamps, and thus control bending and twisting. The strain gauges on both sides of the specimen provide the indications of bending or twisting. At the base of each

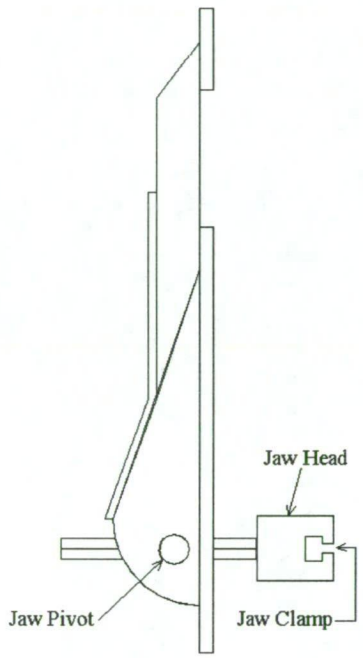

Figure 5.4: Rig Arm.

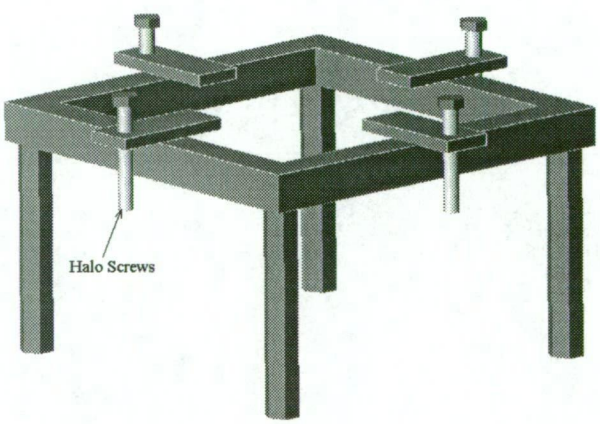

Figure 5.5: The Halo.

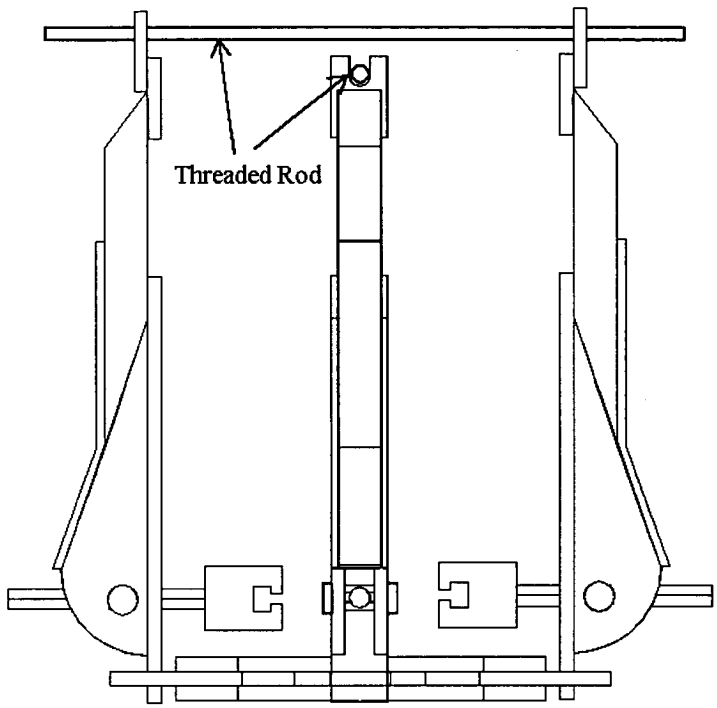

Figure 5.6: The Belle-Wrigley Rig.

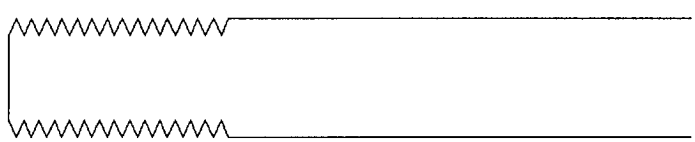

Figure 5.7: Cruciform teeth.

lever-arm it is in contact with the rig-base only via two screws, one on each side. Adjustment of these will also control twisting of the specimen.

The means by which the cruciform specimen is held in the jaws is quite novel. A series of parallel, triangular grooves are cut into both sides of the ends of each of the cruciform arms (Figure (5.7)). A similar set of grooves is in the clamping teeth in the head of each jaw. These teeth are clamped onto the specimen by five screws passing through the top side of each jaw head which press the free moving upper teeth onto the specimen, and the specimen in turn onto the lower teeth. The clamping teeth are located in recesses in the jaw head.

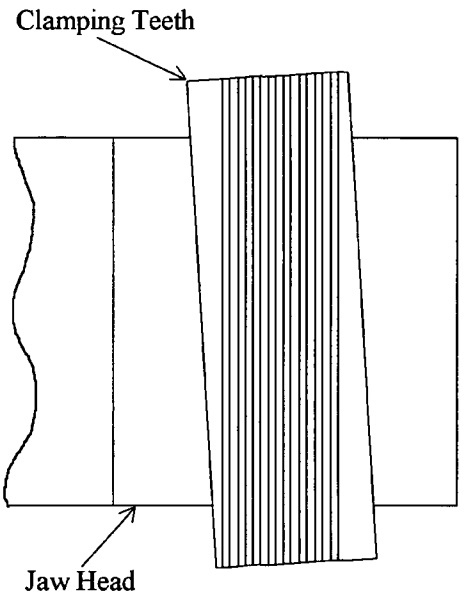

Figure 5.8: Clamping teeth.

Each set of teeth is cut into a rectangular block (Figure (5.8)). The teeth are cut at an angle of 3.4° to the long side of the block, and the recess which houses the block is at the same angle with respect to the end of the jaw head. The angling of the block and recess means that as the block is slid from side to side along the recess, the teeth move backwards or forwards with respect to the end of the jaw-head, but remain parallel with the front of the jaw head at all times. This ingenious design feature enables the clamping-teeth to be independently adjusted so as to mesh with the grooves cut into the specimen, even if the top and bottom face grooves are out of alignment with each other.

The large threaded rods which are mounted across the tops of the stress-arms are in contact with the arms only via the sharp edges of prisms which allow the relative angles of the arms and the rod to change freely. The nuts on the rods (four on each) have long bars welded on two sides so that they may be turned by hand.

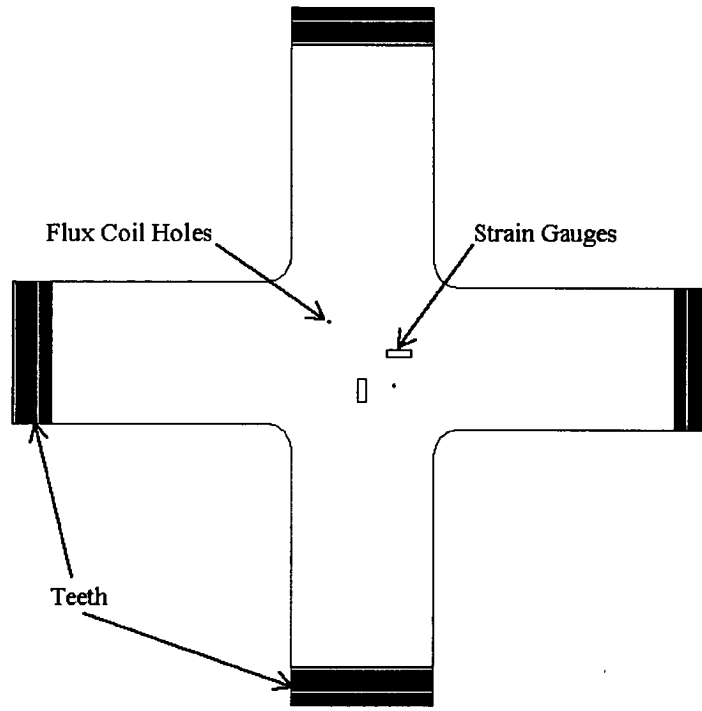

Figure 5.9: The Cruciform.

5.3 The Cruciform

The cruciform was machined from 8mm thick mild steel plate. The details of the design can be seen in Figure (5.9). Two 1mm diameter holes were drilled 35mm apart diagonally across the centre of the cruciform to accommodate the flux-sensing coil. The coil consisted of 10 turns of 36 B&S gauge, rayon-wrapped, enamel-coated, copper winding wire. The coil was wound diagonally to the axes of the cruciform so that a single coil could be used whether the direction of magnetisation be along either the x, or y axis. It also gave a clear path for the flux across the centre of the specimen, whereas two sets of holes will always leave a set of holes and/or a coil parallel to the flux in the middle of the flux path. The flux-coil was connected directly to twin-core mutually shielded cable.

Four resistance strain gauges were attached to the crucifrom, two on each major surface, positioned orthogonally. The strain gauges used were Radio Spares RS 632-168, 5mm strain gauges of nominal resistance 120Ω, gauge factor 2.0,

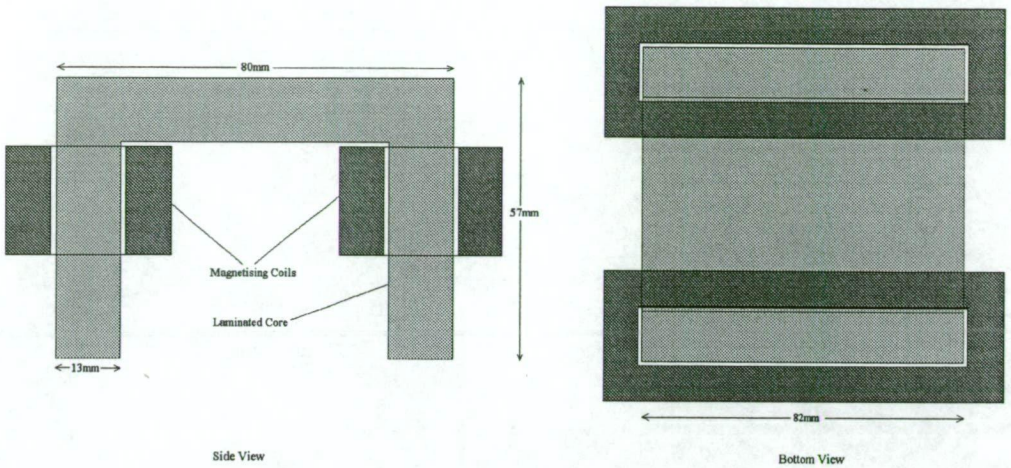

Figure 5.10: The Magnetising U-core

with copper-nickel foil on a polyimide backing. The gauges were attached to the specimen using cyanoacrylate adhesive. A four channel strain gauge amplifier was purpose built using the half-bridge configuration (see Section 5.6). The four channels of strain data were sent directly to the PC30D board in the strain computer, and are read by the Dante-Strain software (Section 6.2.2).

5.4 The U-Cores

Two identical U-core electromagnets are used to produce the field which is applied to the cruciform specimens. The cores are constructed from silicon-iron laminations each 0.3mm thick. The details of the core can be seen in Figure (5.10). Each core has two coils of 0.8mm diameter enamel-coated wire wrapped around it, one on each side. Each coil has 175 turns, and the two coils are connected in series, giving a total of 350 turns per core. Using two coils enabled a design where the middle section of each core was flat and clear so that the twin electromagnets may be clamped to the cruciform. The clamp consisted of two 5mm thick aluminium plates joned by 6mm diameter brass rods. The clamp essentially rested on the top electromagnet, which in turn rested on top of the cruciform specimen, and pulled the bottom electromagnet up to the underside of the cruciform. The

two electromagnets were connected in parallel.

5.5 The Computers and Boards

Two separate systems were required to obtain the data for this project: one for the magnetics data; and one for the strain data. The reason for this was primarily due to the number of real-time, simultaneous processes which were required. A frequency critical output signal was required to control the magnetising field, and frequency critical data acquisition was required to process the magnetic and strain data. Such real-time accuracy could not be achieved with a single processor and bus system.

The magnetic data handling was the more demanding of the two processes and so the bulk of the computing power was dedicated to it. The magnetics computer was a dual-processor 350MHz Pentium II with a 100MHz bus, and 128M RAM. This was responsible for controlling the applied field, and acquiring and displaying the field and flux data. While the Dante (Chapter 6) package was running there were no other active processes on the system so all CPU time was dedicated to it. In order for the input and output functions to operate independently they were in turn handled by separate PC30 data acquisition boards. This enabled them to operate at different frequencies, and at different resolutions so CPU usage could be optimised. The input card was an Eagle Technologies PC30FA high performance analog I/O board, the specifications for which are found in Tables (5.2) and (5.3). The output card was a Boston Technologies PC30D analog I/O board with specifications as shown in Tables (5.4) and (5.5).

The strain computer was a single processor 166MHz Pentium I with 32M RAM and a 40MHz bus. The demands upon this machine were much lower as it was only required to do data acquisition and a minimum of calculations so the smaller processor was more than adequate for the task. The input was handled by another PC30D analog I/O board identical to the one used in the magnetics computer for field control.

Table 5.2: PC30FA Specifications

	Analog Inputs
Number of Channels	16 single ended or 8 differential
Resolution	12-bits (1 in 4096)
Total System Accuracy	±1 bit LSB (for Gain of 1)
Linearity: Integral	±0.05% FS
Differential	±3/4 LSB max.
A/D Input Voltage Range	±5V, ±10V
Data Acquisition Rate	330kHz (G < 1000), 100kHz (G = 1000)
Input Impedance:	
On Channel	10M/20pF
Off Channel	10M/100pF
Offset Voltage	±5 LSB adjustable to 0
Input Bias Current	±100 pA/°C
Input Bias Offset Drift	±30ppm/°C
Input Gains:	
Ranges	1, 10, 100, 1000 or 1,2,4,8
Gain Error	Adjustable to 0
Gain Accuracy	0.25% max, 0.05% typical for gains < 1000
CMRR for various gains	1% max, 0.1% for g=1000
Monotonicity	0 to 70°C
Temperature Drift:	
Full Scale Error Drift	6 ppm/°C
Bipolar Zero Drift	1 ppm/°C
Gain	±30 ppm/°C
Input Over Voltage Protection	±12 V
A/D FIFO Buffer Size	16 samples
Channel Gain/Queue Length	31
A/D Clock:	
Internal Clock	2 MHz or 8 MHz
Clock Frequency Tolerance	0.01%
Clock Drift	10 ppm/°C
Internal Clock Divider	2 x 16 bit stages
External Clock	TTL compatible
External Trigger	TTL compatible
Channel List (queue) Length	31
Block Scan Mode	up to 256 channels per block
Noise Levels (p-p)	G=1: ±1 bit; G=10: ±1 bit; G=100: ±2 bits
Data Acquisition Modes	Polled I/O, Interrupts, Single and Dual Channel DMA

Table 5.3: PC30FA Specifications Cont.

	Analog Outputs
Number of Channels	4
Resolution	Two 12-bit, two 8-bit
Accuracy	±1 LSB (12-bit), 0 LSB (8-bit)
Differential Nonlinearity	±1 LSB max.
Output Ranges	±5V, ±10V, 0 to 13 V
Offset Error	Unipolar: $\frac{1}{4}$ LSB typ., 1 LSB max (12-bit) Bipolar: $\frac{1}{2}$ LSB typ., 2 LSB max (12-bit)
Gain: Ranges Error	x1, x2 2 LSB typ., 5 LSB (12-bit)
Settling time to $\frac{1}{2}$ LSB	10 μs max. in Load of 500 p, 2 kΩ
Throughput Rate	500 kHz
Temperature Drift	100 ppm/°C of full scale
Max. Current Output Source	5 mA max.
Monotonicity	0 to 70°C

5.6 The Electronics

A number of separate, external pieces of electronic equipment were required between the computers and the sample in order to condition the signals.

The field strength adjacent to the surface of the sample was measured using a Linear Hall effect integrated circuit from Radio Spares, the technical specifications of which are shown in Table (5.6). This device features a differential output stage. One output increases linearly in voltage, whilst the other decreases, for a linear increase in magnetic flux density over a ±40 mT range. The Hall IC was connected to a small power supply, the circuit for which is shown in Figure (5.11). The potentiometer allowed the voltage between the two outputs to be balanced, thereby zeroing the output of the probe. The supply to the probe was on continuously so that it was in a state of thermal equilibrium for all measurements so long as there were no large changes in the ambient temperature.

The strain gauges were all connected to a purpose built 4-channel strain gauge supply and amplifier. The circuit diagram of the strain gauge conditioner is shown in Figure (5.12). A separate dummy gauge was adhered to a piece of steel near

Table 5.4: PC30D Specifications

	Analog Inputs
Number of Channels	16 single ended
Resolution	12-bits (1 in 4096)
Total System Accuracy	±1 bit LSB
Differential Nonlinearity	±3/4 LSB max.
Quantisation Uncertainty	±1/2 LSB
A/D Input Voltage Range	±5V, 0 to 10V
Input Bias Current	±25 nA
Input Bias Current Drift	±100 pA/°C
Gain Drift	±30 ppm/°C
Offset Drift	±10 ppm/°C
Input Impedance:	
On Channel	10M/20pF
Off Channel	10M/100pF
Offset Voltage	±5 LSB, adjustable to 0
Monotonicity	0 to 70°C
Data Acquisition Rate	200kHz
A/D Clock:	
Internal Clock	2 MHz, crystal controlled
Clock Frequency Tolerance	0.01%
Clock Drift	10 ppm/°C
Internal Clock Divider	16-bit prescaler, 16-bit divider
External Clock	TTL compatible
External Trigger	TTL compatible
Channel List (queue) Length	31
Block Scan Mode	up to 256 channels per block

Table 5.5: PC30D Specifications Cont.

	Analog Outputs
Number of Channels	4
Resolution	Two 12-bit, two 8-bit
Accuracy	±1 LSB (12-bit), ±3 LSB (8-bit)
Differential Nonlinearity	±1 LSB
Quantisation Uncertainty	±1/2 LSB
Output Ranges	±10V, 0 to 10 V
Offset Error	±0.2 LSB (12-bit), ±3 LSB (8-bit)
Gain Drift	±30 ppm/°C (12-bit) ±0.007%/°C (8-bit)
Throughput Rate	130 kHz max.
Output Compliance	±5 mA
System Accuracy	0.025%
Monotonicity	0 to 70°C

Table 5.6: Radio Spares Linear Hall Effect IC Specifications

Supply Voltage	+4 to +10 V d.c.
Supply Current	3.5 mA (typ.)
Output Current	10 mA
Output Voltage (at zero mag. flux)	1.75 to 2.25 V at 5V supply
Sensitivity	7.5 to 10.6 mV/mT
Frequency of Operation	0 to 100 kHz
Operating Temperature Range	0° to 70° C

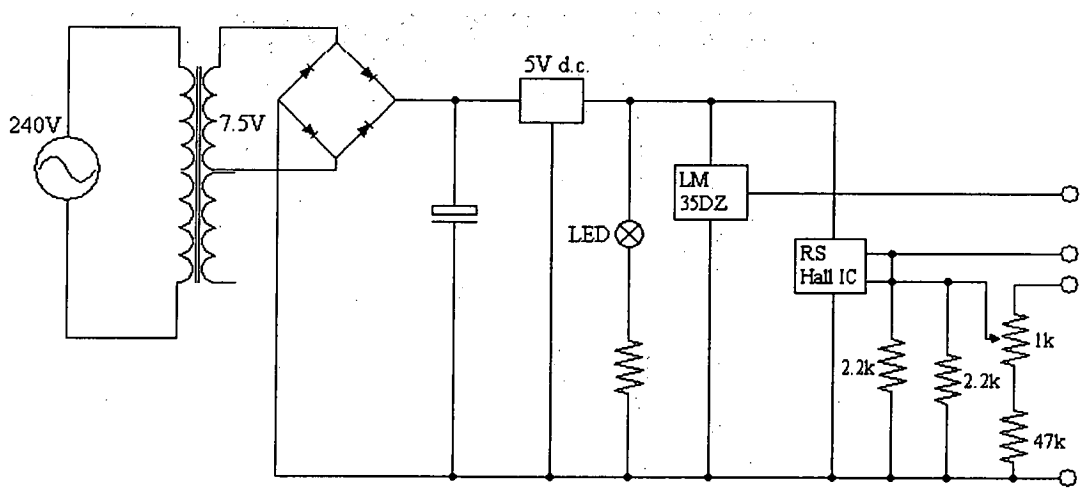

Figure 5.11: Circuit Diagram for the Hall Probe Supply

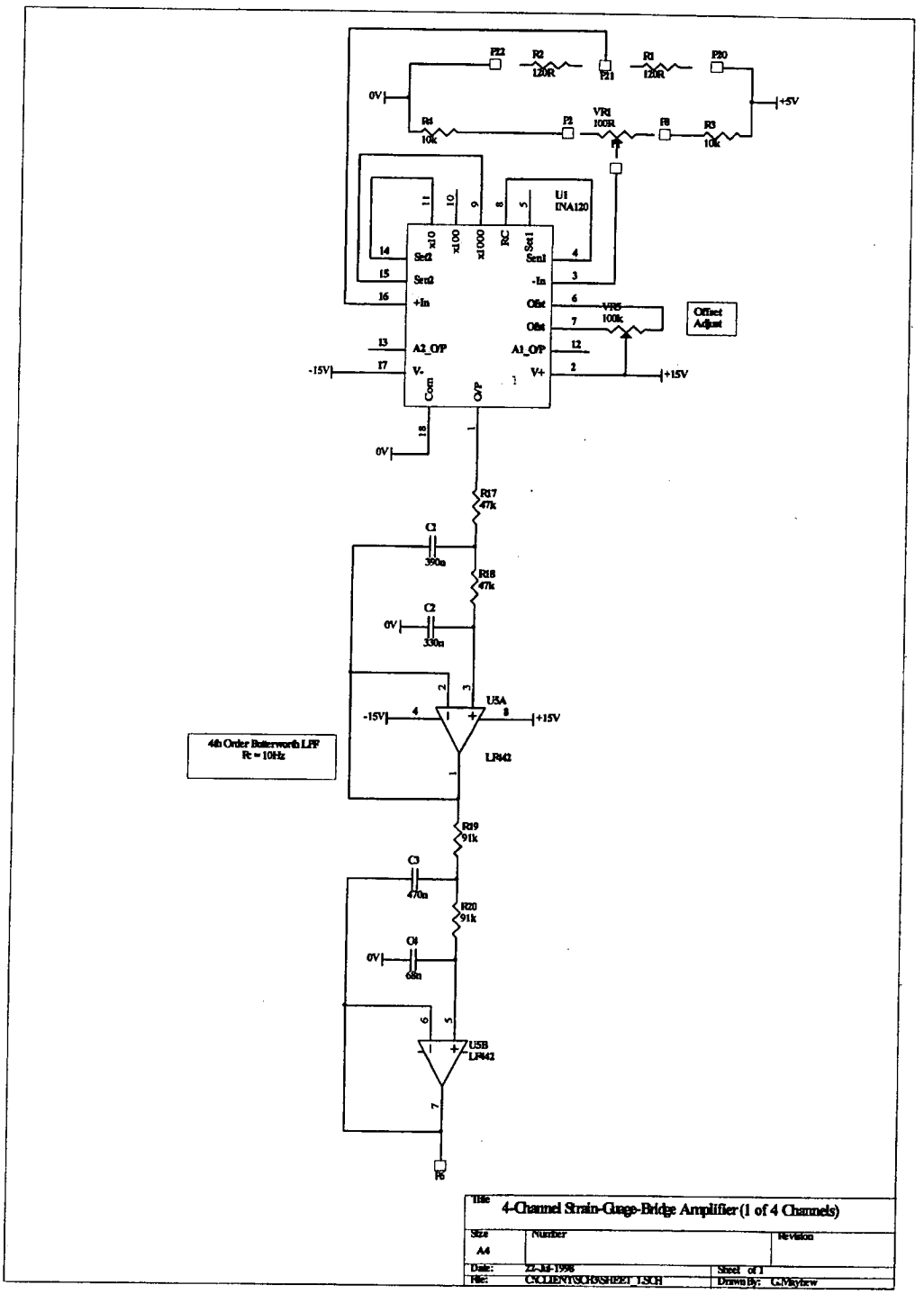

Figure 5.12: Circuit Diagram for the Strain Gauge Supply and Amplifier.

Table 5.7: HP 8875A Specifications

Gain Accuracy	±0.1 %
Gain Stability	± 0.01 %
Input Circuit	Balanced differential
Differential Input Impedance	20 MΩ in parallel with < 0.001μfd
Voltage Drift	±3μV referred to input ±0.2mV referred to ouput
Noise	Measured with respect to input with 1K signal source impedance at gain of 1000. Noise measurement with respect to input is Bandwidth: dc – 10Hz Noise: 1μV peak to peak
Output Circuit	±10 volts across 100Ω, (100 mA), and 0.2 Ω max.
Non-Linearity	less than 0.01% of full scale value, 10 volts

the apparatus for each channel with each of the eight gauges connected to the conditioner by identical length leads. Due to the fact that in general only static stresses were to be considered, it was desirable to use a low pass filter with a very low threshold frequency so that any ambient electromagnetic noise (most of which would be at 50 Hz) could be filtered out. Therefore, a 4th order Butterworth 10 Hz low pass filter was employed along with a gain factor of 1000 to boost the signal before sending it via 6m long cables to the computer. Each output had a 10 turn potentiometer to zero the signal. The strain gauge circuit used was a temperature compensated Wheatstone half-bridge [33].

The signals from the output of the Hall probe and the flux sensing coil were amplified using Hewlett-Packard 8875A Differential Amplifiers. The filters were set at 2 Hz as only very low frequency (< 0.5 Hz) signals were ever considered. During most of the investigation the gains were set at 20 for the field strength, and 50 for the flux density. The specifications for the amplifiers are shown in Table (5.7). [32]

The current to the magnetising U-cores was provided by a Goodwill Dual Tracking GPC-3060 laboratory power supply with the two outputs connected in series, capable of ±6 amps, and ±30 volts controlled by an inverting power oper-

ational amplifier with a gain of 1, which was in turn controlled by the computer. During the investigation the power supply was limited to 12 volts.

5.7 The Permeameter

In order to obtain standardised data which could be acknowledged as true values, a permeameter was required which fell within the recognised design parameters [17]. The permeameter used was a standard twin-yoke design using silicon-iron laminations to complete the flux path. The laminations were in three rectangular shaped sections on each side (six in total), each section was approximately 90 mm x 40 mm in cross section. The average flux path was approximately 675 mm in length per side.

The magnetising field was provided by a solenoidal coil located centrally over the specimen. The coil had an inner diameter of 75 mm, an outer diameter of 155 mm, and a length of 130 mm, with 551 turns wound in multiple layers.

In general the field strength was measured using the Hall probe described in Section (5.6), and the flux density was measured by means of coils wound tightly around each sample.

Chapter 6

Software

6.1 The Task at Hand

Due to the very large amount of data required for the project, the only viable method of acquisition was to use dedicated software, and hardware controlled by a fast PC. Previous software packages which use a PC and data acquisition boards to control field strength and obtain data were unacceptable, because of the rate at which computing power is evolving; older software tends to be slower and simpler than that which can be attempted now.

Due to the complexity of the program required the software programming language 'G' was selected as used by the LabView programming environment. National Instruments' LabView is designed primarily for data acquisition and control, to be used by scientists rather than programmers, and thus was ideal. The PC30 range of data acquisition boards were already commonly used in the School of Engineering for computer-based control and measurement, and as these work well with LabView, they were chosen as the hardware interface (Chapter 5).

6.2 Dante

The software package was given the title "Dante: Magnetic-Stress Interaction Control Environment". The full system requires 3 data acquistion boards and 2 independent computers, and actually consists of two separate programs, one to control and measure the magnetics data and one to measure the strain data.

6.2.1 Dante Magnetics Software

The program to control the magnetics side consists in itself of two parts, as it must both control the applied field, and measure the flux density and field strength. Firstly we will consider controlling the applied field. The key limiting factors to consider when developing this part of the software are hardware ones: primarily the time resolution available to the software from the computer; and the voltage resolution of the data acquisition card. The processor must be capable of performing the required calculations between tasks which are to occur in real-time, and outputs on the card must be capable of resolving the voltages at the accuracy requested by the software. The specifications of the computers used, and the PC30 boards are in the hardware chapter.

Another limitation of the PC30 boards is that once they have been set a certain input task at one frequency they cannot be monitored on different channels at any other frequency (for more detail see Appendix A). For this reason separate PC30 cards had to be employed for the input and the output. The details of the software controlling the applied field will be considered first.

The Output

The waveform required for the magnetising current was at first a simple, constant-frequency triangular wave. At the frequencies used here, the effect of the inductance of the magnetising coils was negligible, and so a triangular voltage would produce a triangular current of the same frequency and zero phase difference. As the output was digital however, a true triangular wave was strictly impossible,

rather a stepped voltage ramp was the best achievable function. The current waveform would be smoothed by the inductance of the coils. The voltage step resolution was 0.01 volts. The time spent at each voltage was determined by

$$t = 1000\left(\frac{V_s}{2\nu V_{\max}}\right) \quad \text{milliseconds,} \tag{6.1}$$

where V_s is the value of the voltage step (0.01 V), ν is the frequency, and $V_{\max}$ is the total change in voltage over the ramp function. The number of steps required to complete the ramp (half of one cycle) was calculated, and a *FOR* loop was employed to step through the voltages. The voltage output during each step was checked via an active feedback loop; the voltage across the magnetising coils was read and compared with the desired voltage. If there was a difference between them then it was added to the output voltage and the coil voltage was again checked with the desired voltage. This cycle was repeated until either the voltage across the coils was within 0.01 volts of the desired voltage, or 100 iterations had occurred. If the voltage was correct the program would continue, and if not the program would halt and inform the user that something was wrong. In this way if any connections were incorrect, or if a power supply was under voltage, false readings would not be obtained.

This piece of code produced an accurate voltage ramp from a starting voltage to a final voltage at a particular slope with the parameters being defined by the user. This ramp function was embedded within a *WHILE* loop. The controlling event of this loop was the activation of a stop button by the user (Figure (6.1)). The *WHILE* loop also determined the extreme values (i.e. starting and final values) of the voltage ramp. This describes the basic "engine" driving the output waveform.

The user interface provides possibly the simplest way to explain the actions taken by the program. The opening screen provides the user with three configuration options and one execution option. The configuration options are Configure Amplification, Configure Cards, and Configure Equipment. The amplification option gives the user the ability to define any amplification factors being used either internally (on the card) or externally (see Chapter 5) on any of the inputs

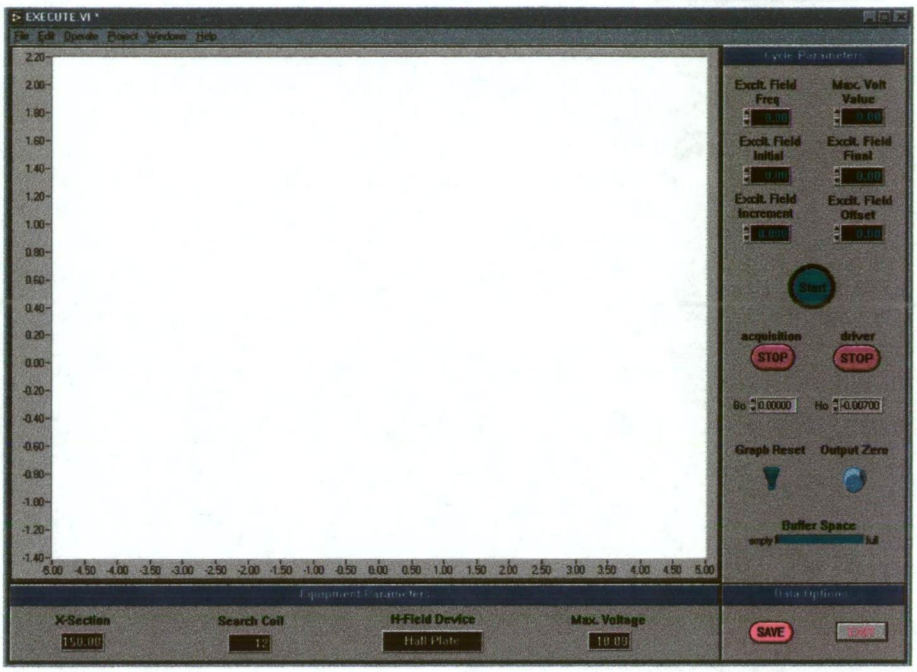

Figure 6.1: The Execute screen of the Dante Software System.

or outputs. The default values are all set to 1; all voltages considered in the program are divided by these amplification values. The options include: magnetic induction voltage; magnetic field strength voltage; and excitation voltage.

The Configure Card option allows the user to set the specifications of the data acquisition boards. These are:
the magnetic induction input channel;
the magnetic field strength input channel;
the excitation voltage input channel;
the excitation voltage output channel;
the input board number;
the output board number;
the I/O card timer divider; and
the I/O card timer prescaler.

The Configure Equipment option allows the user to set the values of external variables required by the program. These include the cross-sectional area of the sample, perpendicular to the applied field, enclosed by the flux search coil (see

Section 5.3); the number of turns in the search coil, and the conversion factor from volts to kAm^{-1} for the device being used to measure the field strength.

The Execution option presents the user with a screen (Figure (6.1)) with a section to enter the cycling parameters and the start and stop buttons which control the excitation and the data acquisition, alongside a display which presents the acquired Bvs$H$ data in a real-time x-y plot format. The cycle parameters to be entered are: the excitation field frequency; the initial excitation field voltage; the final excitation field voltage; the excitation increment field voltage; and the excitation field offset voltage.

The excitation field frequency is simply the frequency at which the field is cycled. The initial excitation field voltage is the first maximum which the excitation voltage will be ramped to, this may be any value, positive or negative, which the hardware is capable of attaining (see Chapter 5). The voltage starts at zero and will ramp to the given voltage in one quarter of the waveform period.

Initially a simple triangular waveform was to be used. However, during preliminary testing it was found that the flux density lagged behind the magnetic field strength due to eddy currents in the specimen (see Appendix A). In order to ensure that all changes in flux density due to the increasing field had occurred before the magnetising current peaked, a 2 second 'wait function' was inserted into the program at the end of each voltage ramp function. Close inspection of initial curves and remanent flux density values of initial hysteresis loops showed that the wait had no adverse effects on the quality of the data and ensured that at low field strengths and higher cycling frequencies (i.e. during demagnetising) the magnetising process was as accurate as possible. The result of this is that a clipped-triangular waveform was used for the applied field.

At the end of the wait, the voltage ramped back to the next extreme voltage, the value of which would be determined by two factors: the final excitation field voltage; and the excitation field increment voltage. In order to demagnetise a specimen or produce a Normal Magnetisation Curve, the amplitude of the applied waveform needs to be decreased or increased accordingly. If the field is

to be cycled between two constant values the voltage will simply ramp up and down between the two appropriate voltages until the user ends the cycle. If, however, other field forms are required, the final excitation field voltage can be set at a different value to the initial voltage (i.e. zero for demagnetising) and at the end of each voltage ramp the maximum field voltage will be altered by the excitation field increment voltage until the field maximum is equal to the final excitation field voltage. The voltages may also be offset in order to ramp between two positive or two negative values rather than cycling about zero applied field, allowing anhysteretic data to be obtained.

The Input

The section of the software which controlled the acquisition of the field and flux data was much simpler than that which controlled the applied field. Digital voltage data was read off two channels of the input PC30 board with a sampling frequency of 2 kHz. Each 100 samples (per channel) were fed into an array. The field strength data was averaged, divided by the amplification value (Chapter 5), multiplied by the volts-to-kAm^{-1} factor and fed to the x-y plot. The flux density data was divided by the amplification, then fed into the integration equation

$$B = -\int \frac{V_B}{NA} dt \quad \text{Tesla}, \tag{6.2}$$

where V_B is the voltage across the flux sensing coil, N is the number of turns in the coil, and A is the cross-sectional area, perpendicular to the applied field, enclosed by the coil. The integration was performed by a numerical integration method. For the sake of speed of execution the Trapezoidal Method was used as it was the simplest available to the software, yet was accurate enough for the task. The trapezoidal method is defined by

$$\int x\, dt = [x(i) + x(i+1)]dt, \quad k = 1, \tag{6.3}$$

$$\text{for i} = 0, k, 2k, 3k, ..., \text{Integral Part of } [(n-1)/k],$$

where n is the number of data points, k is an integer dependent on the method, x is the input array, and dt is the interval size which represents the sampling step

size used in obtaining the input array data from the function (in this case 0.001 seconds). The result of each integrated array was then added to the sum of all previous integrated arrays to produce the flux density value in Tesla which was fed into the x-y plot.

In this way 100 samples were taken per point plotted, and 10 points were plotted per second, thereby providing the user with a real-time, true-value Bvs$H$ graph on the screen during the sampling cycle.

Prior to beginning an acquisition sequence the software would determine the offset on the flux density channel. There is always a small voltage offset on the input channels so that when the input is connected to the ground via a 1kΩ resistor, the channel does not quite read zero. The offset is typically less than 10 mV. This can easily be accounted for on the field strength channel as an approximate average value may be subtracted from the input. Small errors in this will only cause the final graph to be minutely offset to the left or right, and may be easily corrected at the data analysis stage.

The flux density channel is another matter entirely. Small offsets on this channel will be integrated over and over, hundreds of times per cycle, the errors being cumulative. For this reason the voltage at the flux density channel input is read 2000 times, the values of these samples are averaged, and the result is subtracted from all subsequent values read.

These tasks are performed first when the start button is pushed, before anything else occurs. When there is no change of flux in the sample, the search coil approximates a resistor shorting the inputs. It also serves to act as an aerial and samples the ambient electromagnetic noise which is present, and cancels voltages caused by this noise. In this way the zeroing offset may be accurately determined prior to each sampling cycle.

Presenting the Data

During this research three different methods of obtaining and presenting Bvs$H$ data were used: Normal Magnetisation Curves; Initial Magnetisation Curves;

and Symmetric Hysteresis Loops. The appropriate forms of B and H values were extracted from the complete data set by the following methods.

The Normal Magnetisation Curves were obtained by applying a cyclicly increasing field up to a maximum value then extracting the largest obtained B value, and its corresponding H value for each cycle. As the cycling frequency was constant, the same number of points was obtained for each cycle so data could easily be divided up into one-cycle blocks to retrieve a maximum. An array constructed from these data-point pairs was converted to a tab-delimited spreadsheet file.

An Initial Magnetisation Curve was obtained by applying a single voltage ramp from zero to a maximum value and inserting the complete set of plotted points into a spreadsheet file. The Bvs$H$ hysteresis loop data points were obtained by creating an array of points from one complete, closed cycle and inserting it into the spreadsheet.

6.2.2 Dante Stress-Strain Software

The software which monitored the four strain gauges adhered to the test specimen was by far the simplest of all software used. For independence in sampling frequency (see Chapter 5) this software package was run independently to the magnetics software on a separate machine using completely independent hardware. The program monitored the four channels sequentially at a sampling frequency of 10 kHz, each block consisted of 1024 samples, 256 per channel. Each set of 256 samples was averaged then multiplied by a conversion factor determined by

$$C = \frac{g}{nA_sV_s} \cdot 10^6, \tag{6.4}$$

where g is the gauge factor, A_s is the amplification of the strain signal, V_s is the supply voltage, n is the number of samples, and 10^6 is the conversion to microstrain. The four strain values were then displayed as large font numerics on the screen so they could easily be seen while adjusting the Belle-Wrigley rig approximately 3m away.

Chapter 7

Results

7.1 The Method

The magnetic/stress data were obtained from the mild steel cruciform by first demagnetising the specimen *in situ* using the twin U-cores. The magnetising field was cycled with a maximum of 2V across the coils, which produced a flux density approximately 10% above the knee of the initial curve for mild steel, at a frequency of 0.3 Hz, and the maximum voltage was decreased by 0.01V per cycle. Once the demagnetising was complete the desired biaxial stress pattern was applied with an accuracy of ± 5 microstrain. It was necessary to use the eight halo screws to ensure that no bending or twisting was caused by applying the stresses (see Chapter 5). The stresses covered in this investigation are shown in Table (7.1). Every possible combination of these stresses for the x and y directions gave 49 different stress patterns in total.

For system symmetry the sample was then demagnetised again using the same method as indicated before. The reason for this second demagnetisation will be explained shortly. The magnetising coils were then driven to a maximum of 4V at a frequency of 0.02 Hz to obtain a positive initial curve. The sample was then demagnetised again, and the coils driven to -4V at 0.02 Hz to produce a negative initial curve. The coil voltage was then increased to a maximum of 6V, and cycled between that and -6V at a frequency of 0.04 Hz to produce a symmetric

Table 7.1: The X and Y Stresses Applied to the Specimen.

Stresses
-120 MPa
-80 MPa
-40 MPa
0 MPa
40 MPa
80 MPa
120 MPa

hysteresis loop.

The specimen is demagnetised directly after the stresses are applied because demagnetising and then applying stress will produce a different domain arrangement to that which occurs if a stress is applied to the sample and it is then demagnetised. As a result of this, demagnetising had to occur after the stresses were applied so that the conditions for the positive initial curve and the negative initial curve were the same (i.e. stress, demagnetise, magnetise). Attempting to demagnetise, stress, magnetise, unstress, demagnetise, stress, magnetise would produce far too many errors as the differences in the two stress patterns would be large. The process would also be exceedingly time-consuming. The sample must also be demagnetised before the stresses were applied in order to remove any residual magnetisation which would otherwise cause magnetostriction and lead to errors in the strain produced by the applied stresses.

Both positive and negative initial curves were required so that it could clearly be seen that the specimen had been accurately demagnetised [48]. The positive and absolute value of the negative curves could then be averaged which would also account for any drift (which would tend to be in the same direction for both curves) (see Section 4.2). On average around 130 points were obtained for each initial curve, and around 300 points for each Hysteresis loop.

Once 98 initial curves and 49 symmetric hysteresis loops were obtained, the data needed to be presented in a way which allowed the stress-related features to

be interpreted. The simplest way to compare the data seemed to be to superimpose multiple curves or loops taken at different stresses onto a single set of axes. In this way, increases and decreases in flux density are obvious, crossover points where data sets intersect can be seen, changes in remanence and coercivity are clear, and general changes in shape can be viewed. Complex 3-dimensional representations were considered, but the superimposition method offered both ease of interpretation, and the ability to be easily recognised by anyone familiar with magnetics.

Each data set was also graphed individually so that any acquisition anomalies could be seen at the time of acquisition and it could be repeated if required. Anomalous voltage spikes, and ambient noise, or user mistakes can also be seen immediately. Therefore, a complete record of all data acquired is available for further analysis if such is desired. Analysis of the features of individual loops is also best done with only one loop per graph.

So that the graphs did not become overcrowded, it was decided to have stress variations in only one direction per graph. Thus, each graph has seven loops or curves, each taken with the same stress applied in the y-direction, but with different stresses in the x-direction. The complete set of these graphs may be seen in Appendix B.

Figure (7.1) shows initial curves obtained using the method described here from a mild steel cruciform in the stress rig using the twin U-cores with no applied stress, and a rectangular-bar shaped specimen cut from the same plate, in the permeameter described in Chapter 5. The flux densities are slightly different, however, the general shapes of the curves are very similar. It was therefore considered that the loops and curves may be compared with others obtained using similar equipment and conditions.

The differences between the curves may be considered in the following way. At relatively low flux densities, flux flow through a cruciform will closely mimic that through a straight bar. As the flux density increases however, the flux tends to "want to spread out" in the bar sample it will be unable to and will

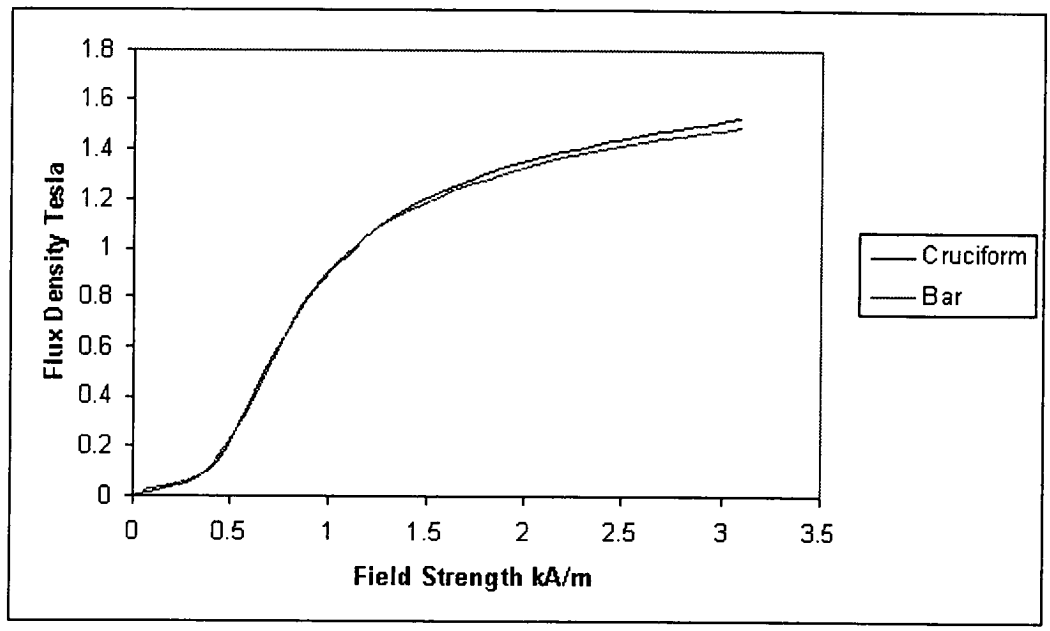

Figure 7.1: Comparison of Initial Curves Obtained from Bar and Cruciform Specimens.

remain primarily within the bar as its permeability is so much higher than the surrounding air. The flux lines will thus be essentially parallel along the length of the bar.

Within a cruciform however, there is room for the flux to "bulge out" at the center of the sample. At low flux densities this effect will be minimal as the flux will generally take the shortest route. At higher flux densities more and more flux will be pushed outside of the section enclosed by the flux sensing coil threaded through the sample thereby reducing the measured flux density, and the true flux density in the center. As the flux density is not measured at a point but across a certain cross-sectional area an average flux density is actually recorded. The bulging will tend to be greater towards the outer regions causing a lower density there than at the center where the field is being measured. Thus the measured flux density will not correspond directly to the field strength.

This will only happen in the samples considered at reasonable high fields, and as all samples considered in the stress analysis had the same geometry the effects would be the same for all curves obtained and thus the data may be compared

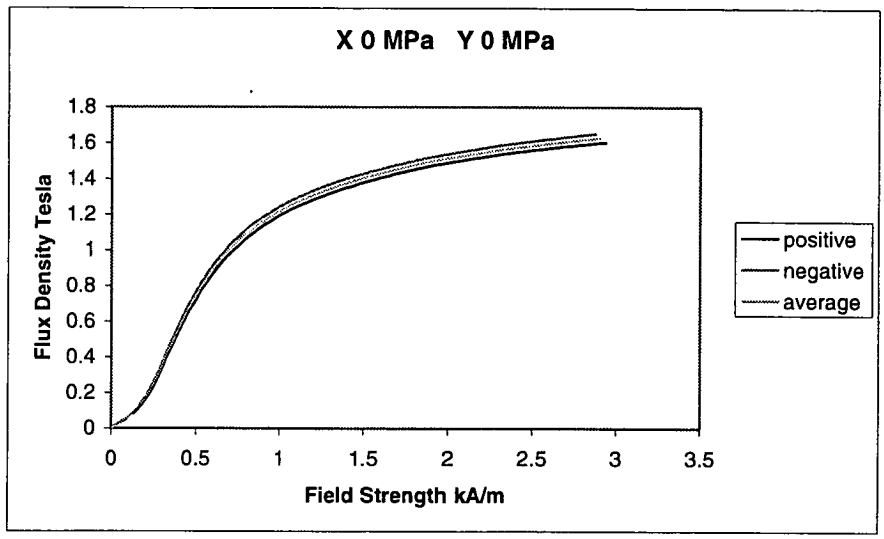

Figure 7.2: Initial Curves With No Biaxial Stress.

with each other without relative errors.

Figure (7.2) shows the positive initial magnetisation curve, the absolute value of the negative initial magnetisation curve, and the average of the two, with no applied biaxial stresses. Figure (7.3) shows a major hysteresis loop obtained from the mild steel cruciform in the stress rig using the twin U-cores with no applied biaxial stresses.

Figure (7.4) shows a superimposition of seven initial magnetisation curves all with zero applied stress in the y-direction (perpendicular to the applied field) and a range of stresses in the x-direction (parallel to the field). All of the graphs produced from the mild steel cruciform at different stresses are presented in Appendix B. The forms of the curves are unremarkable. In general the flux densities of those curves with compression parallel to the applied field, (or tension perpendicular to the applied field) are lower than the zero-stress curve (at the field strengths shown), the degree of change being dependent on the magnitude of the applied stress. The curves with tension parallel to the applied field (or compression perpendicular to the applied field) initially have higher flux densities at the lower applied stresses, but the changes seem to plateau at higher stresses. At higher stresses still, some of the flux densities begin to decrease from their peak

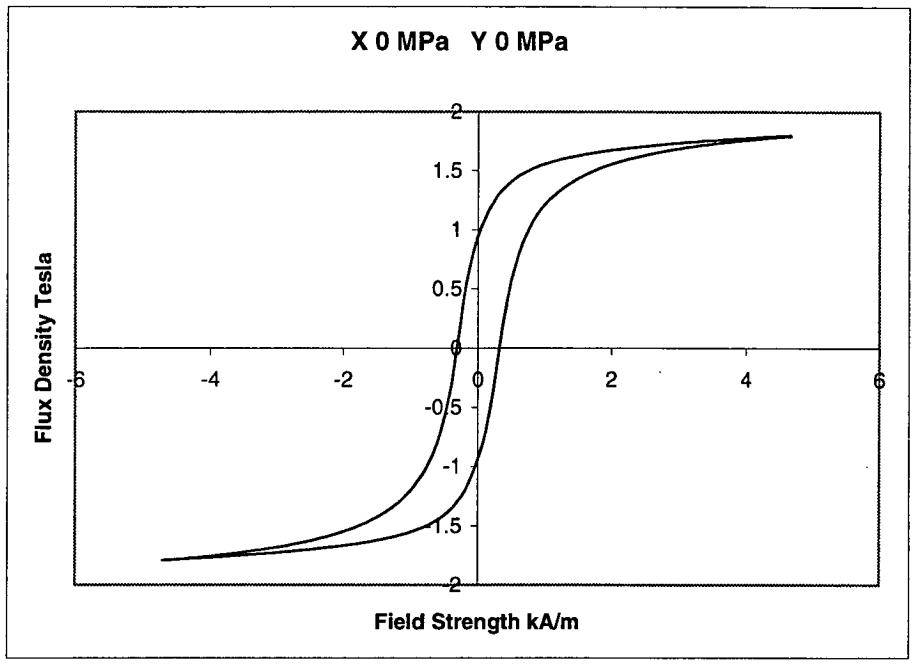

Figure 7.3: Major Hysteresis Loop With No Biaxial Stress.

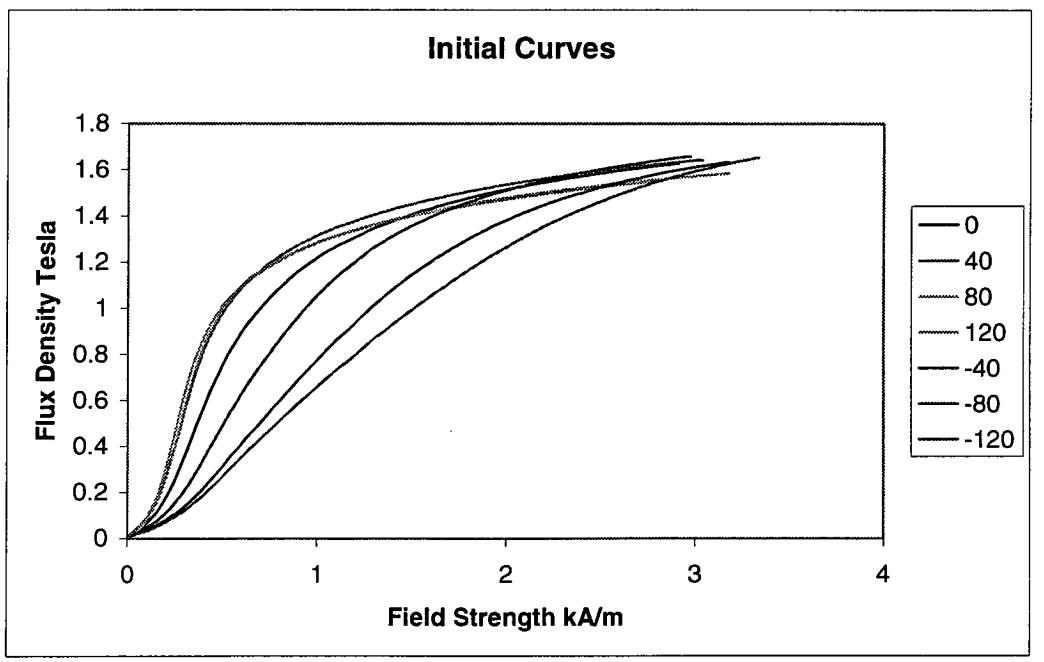

Figure 7.4: Superimposition of Initial Curves of mild steel under different biaxial stresses.

values and once again approach the zero-stress curve values.

Villari reversals are apparent on all of the initial magnetisation graphs presented, where the curves which are initially at higher flux densities cross over the ones which were lower at lower applied fields.

These findings are in agreement with results previously produced by most of the researchers whose works were reviewed in Chapter 3. An example of the curves produced by Bozorth is shown in Figure (3.6).

Figure (7.5) could be considered the most important set of results of the thesis. It shows a superimposition of seven curves all with zero applied stress in the x-direction (parallel to the applied field) and a range of stresses in the y-direction (perpendicular to the field). The dominant feature of this graph is the two coincident points which are common to all curves in the second and fourth quadrants, the implications of which are discussed in Chapter 8.

In order to further investigate the nature of these coincident points, a further series of stressed hysteresis loop were obtained with lower maximum applied fields. These curves are presented in Figure (7.6), and as can be seen the points of coincidence occur at approximately the same applied magnetic field strength, but at a lower flux density.

Figure (7.7) shows a major hysteresis loop obtained from the mild steel cruciform in the stress rig using the twin U-cores with -120 MPa (compression) in the x-direction (parallel to the applied field), and 120 MPa (tension) in the y-direction (perpendicular to the field). As can be seen in this graph the gradual "S"-shaped curve which usually forms one side of the hysteresis loop has become more of a line with a sudden discontinuity of slope in the second quadrant, (and fourth quadrant on the other side). It may also be noted that this "kink" in the loop apparently occurs at approximately the same field as the coincident point mentioned previously. Upon re-examining Figure (7.5), it can be seen that, at low applied stresses, the curvature of the upper portion of the loop between the maximum and the coincident point tends to be convex up, and between the coincident point and the negative maximum convex down. This allows the transition

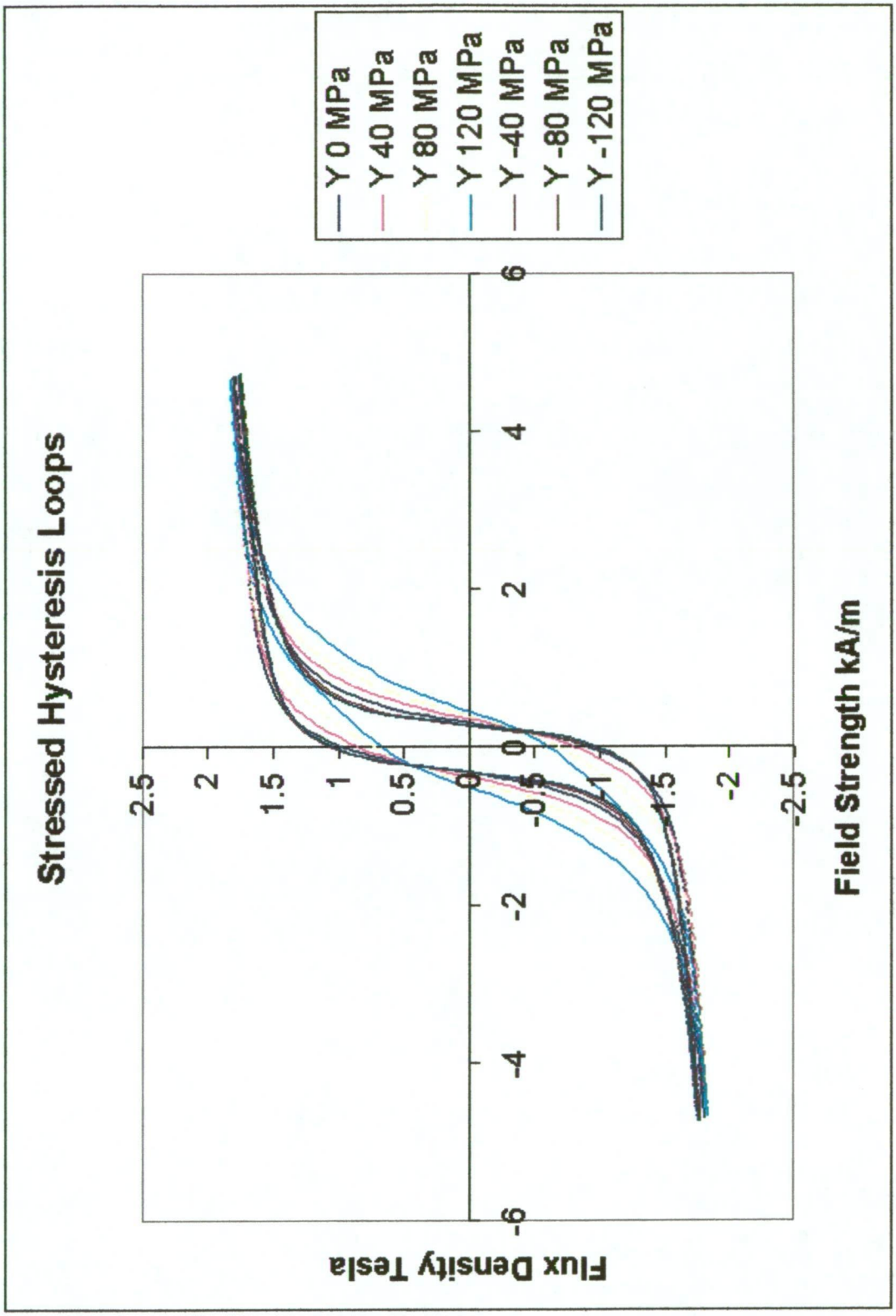

Figure 7.5: Superimposition of hysteresis loops of mild steel under different biaxial stresses. Units are Tesla and kA/m.

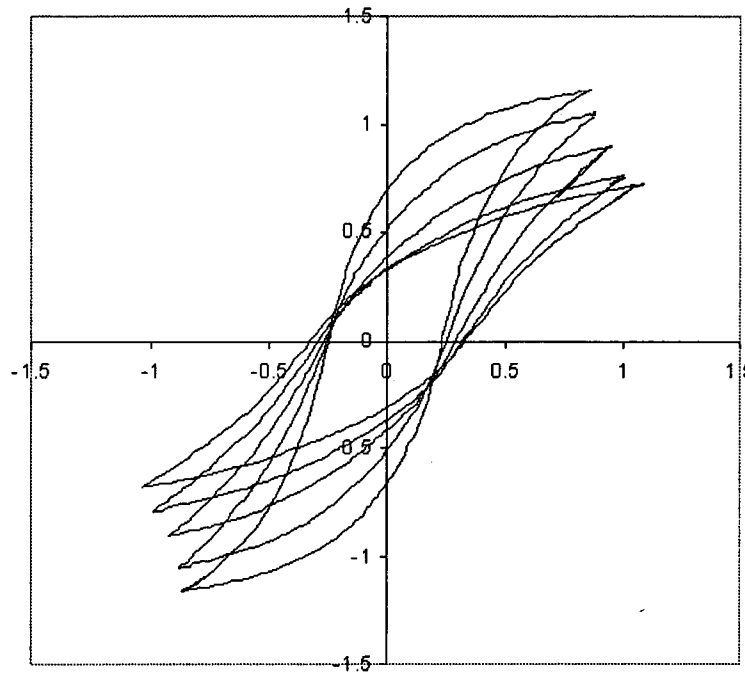

Figure 7.6: Hysteresis loops of stressed mild steel with maximum field values considerably less than the saturation field.

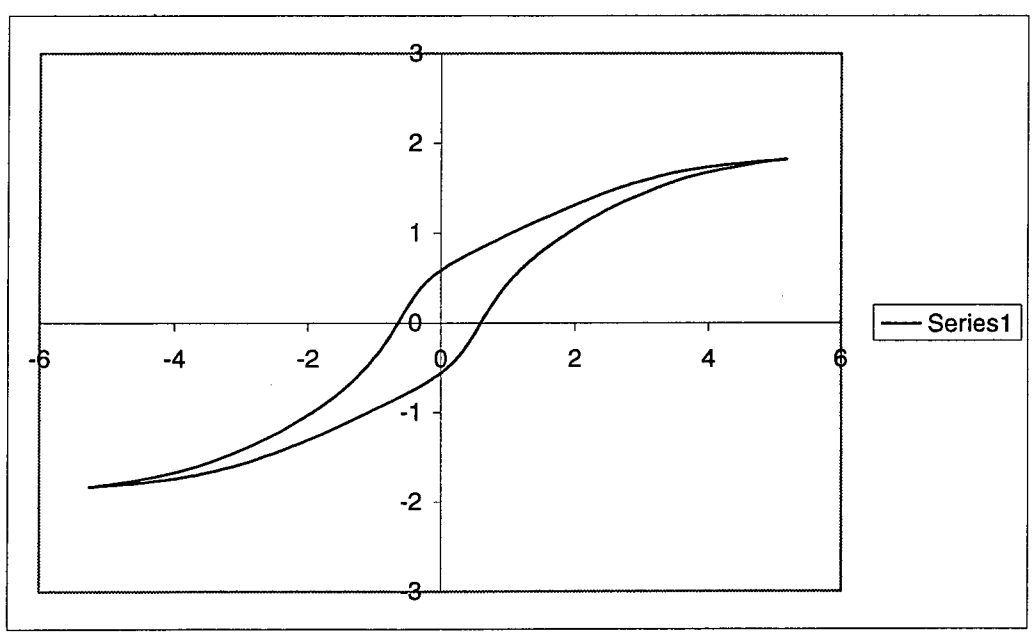

Figure 7.7: Hysteresis loop of mild steel with -120MPa along axis of magnetisation and 120MPa perpendicular to axis.

at the coincident point to be quite smooth. With the application of appropriate stresses these curvatures decrease, and, as the three points do not lie on a straight line, the discontinuity in slope becomes apparent.

As these two features are the most startling and interesting of the results, the validation of the effects was deemed to be vital. Two experiments were designed to attempt to repeat the effects using completely different and independent equipment and materials. In this way if the coincident point and kink were due to the cruciform, the stress rig, the twin U-cores, or the computer/software, and not a true feature of the material, the effects would not be present.

7.1.1 Uniqueness

A close examination of Figures (B.1) through (B.7) in Appendix B shows small, but noticable changes in the flux density at which the coincident point occurs. Each plot is for a different constant stress in the y-axis. The flux density at which the coincident point occurs seems to increase with tension and decrease with compression in the y-axis, however, the field at which it occurs remains constant. the reason for this movement is twofold.

In order to reach the "true" coincident point a full saturation loop is required. The maximum fields used in this investigation are relatively large, however they are not sufficient to guarantee saturation, thus the coincident points shown will tend to be at slightly lower flux densities than the true value. The reason for the stress dependent changes is much more subtle. The structure of the Dante program was such that the output voltage across the coils was controlled rather than the current or the field strength. This was done purely for reasons of simplicity. As a result of this fact and the geometry of the twin U-core yoke system, changes in the permeability of the sample caused changes in both the flux density B and the applied field H for the same voltage across the coils.

An increase in tension in the y-axis is equivalent to a small increase in compression parallel to the applied field (as far as the effect on B), and thus caused a reduction in the permeability in the x-direction. This corresponded to lower

flux densities but higher field strengths at the same voltage. This effect can be seen very clearly in Figure (7.6) as the maximum field strength (H_{max}) is seen to increase markedly with compression although the maximum voltage was the same for each loop. This figure also shows the fact that the flux density at which the coincident point occurs depends only on the maximum field applied.

The ultimate result of these considerations is that under the conditions the fields are applied in this investigation the flux density at which the coincident point occurs appears to be altered by stress, but this is in fact a result of stress affecting the applied field. Redesigning the software so that the applied field was the controlling factor would greatly reduce the spread of the crossing points of the hysteresis loops, and eradicate the apparent stress dependent drift of the coincident point.

7.2 Verification

The first experiment designed employed a cylindrical rod specimen of mild steel with a diameter of 20 mm and a length of 410mm. A flux sensing coil of 50 turns was wrapped around the rod. The rod was placed in a universal testing machine which would apply the (uniaxial) stresses and would also serve to provide a closed magnetic circuit (even though the machine provided a fairly low magnetic permeability path, it is significantly better than air). The magnetising field was applied using the permeameter coil described in Section 5.7, which has 550 turns and an inner diameter of 75mm. The field was measured using a Linear Hall Effect IC. The flux sensing coil was connected to an HP 8875A differential amplifier, which was in turn connected to an analog integrator, the output of which was connected to a Hewlett-Packard 7035B X-Y Recorder (plotter). The Hall probe was also amplified by an HP 8875A and connected to the X-Y plotter.

Hysteresis loops were taken at four different applied stresses, both compressive and tensile in nature. These plots were then scanned and superimposed graphically. The result of this hybrid is shown in Figure (7.8). The errors inherent in this

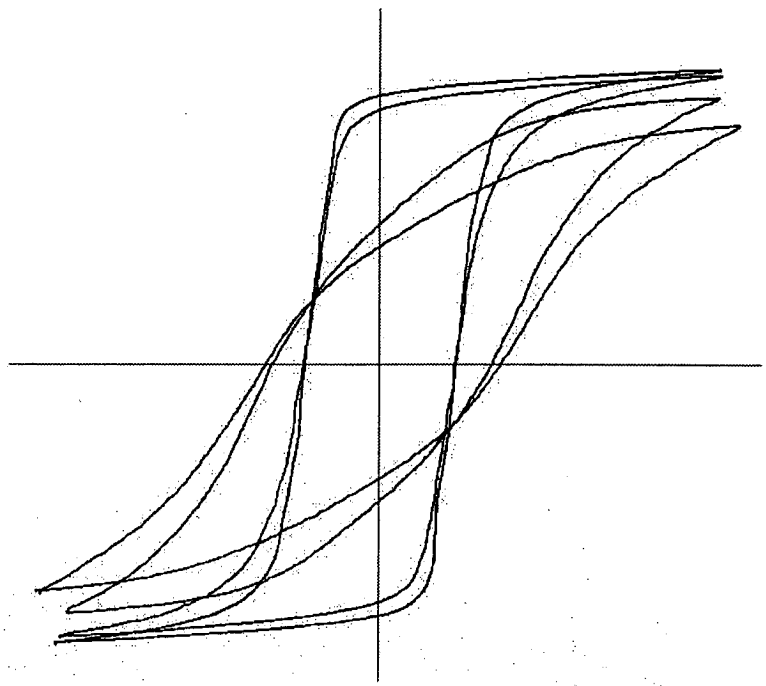

Figure 7.8: Superimpostion of hysteresis loops of mild steel rod with different applied uniaxial stresses taken using alternative equipment.

method are unfortunately much greater than using the rig and Dante software. The graphs were actually superimposed by hand and placed where they looked "as central as possible". However, the coincident point is still strongly indicated by the data.

The stresses applied were -150, -100, 0, and +50 MPa, the maximum applied field was approximately 600 kA/m, and the maximum flux density approximately 0.3 Tesla.

The second experiment designed was to use the same computer and software as used with the cruciform, but using a nickel specimen instead of mild steel. The only usable sample of nickel which could be easily obtained was, unfortunately, a length of nickel wire with a diameter of 1.5 mm. This is far from the ideal form for a specimen to take, however it was the best which could be obtained under the circumstances. The wire was cut to 430 mm in length, and had 4000 turns of fine wire wound closely around it as a flux-sensing coil. It was then placed in

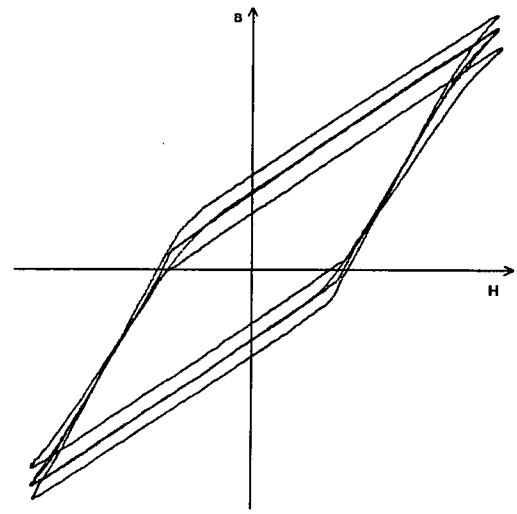

Figure 7.9: Superimposition of hysteresis loops obtained from unannealed nickel wire under different applied uniaxial tensions.

the permeameter described in Section 5.7. A Hall probe was located against the wire as closely as possible.

The end of the wire was connected to a cable which ran over a pulley, allowing weights to be suspended from it, thereby applying tension. Hysteresis loops were taken with just a support hanger suspended on the wire, a 4 lb weight, a 7 lb weight, and an 11lb weight.

The loops obtained were perfect diamonds, i.e. 4 straight lines with sharp discontinuities in slope (see Figure (7.9)). From this it was deduced that the nickel had been plasticly strained during the wire-forming process. In order to remove the internal stresses and dislocations, the wire was annealed [30] in a kiln at $(1050 \pm 10)^\circ$ for 4 hours, then allowed to cool over 12 hours.

The wire was then once again placed in the permeameter and loops obtained at the indicated tensions, these graphs are presented in Figure (7.10). It is immediately clear that the features of these graphs are different to those seen in the mild steel data. In order to obtain more detail about the features of the curves a second series of hysteresis loops were acquired with a greater maximum applied

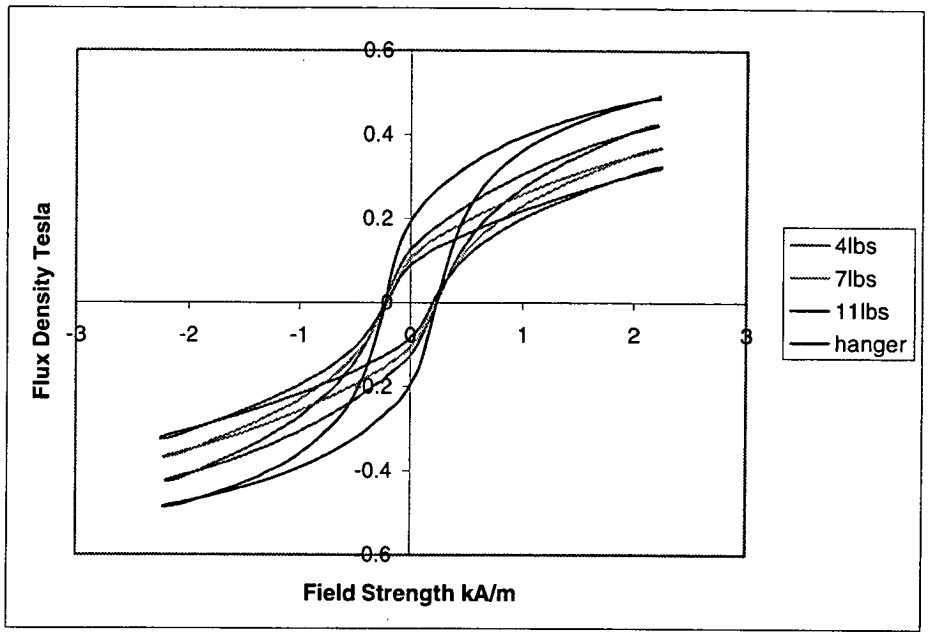

Figure 7.10: Superimpostion of hysteresis loops of annealed nickel wire with different applied uniaxial tensions at low fields.

field. These loops are shown in Figure (7.11).

In contrast with the mild steel graphs the coincident points appear to be at the coercive field in both Figures (7.10), and (7.11). The kinks which are quite prominent for tension in Figure (7.11) are in the first and third quadrants, and are not at the same fields as the coincident points, and thus occur at different flux densities for each applied tension. The kinks do appear to be occurring at the same applied field strength for each curve, however, insufficient data is presented to substantiate this.

In summary, the secondary investigations have confirmed the existence of the coincident points in mild steel and nickel, and the dramatic kink which occurs at higher stresses which result in a lowering of the flux density. The implications of these effects, and the differences between the behaviour of mild steel and nickel under applied external stresses will be discussed in Chapter 8.

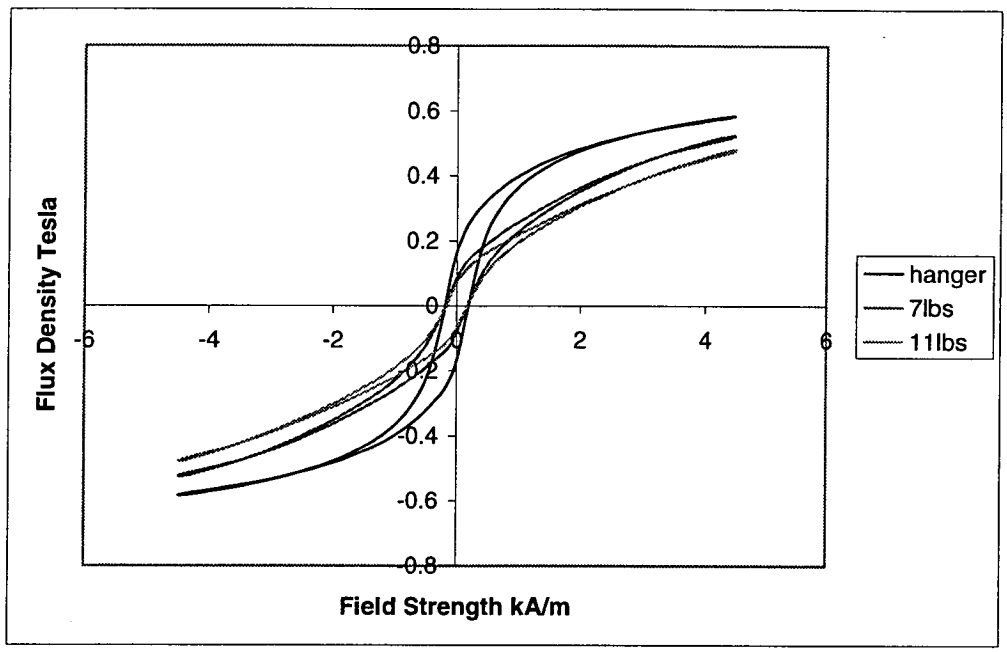

Figure 7.11: Superimpostion of hysteresis loops of annealed nickel wire with different applied uniaxial tensions at higher fields.

Chapter 8

A New Look at Magnetisation Processes

The hysteresis data obtained from the mild steel cruciform may be analysed in a number of different ways. The ways chosen were: (i) looking at individual hysteresis loops at specific stress patterns; and (ii) looking at groups of hysteresis loops at different stress patterns superimposed onto the one set of axes. The first method is good for seeing the shape of the loop, and identifying features and characteristics of the hysteresis loop at a particular biaxal stress. The second method is good for seeing changes which occur in loop shapes at different stresses, and showing points where the flux density is higher or lower at particular stresses, and where the loops intersect each other. The hysteresis loops obtained during this research have been considered in both of these ways, and the implications of the subsequent speculations documented.

8.1 Considering the Graphs

Superimposition of the Bvs$H$ hysteresis loops of steel under biaxial stress clearly shows two new features. The first is the two coincident points (Figure (7.5)) where all of the curves intersect on hysteresis loops at different stresses but identical maximum field strengths. The second is the noticeable kink (Figure (7.7)) in

the hysteresis loops with compression in the direction of magnetisation, which occurs at this intersection. It would appear that at the particular applied field (hereafter referred to as the critical rotation field, H^* [4]) at which the coincident point and kink occur, the magnetisation of the sample is essentially independent of the applied (biaxial) stress.

It seems that the mechanism which connects stress and magnetism is either not present, or rendered inactive by the application of this critical rotation field. The implications of this phenomenon regarding the mechanism by which applied stress and magnetic properties are inter-related are of fundamental importance.

It is important to note that the coincident points are not seen unless the steel is magnetised to several hundred A/m; the critical rotation field (which is approximately $\pm$200A/m for mild steel) must be exceeded by a sufficient amount (the precise minimum field was not determined, however it is certainly present with a maximum applied field of $4H^*$) before the effect is discernible. Hysteresis loops which have maximum applied fields of much less than the saturation field, but are still sufficiently greater than the critical rotation field will show the coincident point at the same field strength (H^*), but at a lower flux density (Figure (7.6)).

In the nickel wire, however, the effects are markedly different. In the data obtained before the specimen was annealed, the kink is very prominent; the discontinuity in the slope being quite dramatic (see Figure (7.9)). However, in all of the nickel data, the coincident point is clearly not at the kink point, rather it is at the coercive field (Figure (7.10)). It must be noted as well that due to the negative magnetostriction of nickel, the effect of stress is in some ways reversed from that seen in iron and steel. Tension parallel to the field tends to reduce the flux density, producing the more lentil/diamond shaped-loops seen for compression in iron and steel. Unfortunately, compression parallel to the field could not be investigated because the sample of nickel wire used was very thin.

8.2 The Magnetisation Process

In order to explain the coincident point and kink found on hysteresis curves of materials under stress, it is necessary to consider in some detail the accepted theory which explains magnetisation processes [53]. Begin by considering a small, relatively perfect crystal of ferromagnetic material in an ideally demagnetised state. The magnetisation vectors within the crystal will be oriented in such a way to form domains. These domains will be alligned with easy directions in the crystal and will form a pattern which creates closed flux paths in a way which minimises magnetostatic and anisotropy energies. If an external magnetic field is applied to this crystal the domain walls will move so that the domains with directions closer to that of the applied field will grow at the expense of the others. This applied field must exceed a certain critical value for irreversible wall motion to occur [4]. Beneath this value the walls will move slightly, or bulge, but would return to their original location were the field to be removed (the true Rayleigh region).

In a real sample of ferromagnetic material, however, the situation is complicated by the fact that theoverall structure is not a regular crystal lattice, rather it is made up of small regions, or grains, within which the structure of the crystal lattice is (relatively) perfect. Domain walls can only move across a region of relatively regular crystal structure (in the materials considered in the scope of this thesis), in which lattice imperfections cause small Barkhausen jumps or Barkhausen Noise, and domain wall "snapping" [7], [31]. At a boundary between grains, the wall will presumably be absorbed by the boundary. Once a field strength has been reached so that all walls have been absorbed by boundaries, each grain is now a single domain. All of the grains differ in size, shape, and orientation. This larger scale structure has a similar effect to domains on the bulk magnetisation of the material. That is, each grain may become a single domain at high enough applied fields, but since the grains are oriented randomly, their individual contributions to the bulk magnetisation will tend to cancel each other

out to a degree. This will result in a global magnetisation which is substantially lower than the theoretical saturation value even though each grain is saturated.

In order for this state to be reached, another effect must also play a part: the irreversible rotation of domain magnetisation, or large Barkhausen jumps [54]. A point is reached during the application of an increasing field when the field is strong enough to spontaneously snap the atomic moments from one easy axis to another. This means that instead of a wall moving gradually across a domain, slowly turning the spins as it goes, whole domains in iron and steel will change direction by 90° or 180° with all of the spins moving effectively simultaneously. Above this field strength the domain walls gradually disappear within the material, until only grain boundaries separate the "Domains".

At even higher fields the increase in magnetisation will be due to the process of reversible rotation of the spins (also referred to as magnetic moments) away from easy directions towards the direction of the applied field. The field required to rotate the spin is dependent on the angle between the easy direction of magnetisation and the field direction (which determines the magnetocrystalline anisotropy energy of the direction). Once a field strength has been reached which is enough to rotate the spin from the easy to the hard direction (ignoring precession effects) technical saturation has been reached as all spins are now experiencing sufficient field to rotate them to the applied field direction [20].

8.3 Applied Stress and Non-Easy Moments

Magnetism can be conceptualised on a number of different levels. The distinctions between these levels is somewhat arbitrary, but a guide is shown in Figure (8.1) from Hubert and Schäfer [34]. These may be simplified yet further into domain, atomic, and subatomic levels. Explanations of magnetic effects have traditionally concentrated on producing theories based in only one of these approaches. Magnetomechanics is an area in which all levels are affected, and thus a theory needs to consider responses to models at each level of complexity, and ideally

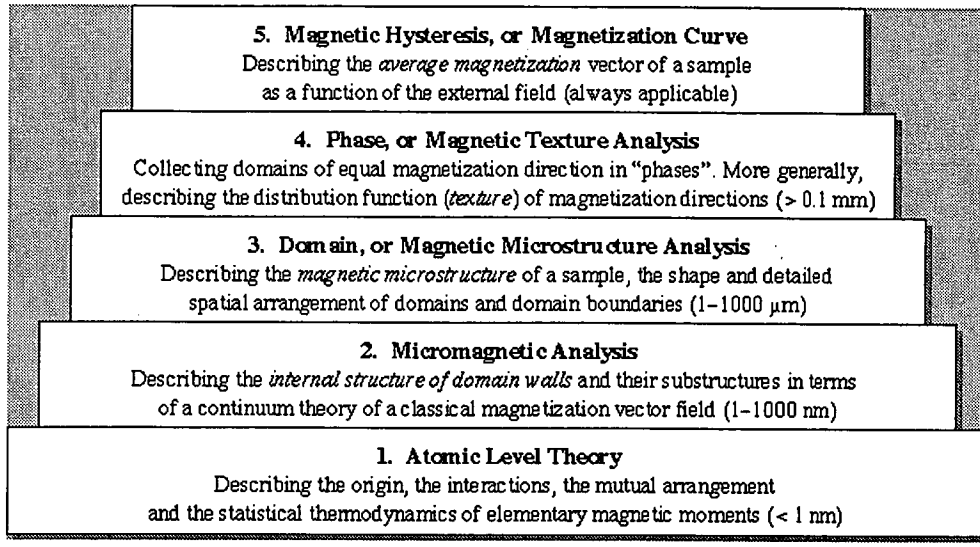

Figure 8.1: Qualitative comparison between different domain observation methods [34].

evolve smoothly from one to the next. For this reason the following hypotheses are explained in terms of domains, crystals, and quantum mechanics, so that the features of the model can be understood from each of these view points.

8.3.1 Domain Walls

When a mechanical stress is applied to a sample, its magnetic behaviour can change dramatically. In iron and steel, compression in the field direction makes magnetisation harder, whilst tension initially makes it easier [3] [50] [60]. These effects will now be explained primarily in terms of the structure of domain walls, rather than their movement as previous explanations have done. [12]

Domains form within a region of coherent crystal lattice and orient themselves in directions of easy magnetisation, which is parallel to the lattice sides in iron and steel [11] [67]. A domain wall consists of gradual rotations of the atomic magnetic moments away from one easy direction towards another (Figure (8.2)shows a 180° wall). In a 90° wall none of the spins within the wall will lie in easy directions. In a 180° wall the centre of the wall will lie in an easy direction but the rest of the wall spins will all be in non-easy directions. The 180° domain wall stretches over

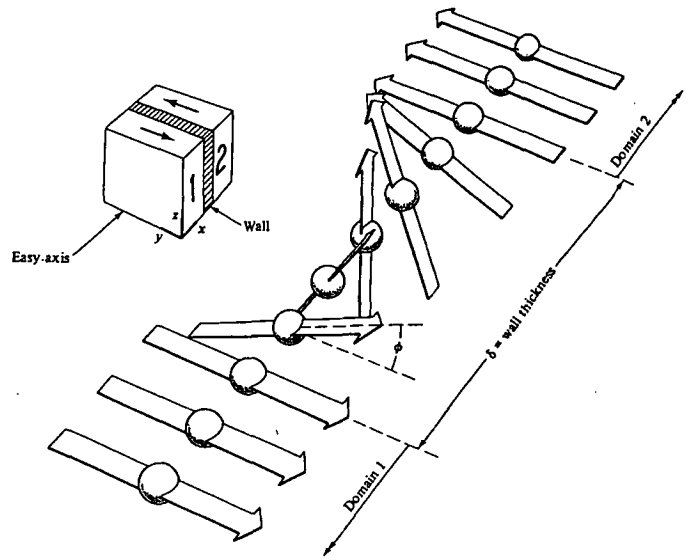

Figure 8.2: Schematic of spin rotations in a 180° domain wall [23].

hundreds of atoms and so almost all of the moments associated with the wall will be aligned in non-easy directions. The spins in a wall are in a way analogous to the reversible rotations of moments within a domain that are induced by large applied fields against the opposing anisotropy forces.

Domain walls exist in order to reduce the total exchange energy across a transition of magnetic moments between domains, by spreading this transition over many atomic sites. Note that a domain wall is not "needed" at a lattice boundary as the spin-spin interaction across a grain boundary is very weak, and the domains can be oriented in different directions while maintaining a low exchange energy [70]. Anisotropy and magnetostatic energy can also be kept low as the global directions of the easy axes of the two grains are unlikely to be parallel. Thus, the atomic moments can be non-parallel across the boundary with little or no increase in the total energy.

8.3.2 A New Hypothesis

Applied stresses distort the crystal lattice. For a cubic lattice this means that the ⟨100⟩, ⟨010⟩, and ⟨001⟩ directions are no longer all perpendicular. Depending on the orientation of the lattice with regards to the applied stress, the angles between the easy directions will increase or decrease, and the relative separations of the atoms will also change. Any non-easy-aligned spins will be affected by these lattice distortions as the energies determining their orientations are determined by the angles they form with the lattice directions. In this way the energy associated with the position of a non-easy-aligned spin is determined by its magnetic anisotropy, which is dependent on the relative angles the moment forms with respect to the three crystallographic directions, and which is also critically interdependent on the exchange energy (see Section 8.4). When the axes and the atoms move relative to each other the changes in anisotropy energy and exchange energy modify the energy required to keep the moments pointing in any given direction. This is of fundamental importance to the magnetomechanical effect.

As domain walls are effectively groups of non-easy-aligned moments, they will be affected by applied external stresses. Wall motion will occur for 90° walls as the effective "pressure" on the the wall caused by the applied stress will be in one direction only. The pressure on 180° walls will be on both sides of the wall but in opposite directions, and so the thickness of the wall will change slightly, but its position will not alter. In the demagnetised state this process alone will not cause magnetisation, as the net magnetisation will remain zero. In iron and steel when the specimen has a non-zero net magnetisation, the stress will affect the magnetisation as it will reduce (compression), or increase (tension) the size of favourably-oriented domains via the movement of 90° walls.

Hysteresis Loops

The behaviour of the material is different again once it has been magnetised and is on the hysteresis loop [40]. As the magnetisation of the material moves along the major hysteresis loop from the tip of the loop in the first quadrant to the negative

coincident point in the second quadrant the applied field is first reduced to zero, leaving some non-zero, positive internal field (the remanence). This internal field is sufficient to maintain some reversible rotation of magnetic moments. As a negative field of increasing magnitude is applied, the point is reached where the net field experienced by the magnetic moments is insufficent to maintain reversible rotation. The net magnetisation of the material is still positive, as it is the sum of the internal and applied fields; however, no magnetic moments are experiencing sufficient field strength to overcome the net anisotropy (crystal, stress, etc.) and thus are aligned in the easy directions which are closest to the direction of the original field. Thus no domain walls will exist within the grains. At this point, there are no non-easy aligned spins, and so the magnetisation is independent of the applied stress, and dependent only on the history, temperature, and applied field. Thus, all hysteresis curves of that sample with the same history, temperature, and field strength will coincide at that point no matter what stresses are applied to the sample.

Measurement shows that the coincident points also occur on loops which have lower maximum applied field values; however, these points will be at successively lower flux density values. At these points 180° domain walls will presumably be present within the material, thus lowering the global flux density, but the magnetisation of the material will still be independent of the applied stress as 180° walls are not affected by stress.

At fields greater than the critical rotation field, reversible rotation will begin taking spins away from the easy directions and so the sample will once again be affected by stress. The greater the number of easy directions which are closely aligned to the field, the more dramatic this change will be. In a sample with all easy directions aligned with the field, a hysteresis loop of the form shown in Figure (8.3a) would be expected [21]. This shows no reversible rotations occurring, and ideally no 90° wall motion; the magnetisation process is carried out purely by 180° irreversible domain rotation. If however, only hard directions were aligned with the field a loop of the form shown in Figure (8.3b) would result. This corresponds

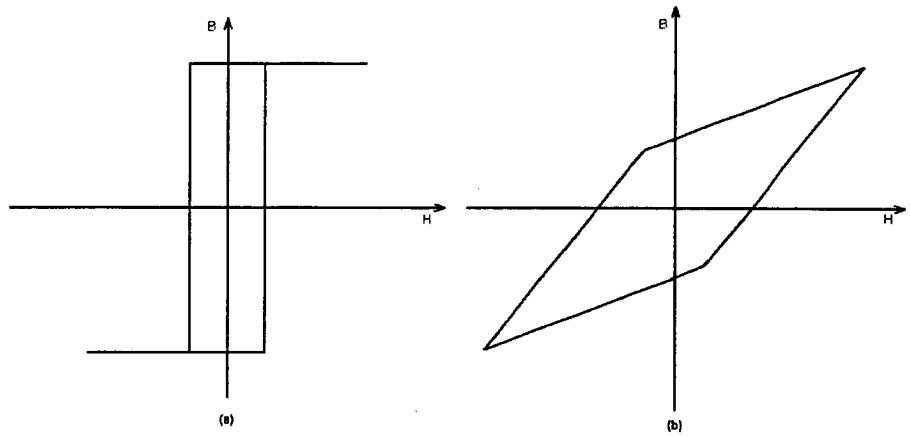

Figure 8.3: Hysteresis loops for ideal materials with (a) all easy directions aligned with the applied field, and (b) all hard directions aligned with the field.

to an arrangement where all magnetisation is due to reversible rotation; from positive saturation to $-H^*$, the moments are rotating back to an easy direction. From $-H^*$ to negative saturation the rotation is from the easy direction to a hard direction, but through a greater angle.

An important question is: why does the slope of the loop change at this point, particularly in the x-direction compression loops? A possible answer is, that it is a matter of degrees. Consider a simple non-stressed crystal unit with a magnetic moment directed along the [111] direction due to an applied field in the z direction, Figure (8.4). Removal of this field and application of a negative critical rotation field will rotate the moment to the [100] direction. Within a single cycle of applied field from positive to negative to positive again any particular magnetic moment will rotate in one plane only describing a flat circle. This is the lowest energy path which the moment can take. The anisotropy energy associated with the [111] direction is the same as that associated with the $[\overline{1}\overline{1}\overline{1}]$ direction, yet the angle through which the moment must rotate from the [100] direction to the $[\overline{1}\overline{1}\overline{1}]$ direction is much greater (125.3°) as opposed to the angle between the [111] and the [100] directions (54.7°). This means that a given change in field strength in the $-z$ direction will result in a percentage change in angle equivalent

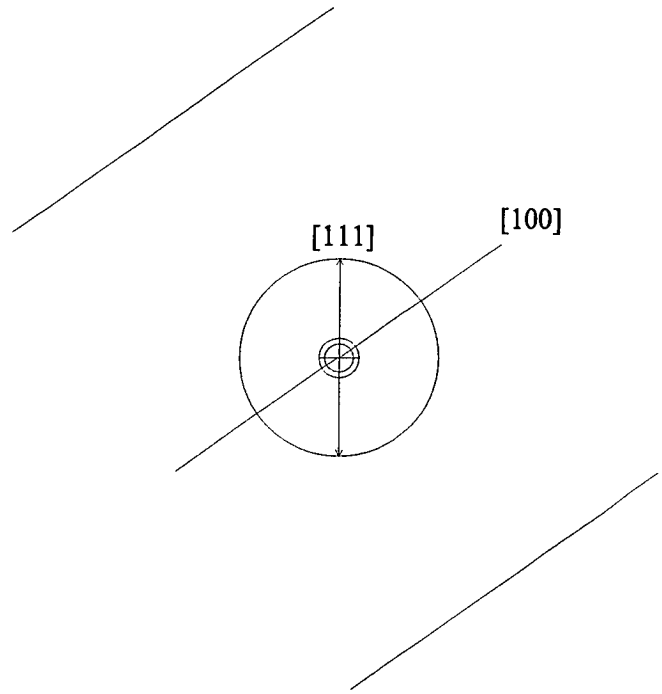

Figure 8.4: Schematic of the {110} plane in a cubic crystal, and the rotation of a magnetic momentaround a major hysteresis loop.

to the percentage change in the z direction, however the magnitude of the change in angle will be greater in the [100] to $[\overline{111}]$ transition due to the larger total change. As the change in flux density is purely a function of the change in angle of the magnetic moment, an increase (negative) in the magnitude of the applied field in the [100] to $[\overline{111}]$ region will result in a greater change in B than would result in the [111] to [100] region. Thus the slope of the curve is steeper in this region of the curve. The proportions of the changes in flux to angles would only be equivalent in an ideal crystal at appropriate fields.

The Stoner-Wohlfarth model uses an ideal crystal with 90° between the easy and hard axes and thus does not show these effects. The hysteresis loops produced by this model are symmetrical and are linear for the hard direction. Such a model though useful in many respects, does not give a very accurate representation of iron or nickel as the assumptions made regarding the properties of the crytals and domains are inaccurate.

In real-world samples there is a distribution of lattice directions due to each grain having its own orientation with relation to applied fields or stresses. This will result in the curved hysteresis loops which are more familiar. Externally-applied stresses will cause an iron or steel sample to behave as if it has either more (tension) or fewer (compression) easy axes aligned with the applied field due to stress-induced anisotropy. As the anisotropy energy of each particular direction changes, the field required to force the magnetic moments towards that direction also changes. Thus, the number of magnetic moments which are experiencing sufficient field to become aligned with the applied field is dependent on the stress. At some fields, 90° and 180° wall motion will occur simultaneously with reversible rotation in different grains depending on their orientation. Inclusions, dislocations and different internal stresses will all combine to smooth out the curves under most conditions.

During an initial magnetisation there are many domains and walls in the material, and the closure domains are some of the last to be removed. Thus, all walls may not have been swept from the material (particularly if compressed) when the critical rotation field is reached. There may also be a region on the initial curve where both rotation and wall motion processes are active. For these reasons the coincident point does not appear on the initial curve.

8.3.3 Nickel

In nickel the processes involved are similar, but important differences produce results which are markedly different from iron and steel. Nickel has $\langle 111 \rangle$ easy directions, which means that it can have 71°, 109°, and 180° domain walls. The walls which are affected by stress are the 71° and 109° walls. If, for example, the applied field were parallel to the [100] direction (hard), when the field was reduced and brought to the kink point, all moments would be in easy directions. However, the easy directions closest to the field direction are [111], $[1\bar{1}1]$, $[11\bar{1}]$, and $[1\bar{1}\bar{1}]$ therefore the sample will contain only 71° and 109° walls, and still be very dependent on any applied stresses.

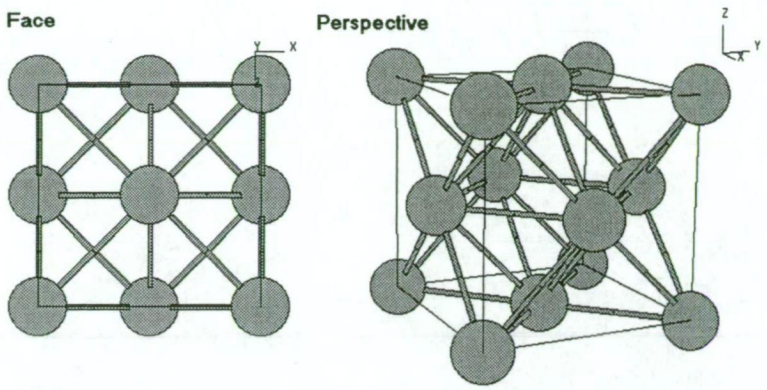

Figure 8.5: Schematic diagram of a face-centred cubic crystal unit.

When the field reaches the negative coercive value an amount of 180° rotation has occurred due to wall motion so that the number of moments in the [111], $[1\bar{1}1]$, $[11\bar{1}]$, and $[1\bar{1}\bar{1}]$ directions is equal to the number in the $[\bar{1}11]$, $[\bar{1}\bar{1}1]$, $[\bar{1}1\bar{1}]$, and $[\bar{1}\bar{1}\bar{1}]$ directions. This will ideally result in all of the walls being 180° walls, and therefore the magnetic properties of the material will be independent of any applied stresses. If however, the applied field was parallel to the [111] direction, a loop of the shape shown in Figure (8.3a) would result, as magnetisation would only be a result of 180° rotations.

The fact that the response of nickel is opposite to that of iron and steel in some respects is partially due to the fact that the easy and hard directions are reversed. Therefore, stresses which result in alterations to the crystal lattice structure which favour either the ⟨111⟩ directions, or the ⟨100⟩ directions will naturally have opposing effects in the materials.

8.4 Spins and Lattice Mechanisms

An externally applied stress does more than apply an effective pressure on domain walls; it also alters the relative positions of atoms within the lattice. The interactions between nearest neighbours in a metallic crystal like iron are very complex. The fundamental relationships [23] are shown in Figure (8.6), these being the Spin-Spin, Spin-Orbit, Spin-Lattice, and Orbit-Lattice interactions. The

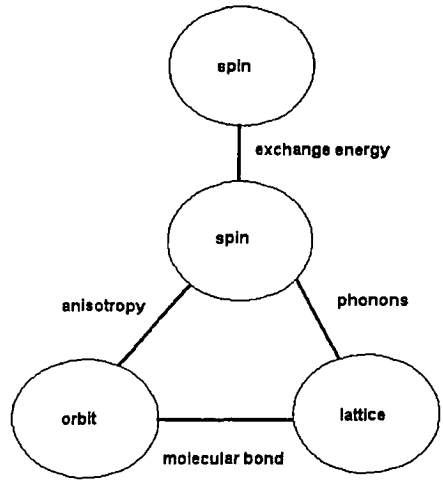

Figure 8.6: The fundamental relationships within ferromagnets.

key relationship which forms the basis of ferromagnetism is the Spin-Spin interaction, which depends on the exchange energy (or exchange force). The exchange energy is most commonly presented [23] in a form similar to

$$E_{\text{ex}} = -2J_{\text{ex}}\mathbf{S}_i \cdot \mathbf{S}_j = -2J_{\text{ex}}S_iS_jcos\phi, \tag{8.1}$$

where J_{ex} is the exchange integral. This is essentially the Heisenberg model of ferromagnetism [23] which can be determined via the Heitler-London approximation [38].

The analysis of atoms heavier than hydrogen is currently beyond modern physics so problems are generally simplified to smaller hydrogen-like systems, and therefore, such systems will be considered in the remainder of this section, as a result numerical estimates relevent to iron and other heavy elements are not possible. The spin of a two-electron system is dependent on the singlet-triplet energy splitting. When the two nuclei are far apart, the ground state describes two independent atoms and is therefore fourfold degenerate. When the atoms are closer together, there is a splitting of the fourfold degeneracy due to interactions between the atoms [2]. However, this splitting is small compared with the other excitation energies of the two electron system, and analysis is often simplified by ignoring the higher states, thus representing the molecule as a simple four-state system. Within this system an operator is defined, known as the Spin

Hamiltonian

$$H^{\text{spin}} = -\sum J\mathbf{S}_1 \cdot \mathbf{S}_2, \tag{8.2}$$

whose eigenvalues are the same as those of the original Hamiltonian within the four-state manifold, and whose eigenfunctions give the spin of the corresponding states.

It is important to note that the coupling in the Spin Hamiltonian depends only on the relative orientation of the two spins but not on their directions with respect to the locations, or separation of the atomic nuclei. This is a consequence of the spin independence of the original Hamiltonian, and holds without any assumption about its spatial symmetry. Terms that break rotational symmetry in spin space, such as dipolar interactions or spin-orbit coupling, must be included in the original Hamiltonian in order to produce a Spin Hamiltonian with anisotropic coupling.

It must also be noted that for only products of pairs of spin operators to appear in equation (8.2), it is necessary for all magnetic ions to be far enough apart that the overlap of their electronic wave functions is very small.

8.4.1 Implications for the Magnetomechanical Effect

A consequence of these considerations is that the exchange energy, which determines the strength of the spin-spin interaction, is actually dependent on both the relative separation, and relative orientation of the atomic nuclei about which the electrons are orbiting. Therefore, so is the spin-orbit coupling which determines the magnetocrystalline anisotropy. Consequently, externally applied stresses may also alter the energies determining the number, and locations, of domain walls, as well as the anisotropy energies for given crystallographic directions.

Stress-induced anisotropy which favours one easy direction above another is in part caused by an asymmetry of the overlap of electron distributions on neighbouring ions [42]. Due to spin-orbit interactions, the charge distribution of an ion is spheroidal, not spherical. This asymmetry is linked to the direction of the spin, so that the rotation of the spin directions relative to the crystal axes changes the exchange energy and also the electrostatic interaction energy of the charge

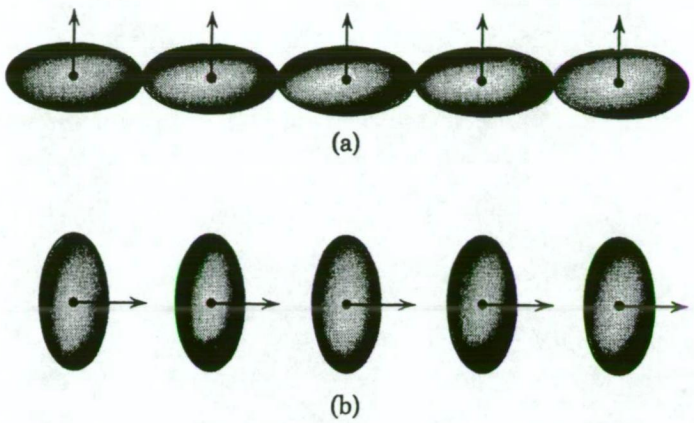

Figure 8.7: Anisotropy of easy directions leading to magnetomechanical effects and magnetostriction [42].

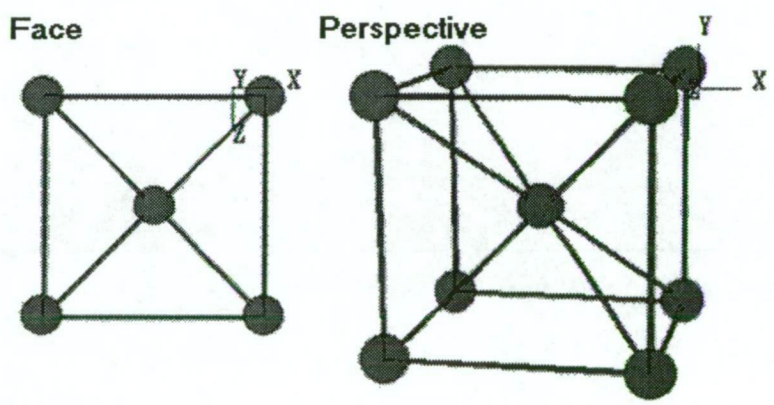

Figure 8.8: Schematic diagram of a body-centred cubic crystal unit.

distributions on pairs of atoms. Both effects give rise to an anisotropy energy. In Figure (8.7a) the relative values of the interaction energies between ions is not the same as in (8.7b).

8.4.2 Iron and Steel

Applied stresses will distort the structure of the crystal lattice. As the energy required to maintain the orientation of a non-easy-aligned spin is dependent on its angular separation from the easy axes, the orientation will change as the lattice distorts. As the atomic spacing changes so do the forces acting on non-easy-

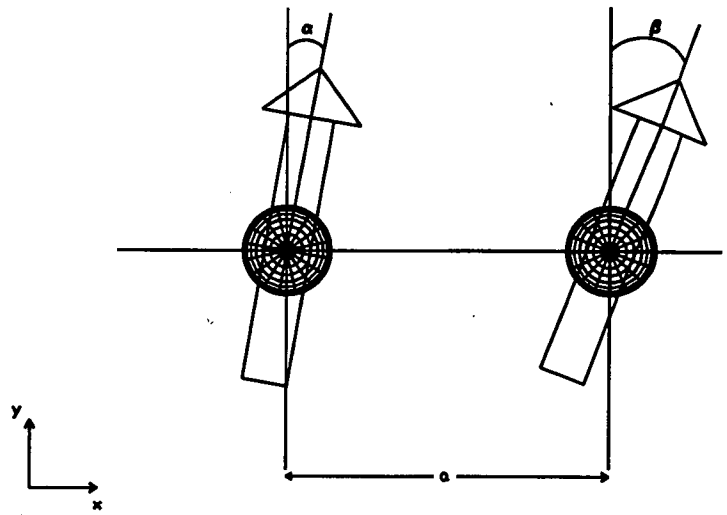

Figure 8.9: Adjacent spins in a domain wall.

aligned magnetic moments. Consider a 90° wall region where two adjacent spins are not parallel due to the gradual rotation present in a domain wall (Figure (8.9)). There are a number of forces on the spins which are in equilibrium in the absence of an external field or applied stress.

If an external stress were applied so as to minutely reduce the atomic spacing to some distance $l < a$, where $l \equiv a - \Delta a$, the directions of the spins would in turn alter to bring the arrangement back into a state of equilibrium. In this case the difference between the angles α and β would be reduced since the spin-spin interaction would have an increased effect which tends to force the two spins closer to parallel in direction. As this effect would also be occurring on all such pairs of non-easy-aligned spins, the overall consequence of the applied stress would be to move this particular wall in the direction of positive x until a stable energy configuration is reached, thus increasing the size of the domain which is oriented in the y direction. An applied stress which would achieve this in iron or steel would be either tension in y or compression in x.

8.5 Implications

Once the coincident point was discovered a satisfactory explanation of the effect was sought. It is apparent that the magnetic properties of the material become independent of the applied stress under these conditions. It is also generally accepted that stress applies an effective pressure on 90° domain walls. Therefore it seems reasonable to deduce that no 90° domain walls are present in the material. The nature of domain walls then became the focus of the investigation.

If one considers a domain wall as a series of non-easy-aligned magnetic moments (Figure 8.2), and acknowledges the preferential directions created by stress, then it is a logical step to assume that applied stresses might only affect non-easy-aligned spins such as those found in domain walls, and in materials in very high fields. This implies that no 90° domain walls, and no reversible rotations are present at the coincident point. If the loops are then considered with this in mind, it would appear that the critical rotation field is the field required to produce an irreversible rotation of the magnetic moments (or large Barkhausen jump).

The key features of a hysteresis loop are generally considered to be the saturation point, the remanence, and the coercive field. The kink in a compression loop is a feature which may be determined quite accurately when a number of B vs H loops are superimposed on each other, as it occurs at the same field as the coincident point (in iron and steel).

There are essentially two mechanisms working together to create the magnetomechanical effect. The first is simply the change in exchange energy which leads to an anisotropy between the easy axes (Figure (8.7)) thus applying pressure on 90° domain walls for iron and steel. The second is related to this effect, but is subtly different: that being the relative changes in the anisotropy energies for each direction, which may change the directions which are easy or hard (different materials and conditions will determine the limits of this).

The application of tension in iron or steel alters the shape of the hysteresis

loops, tending to make them more square. The implication is that if sufficient tension were applied, ultimately the stress-induced anisotropy would overcome the magnetocrystalline anisotropy and a square-loop could be obtained from a sample with ⟨111⟩ directions parallel to the applied field and tension. This assumption would require the reaction of the material to be linear with tension up to the required stress. The response of metals to stress is of course not a simple linear relationship at all values. The response may be elastic or plastic and the material will fail at high enough stresses. It is a simple task to determine if sufficient stress may be applied to a metal for stress-induced anisotropy to rival the magnetocrystalline anisotropy. In fact this has already been determined by Cullity [23] who derived the equation for the anisotropy constant

$$K_\sigma = \frac{3}{2}\lambda_{si}\sigma, \tag{8.3}$$

where λ_{si} is the isotropic mgnetostriction, and σ is the applied stress. For the crystal and stress anisotropies to be equal

$$K_1 = \frac{3}{2}\lambda_{si}\sigma, \tag{8.4}$$

thus the stress required for this to occur is

$$\sigma = \frac{2K_1}{3\lambda_{si}}. \tag{8.5}$$

For nickel this stress is $\approx$ 105 MPa, which is relatively easily attainable, however for iron the stress is $\approx$ 4600 MPa which is about ten times the fracture stress of iron and is therefore unattainable.

Chapter 9

Conclusion

9.1 Review of Thesis

The intention of this chapter is to summarise the results obtained, and to re-appraise the successes and shortcomings of the theory introduced in the earlier chapters.

Chapter 2 introduced the reader to the important basic concepts of magnetism which were required to understand the developments in subsequent chapters. Chapter 3 was a review of the literature which deals with the magnetomechanical effect including experimental methods and results, and theories. The general result of this review was that there is good understanding of what to expect when ferromagnetic materials are stressed, but that very little exists which gives much insight as to why materials behave in these ways. There are many good models which explain magnetomechanical effects, and systems for predicting these changes; however, most work is empirical in nature, based on numerical models rather than fundamental theory.

Chapter 4 is the beginning of the sections which cover the work done in this investigation. The concepts dealt with in this chapter could be considered to be controversially obvious as the normal magnetisation and the initial magnetisation curve are equated. This chapter contained a miniature literature review of its own which detailed the history and evolution of the two curves, or rather the

two methods of obtaining the same curve. Although the two curves have been considered to be equivalent by many respected researchers in the field, there are also areas of experimental magnetism which have inherently assumed the two to be different. The experimental data presented in this chapter strongly support the proposal that the two methods do indeed produce identical data sets for the materials considered. Some of the implications and ramifications of this suggestion were considered. Chapter 4 is the justification for presenting data in the initial magnetisation curve format later in the thesis.

Chapter 5 is a detailed description of the equipment, hardware, and electronics used in the experimental phase of this research. Most of the equipment used is not based on new concepts, but uses proven methods of obtaining stress and magnetics data, even if this particular combination of techniques has never been used before. The twin U-cores, or yoke method of applying a magnetic field to a sample has received some critisism from various sources, but all methods have their own inherent shortcomings. The errors introduced by the yoke system are considered acceptable under the conditions and limitations imposed by other factors in the system [5] [72]. The sample sizes and shapes were limited by what was required by the Australian Defence Science and Technology Organisation, and by the physical constraints imposed by the Belle-Wrigley rig which already existed at the start of this research. The intention of Chapter 5 was to provide the reader with a fundamental understanding of all of the limitations and features of the system used, so any effects which may be due to the equipment may be foreseen. With the aid of the information presented here the experimental procedures could also be replicated by others in order to verify the results presented later.

Chapter 6 follows on from the hardware chapter to present the software which was written to control the data acquisition and the magnetising field. Due to the graphical nature of the LabView language "G", it was impossible to present the code of the program on 2-dimensional pages of this size in any decipherable manner. Instead of the code, the steps which the software takes, the speed at which it acts, the response times, and the voltage values considered at the

inputs and outputs were listed. In this way the effects of the program may be determined, and the limitations of the system can be seen. The calculations performed by the program were also presented so that numerical procedures and methods are transparent. From these details software could be written which performed identical tasks at the input and output of any system and the data presented to the user would be the same as was obtained using the Dante package even though the individual tasks performed may be completely different.

Chapter 7 presented a sample of the data obtained during the research, and detailed the steps taken during its acquisition. The evolution of the research was quite fluid as the results from one approach were analysed and new questions subsequently raised before the next step was designed. The full set of data for the mild steel cruciform is presented in Appendix B, so only examples which show the salient features of the data were required here, as in general the differences between one curve or loop and the next is very subtle. Bvs.H loops and curves were also shown for a rectangular section of mild steel plate, a stressed mild steel bar, and stressed loops taken from a length of nickel wire. All of this data is compared in order to interpret the features found on the loops and curves produced.

Chapter 8 is considered the most important chapter in the thesis as it contains the detailed analysis of the results of the experimental phase of the research. The new features of stressed major hysteresis loops which were introduced in this chapter were, as far as the author is aware, previously unknown. The kink in the compression hysteresis loops which occurs at the coincident point common to all stressed major hyteresis loops was immediately recognised as the manifestation of some crucial mechanism of the magnetisation processes on the symmetric loop. The task of explaining what was occurring at this point took considerably more time. The mechanism by which stress and susceptibility are linked needed to be rendered inactive by the application of this particular field. Even then the mechanism needed to be such that it explained: (i) the behaviour of iron when stressed in different directions; and (ii) the negative magnetostrictive behaviour

of nickel. Many preliminary hypotheses were discarded by the author as flaws in them were discovered.

Finally, the hypothesis chosen as by far the most robust was that which linked the exchange and anisotropy energies, and proposed that magnetic moments aligned in easy directions (in iron and steel) are independent of effects caused by the application of external stresses. Much of the extra experimental research outlined in Chapter 7, Results, was in fact designed to test this hypothesis, which proved to withstand all assaults and even predicted some of the effects seen in nickel.

The implications which this theory has on our understanding of the magnetisation and hysteresis processes are many and varied. The evolution of domain patterns during field changes is given new insight. Methods of determining stress-independent properties of materials in non-destructive testing are possible as the H and B values of the coincident/kink point may be unique to different materials. Divergence from these values may indicate plastic straining of the material. Equations for predicting the hysteresis loops of materials could possibly be determined from the saturation points, the coincident/kink points, and a statistical evolution of the curves connecting them as percentages of the $\langle 100 \rangle$ shape and the $\langle 111 \rangle$ shape. In fact, once the coincident point is found the remanent point alone may provide enough information to deduce any strain in the material.

Although the possibilities are very promising a great deal of work is yet to be done to support the theory. Considerably more numerical verification is required before the theory could even be considered to be complete and ready for testing. It may well be that some of the assumptions which have been made regarding interactions are not viable, however, the testing of them was not possible using the equipment available, nor was there sufficent time to thoroughly address all concerns.

Further research which would be of much interest could include experiments where a sample was magnetised and cycled on a symmetric hysteresis loop, and the field then paused at the critical rotation field and a change made in the applied

stress. The resulting change in flux density (if any) would certainly provide considerable information about the magnetisation mechanisms. Extending the research already done to include a greater variety of metals and alloys would also be of considerable benefit.

The development of an equation, even one empirical in nature, based on this theory could be of much practical benefit also. The amount of data required to produce the necessary values for inclusion is relatively small and easy to obtain, and therefore would make empirical models quite simple to construct.

There are still many facets of the theory and model presented here which need further investigation. Correspondence with the Jiles-Atherton model [36] seems to be missing, although that model is based more on constant field and changing stress when predicting magnetomechanical changes. A theoretical analysis of the concepts involved would also be very useful in providing supporting evidence as many areas have been dealt with at a very conceptual level in the development of these ideas.

It is sincerely hoped by the author that the work presented here will provide new insights into the understanding of the magnetomechanical effect and ferromagnetics in general.

Appendix A

Problems Encountered

The technical requirements of this project were substantial. Although each individual task was not necessarily a new development, the integration of many different pieces of equipment and software was required. Many of the tasks performed had not been attempted with the equipment available, and therefore many complications arose which had not been foreseen.

Although the means by which these hurdles were overcome is not essential to the understanding of how the project was carried out, a discussion of some of the solutions provides an insight into the complexity of the task as a whole.

The problems can be neatly divided into two areas; these being hardware related, and software related. The segregation is not quite this simple as many problems arose due to combinations of the two, however the solutions generally lay in only one of the two areas.

A.1 Hardware Difficulties

The very first task in the project also provided an introduction to the sorts of difficulties which would have to be overcome. The design and construction of the cube was an excellent example of combining theoretical requirements with practical ones. A low-field volume needed to be created which was large enough to contain the Belle-Wrigley rig, yet the structure needed to be small enough

to fit into a room, and (when dismantled) be transportable. The inner region also needed to be easily accessible so that the Belle-Wrigley rig and the specimen could be reached during operation.

The 3-coil system was chosen over the traditional Helmholtz pair as the design offered a larger volume of homogenous field for the given diameter of the coils. It also enabled the true cubic shape to be used as Helmholtz pairs need to be one quarter of the side length from each face, greatly complicating the 3-axis structure. The 3-coil system also leaves a large amount of unobstructed floor space inside the cube, and a sphere with the same diameter of the coils completely empty. Access to the inside of a 3-axis Helmholtz system is difficult as the coils are all close to the centre. By making the support structures of the central coils of each 3-coil group small and flexible, a very large easily accessible work environment is created.

The design of the cube also allowed it to be dismantled easily into six squares and three hoops, each approximately 2.4m across, which would fit diagonally through a standard doorway. The six sides of the cube were held together by brass screws, but each side was independently removable. The hoops were suspended from craftwood hangers and fine cord, and could easily be pushed aside or completely removed to allow free access, or to dismantle the cube.

A table/stand was also specially constructed from non-magnetic materials which supported the Belle-Wrigley rig centrally, yet allowed the two horizontal-axis central coils to be removed without moving or lifting the stand. The table also functions as a manger for christmas plays when tipped on one side.

Another of the obstacles encountered was the inadequacy of commercially available strain-gauge amplifiers. A professional strain gauge conditioning board was purchased to provide both the 5 volt supply, and an amplifier and filter for the signals. The amplification had a gain factor of 10, and the filter a cutoff frequency of 1000Hz. The conditions under which this piece of equipment was designed to be used are unknown. However, for this application, these specifications proved to be completely inappropriate. In general the strains measured were static or at

least changing very slowly, and the majority of the ambient electrical noise was at 50Hz. For these reasons a 1000Hz filter is useless, 10Hz is more appropriate.

The signals from the gauges were also quite small and a considerable length of cable lay between the amplifier and the data acquisition board, thus a greater amplification would be desirable, for example a gain of 1000. The commercial board was soon discarded and a supply/amplifier/filter was designed and built which better suited the applications for which it was required.

One of the earliest computer glitches encountered was the limitation of the PC30 boards regarding interrogation frequency. Once one input channel is being interrogated by the software at a particular frequency, the other channels cannot be monitored at different frequencies. As the input and output functions needed to occur at different frequencies, separate boards were required for the input and the output. Similarly, the strain data acquisition was occurring at yet another frequency, and so another another board was required for this task. However, no more appropriate ISA slots were left in the acquisition computer, so a second computer needed to be used to house the third PC30 board. As a result of this the software needed to be altered and a separate strain data package written.

A.2 Software Difficulties

As a result of the two separate boards being used in the magnetics computer at two different frequencies, two independent functions were required to control the data flow. This made for many complications in the programing for it was essential that the input and output run synchronously.

If the input and output instructions are part of the same function it is easy to determine any particular data point relative to the output which corresponded to that point. However, if the functions are separate there is no cross-indexing to link an output command to an acquired data point. This makes tasks like producing a normal magnetisation curve difficult as the point which was obtained at a peak applied field can be found only by considering the acquired data. To

do this the entire data set (a 2xN array) has to be broken up into subsets each with the data from one cycle only, and the minimum and maximum points taken from each subset to create the full normal magnetisation curve. The problem is; how many points are there per cycle? In an ideal system that would be a simple calculation, however computers do many things beneath the surface which can affect the speed at which commands are executed. This can result in tasks not occurring at the frequency at which they had been instructed to run.

If the data subsets are too small (i.e. less than one cycle) the peak(s) may not be included. If the subsets are too large two peaks may be included, only one of which would be foundleaving the next cycle-set without that peak. It is essential therefore that a procedure be used which will correctly recognise data points.

A side effect of these requirements is that the computer has to be fast enough, and powerful enough to do all of its assigned tasks without them interfering with each other. It was for this reason that the dual processor Pentium II 350MHz machine was chosen. Initially a single processor 166MHz machine was to be used but it was noticed that the output waveform did not run at the requested frequency but approximately 10% lower when the input functions were also running, as the processor was not powerful enough to perform all tasks required.

One of the benefits of having the input and output functions separate was the ability to run them independently, thus greatly increasing the flexibility of the software. The computer could then be used as a digital oscilloscope with recording, processing, and spreadsheet functions when only the input was running. It could aslo perform as a function generator with active feedback monitoring. These features enabled the parts of the software to be tested independently when determining their accuracy, and verifying the results obtained.

One of the more physical problems which had to be overcome during the research was that posed by eddy currents. Due to the relative thickness of the samples used, quickly changing fields will induce eddy currents beneath the surfaces of the specimens which will tend to shield the interior. By only using very slowly changing fields (i.e. less than 1Hz at relatively low maximum fields) most

of the problems associated with eddy currents can be avoided. It is not possible however, to be absolutely sure that no eddy current effects are present. A simple way of being sure that all flux density changes occur as desired (something which is critical when demagnetising) is to wait for them to finish.

The eddy current shielding means that the response of the bulk of the specimen lags behind the applied filed. This means that flux density changes may not be completed when the applied field reaches its peak and starts to reduce again. The exact consequences of such circumstances are not known, but any complications which can be avoided, should be. For this reason the 2 second pause was introduced at the peaks of the applied field, creating the clipped triangular waveforms used.

At low fields and using a triangular waveform, the flux changes were tracked against applied field using a digital oscilloscope, and it was seen that the majority of flux changes occurred between zero applied field and the peak. The flux changes were completed at almost the same time at which the peak was reached and the field was then reduced, raising concern that a conflict may be created.

A useful side effect of the pause was the ability to see drift on the flux density channel easily during the pause. This facilitated dynamic correction of drift problems.

Appendix B

Data

The complete set of data obtained from the mild steel cruciform is presented here. The formats of the graphs are such that seven loops or curves are shown on each set of axes. For each graph the externally applied stress in the y-axis is constant, and each curve or loop is for a different applied stress in the x-axis. The seven sets of hysteresis loops are shown first, followed by the seven sets of initial magnetisation curves.

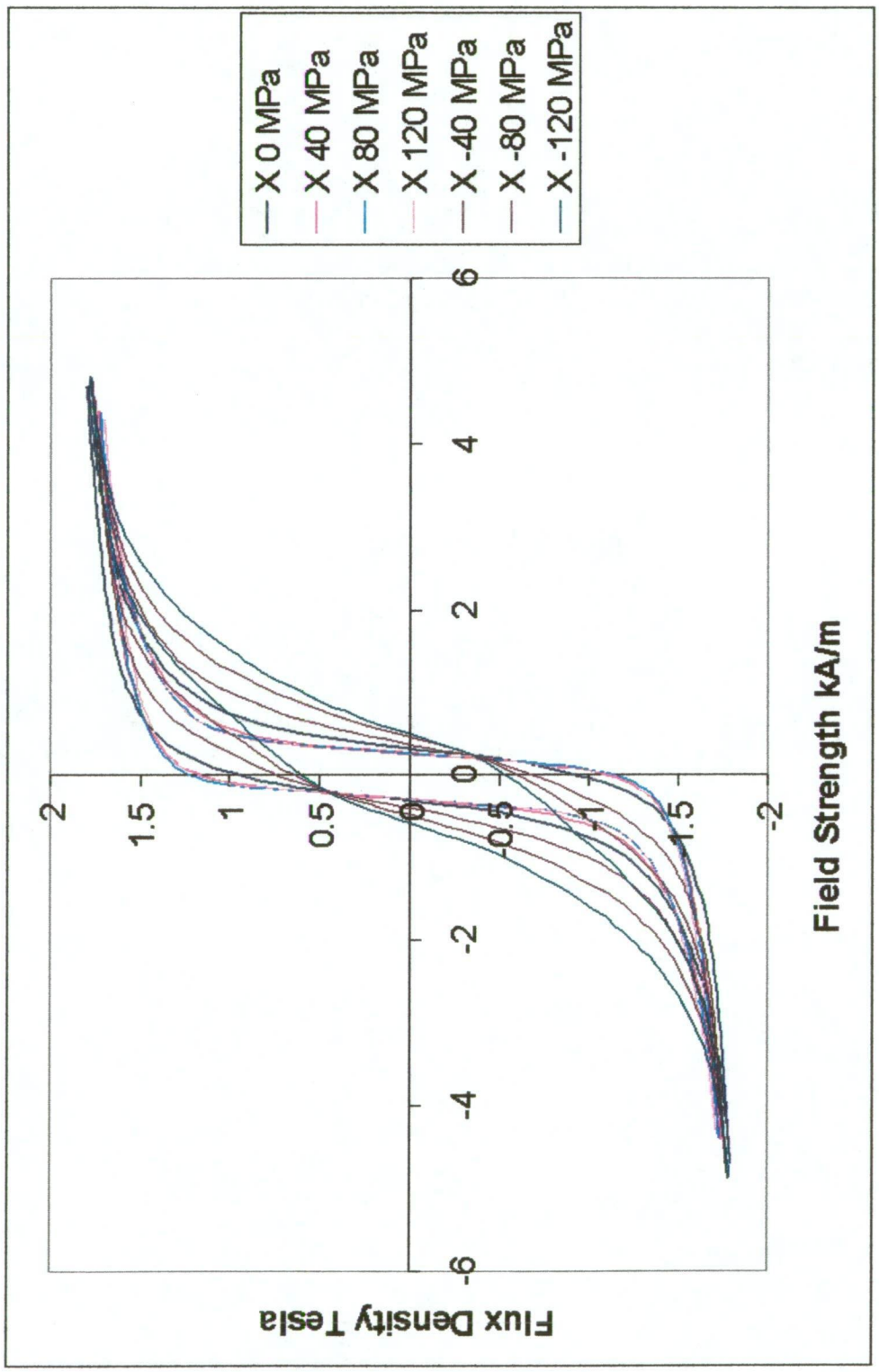

Figure B.1: Loops with 0 MPa in the y axis.

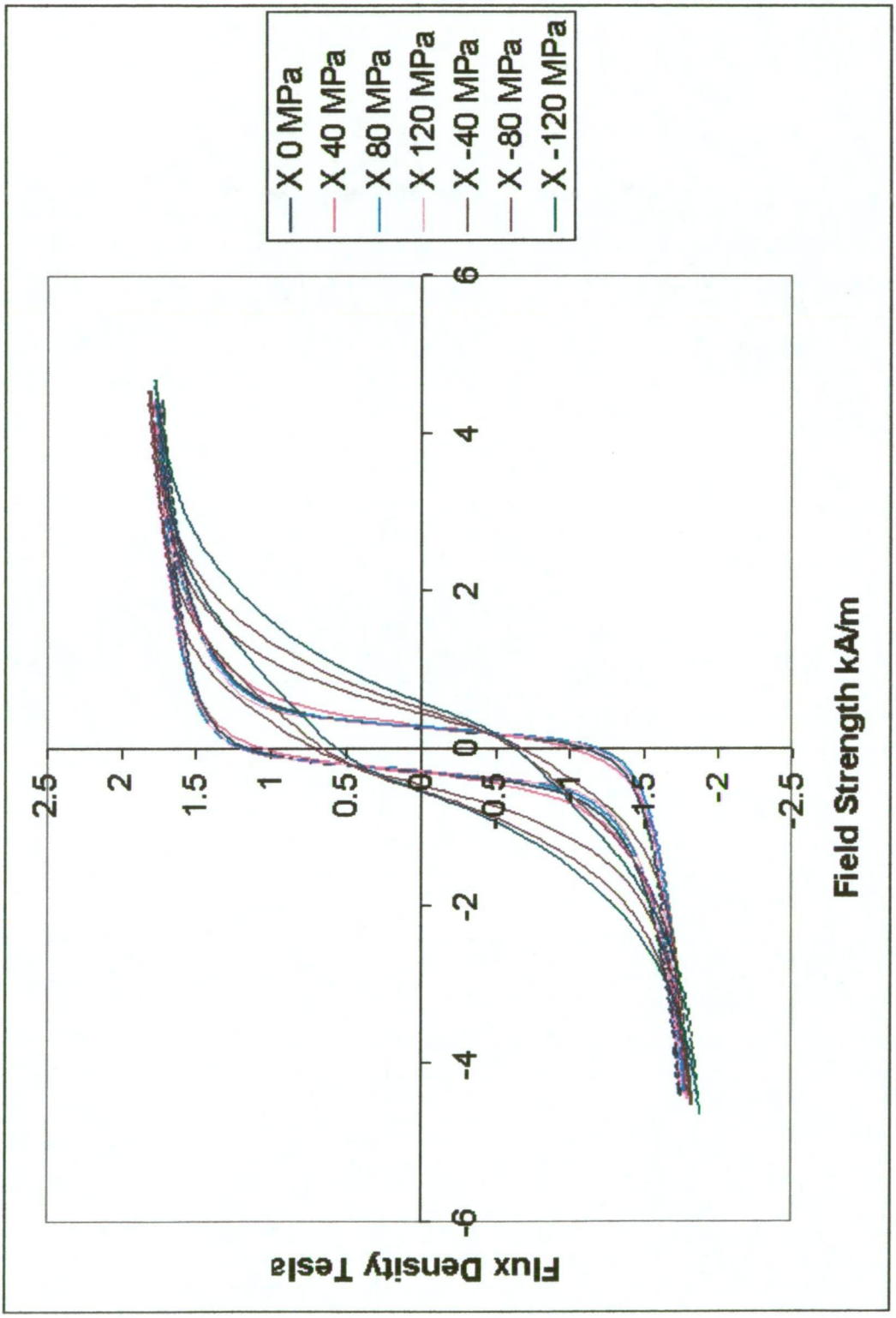

Figure B.2: Loops with 40 MPa in the y axis.

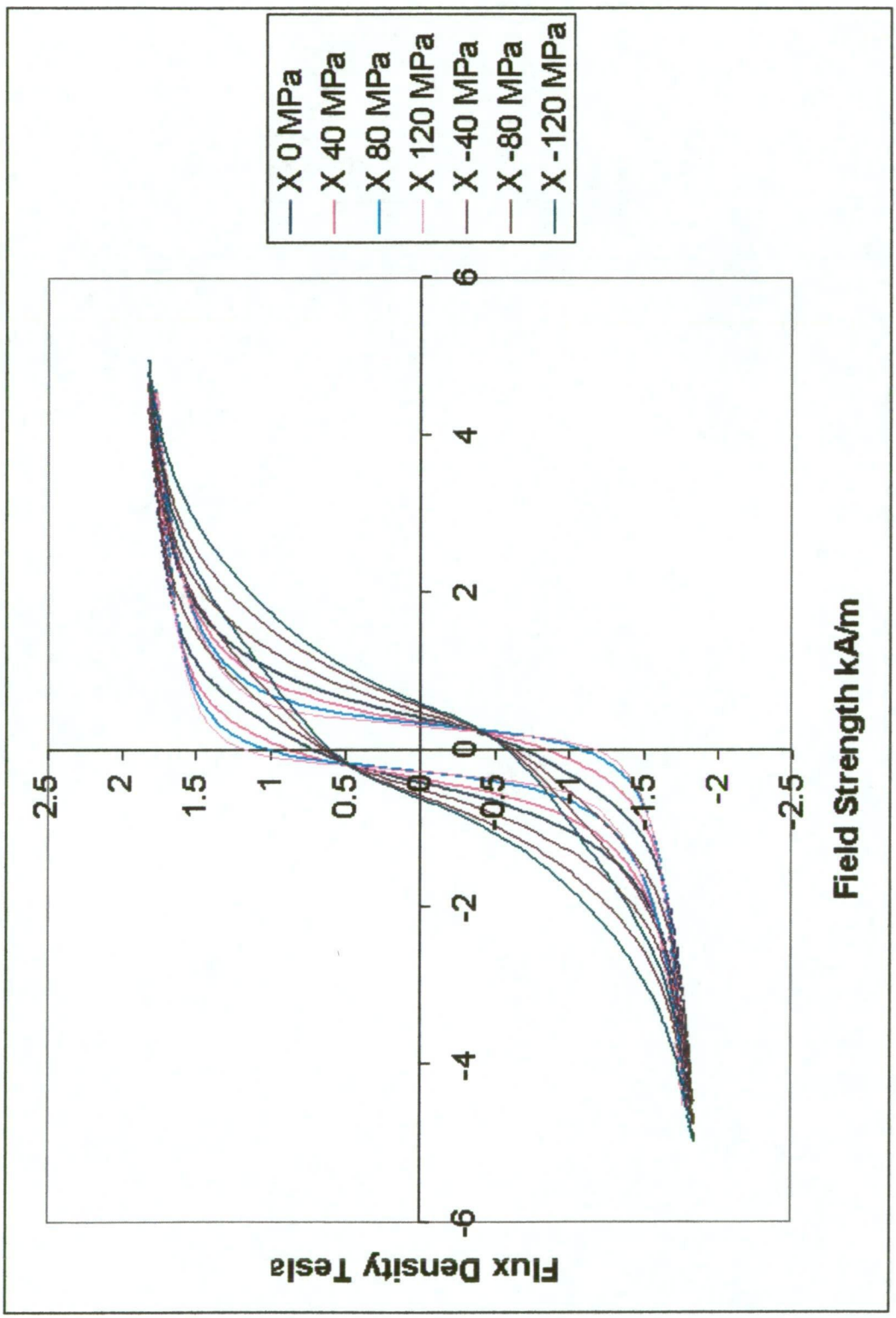

Figure B.3: Loops with 80 MPa in the y axis.

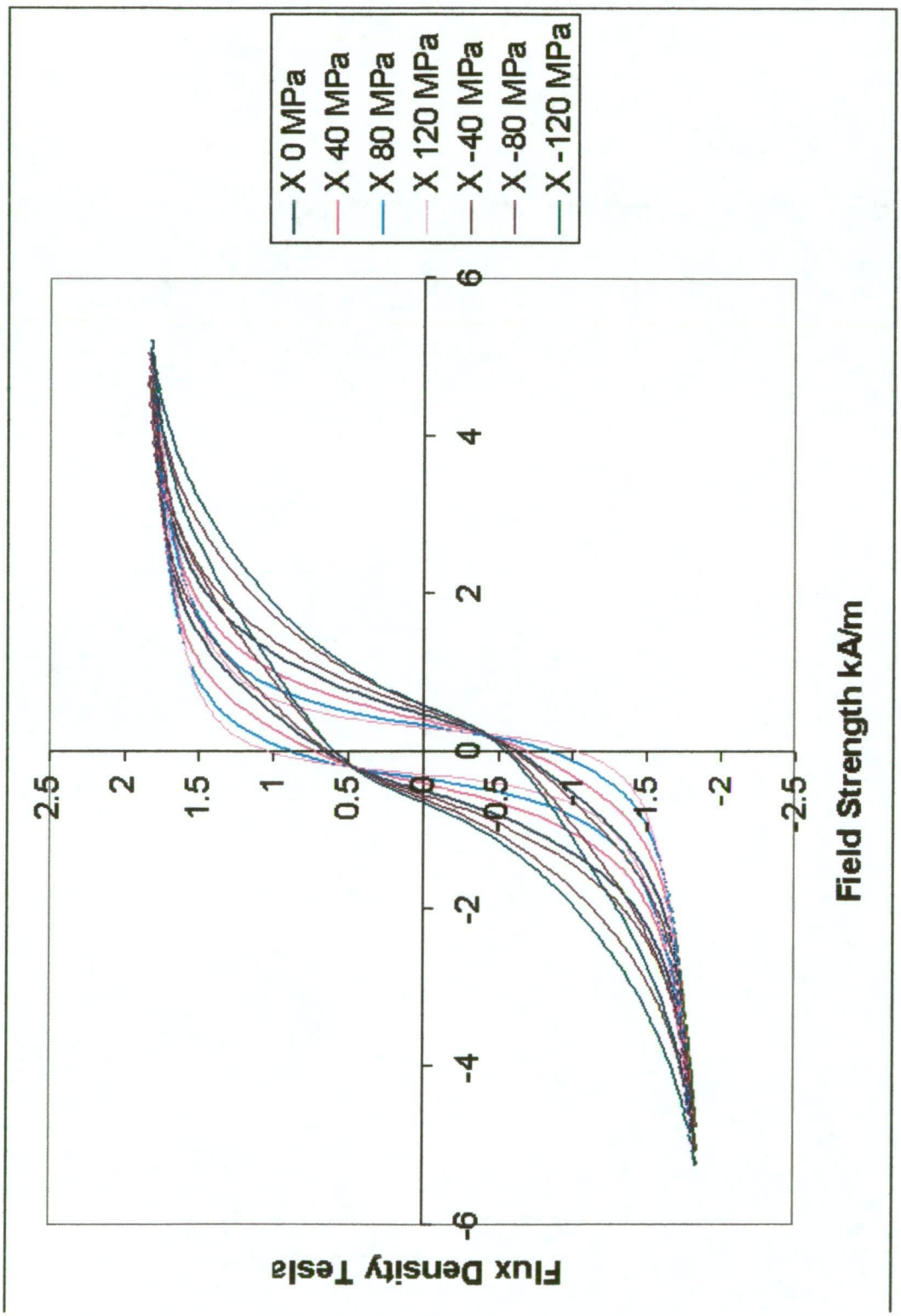

Figure B.4: Loops with 120 MPa in the y axis.

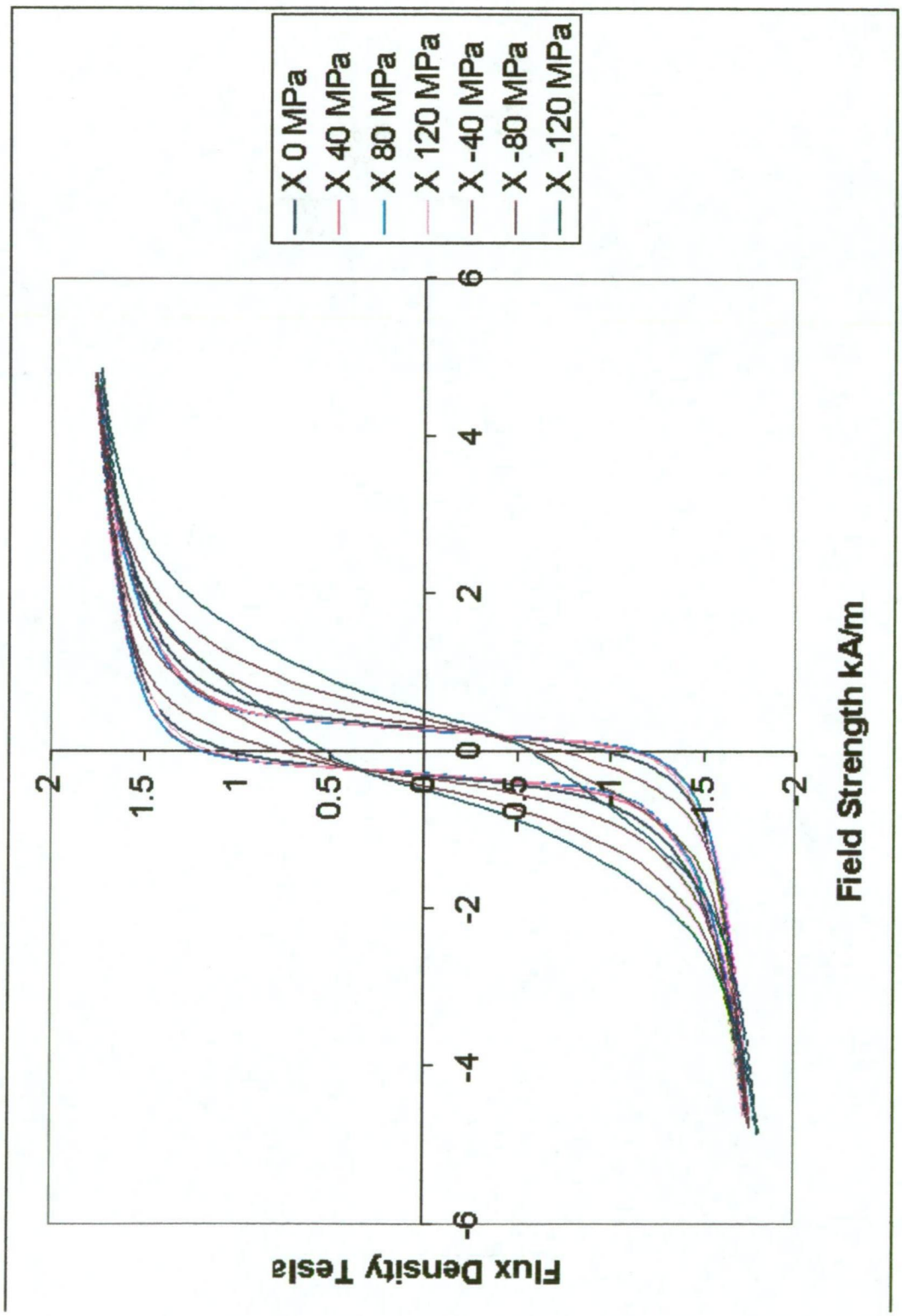

Figure B.5: Loops with -40 MPa in the y axis.

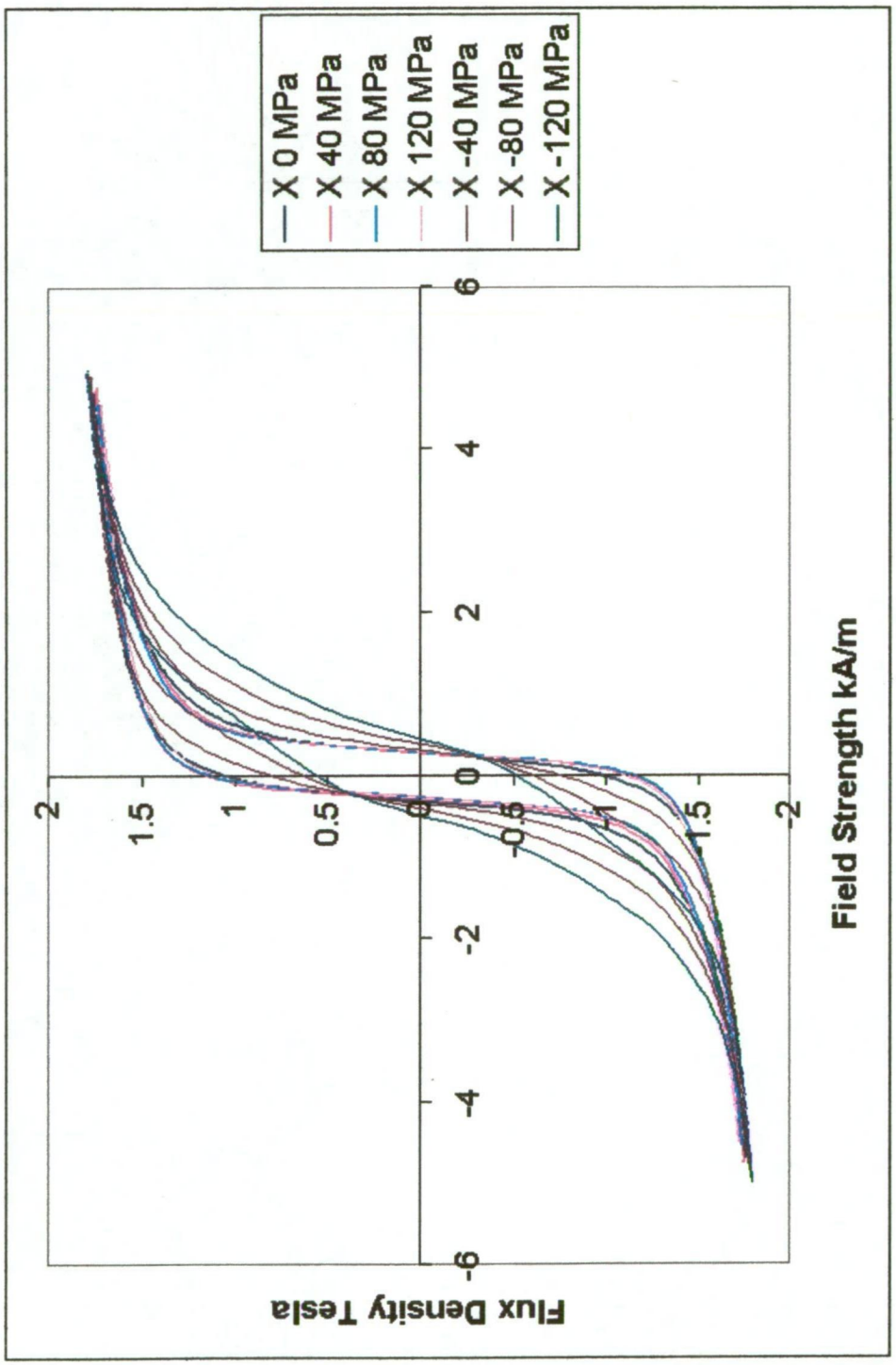

Figure B.6: Loops with -80 MPa in the y axis.

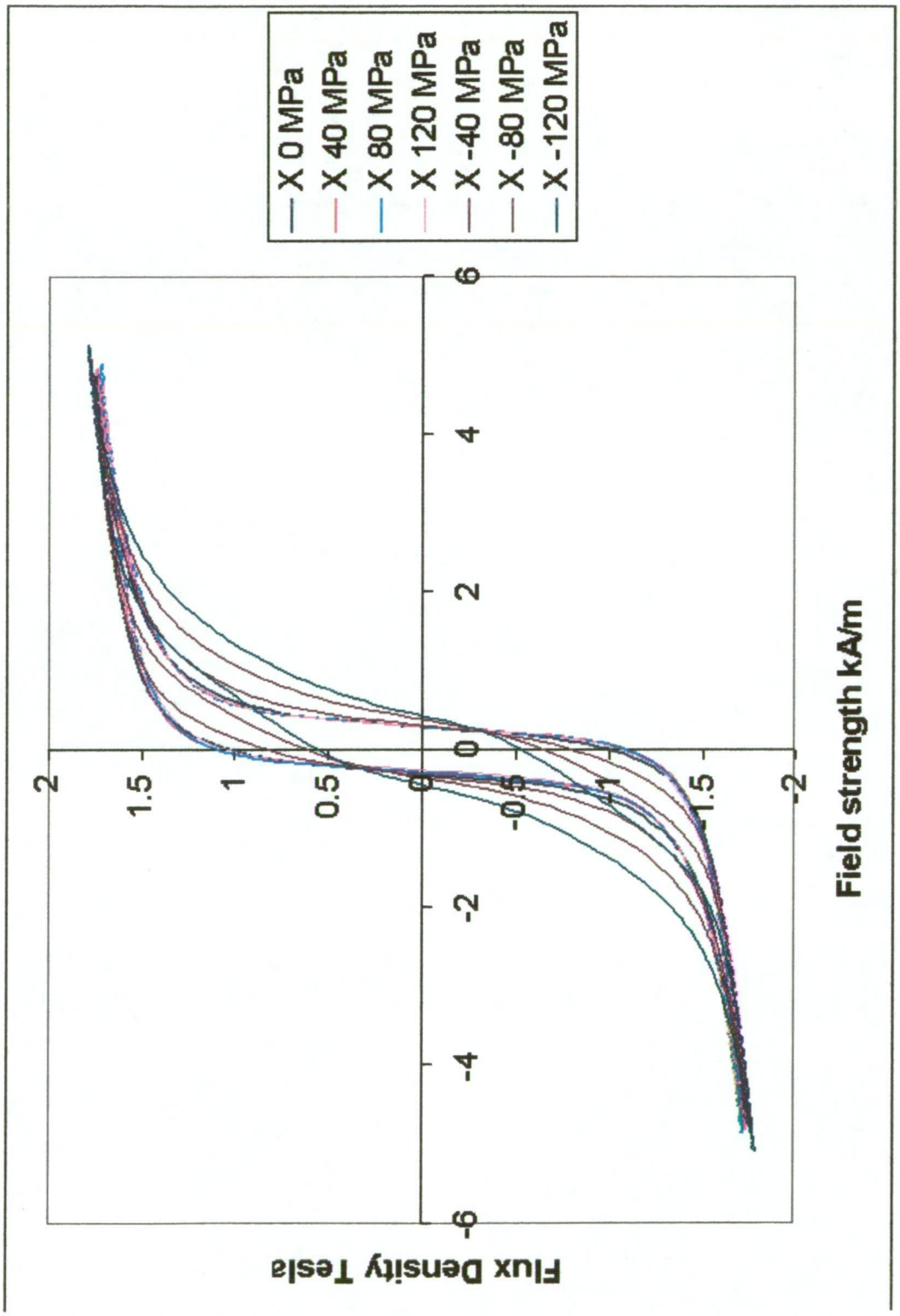

Figure B.7: Loops with -120 MPa in the y axis.

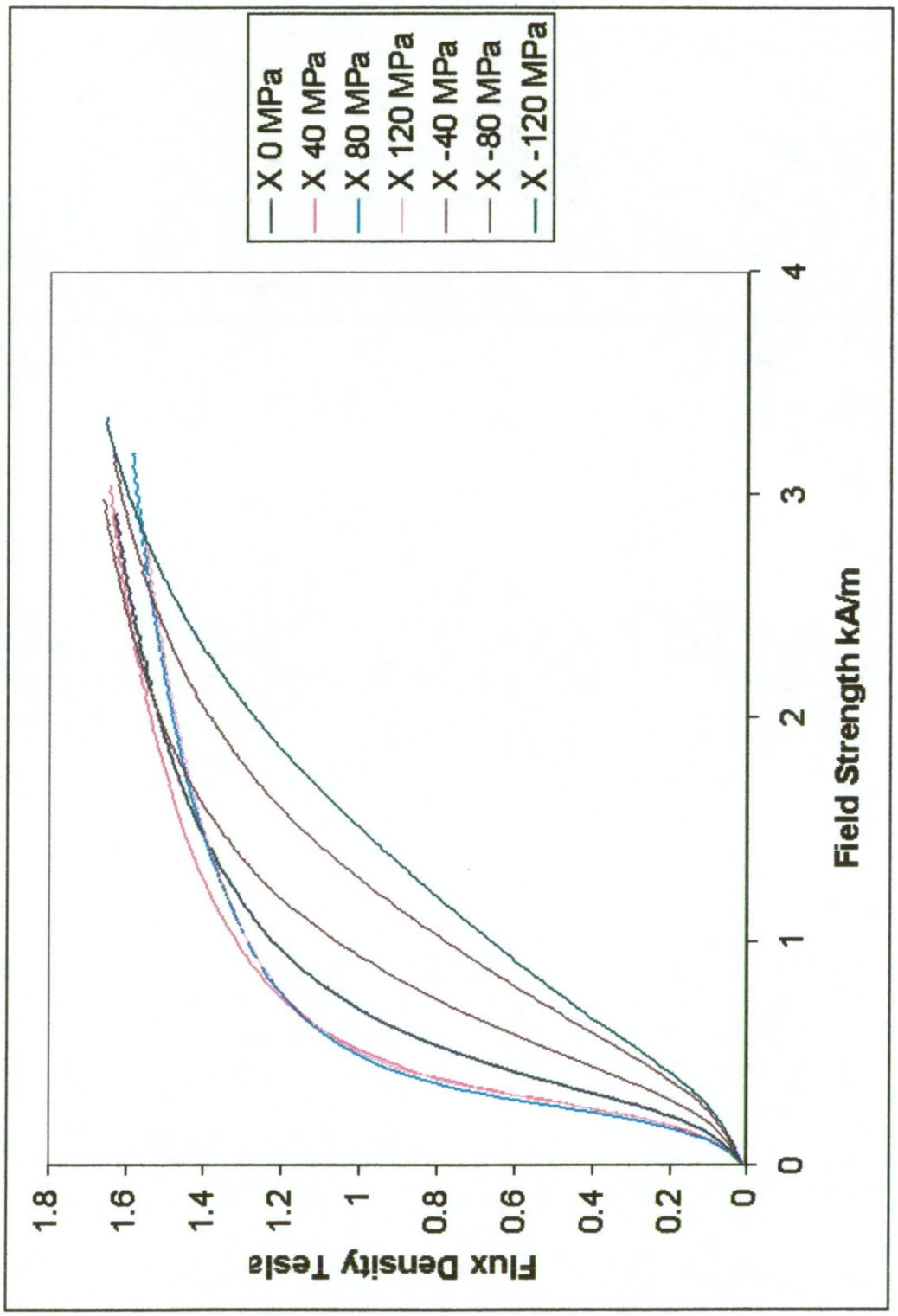

Figure B.8: Curves with 0 MPa in the y axis.

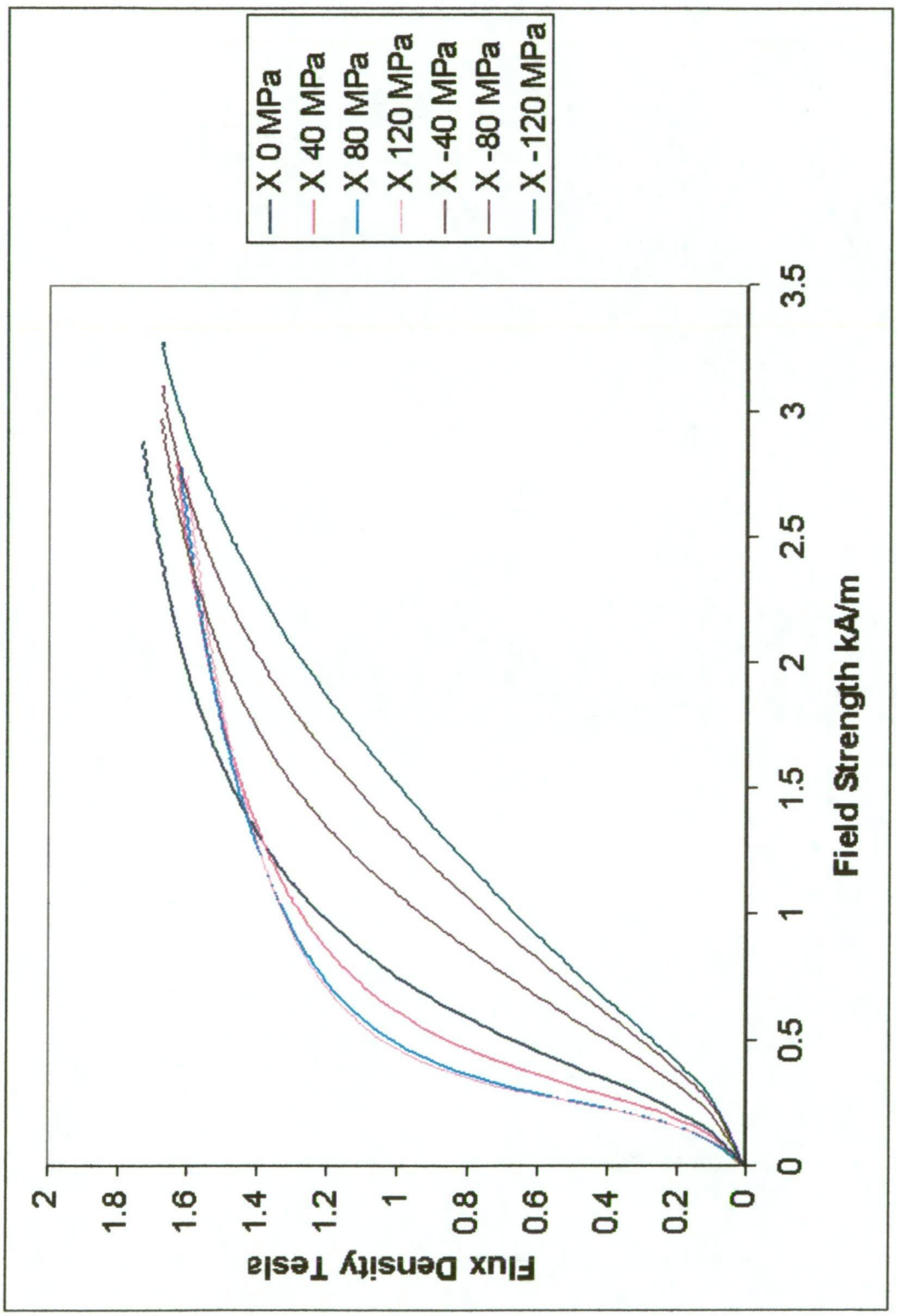

Figure B.9: Curves with 40 MPa in the y axis.

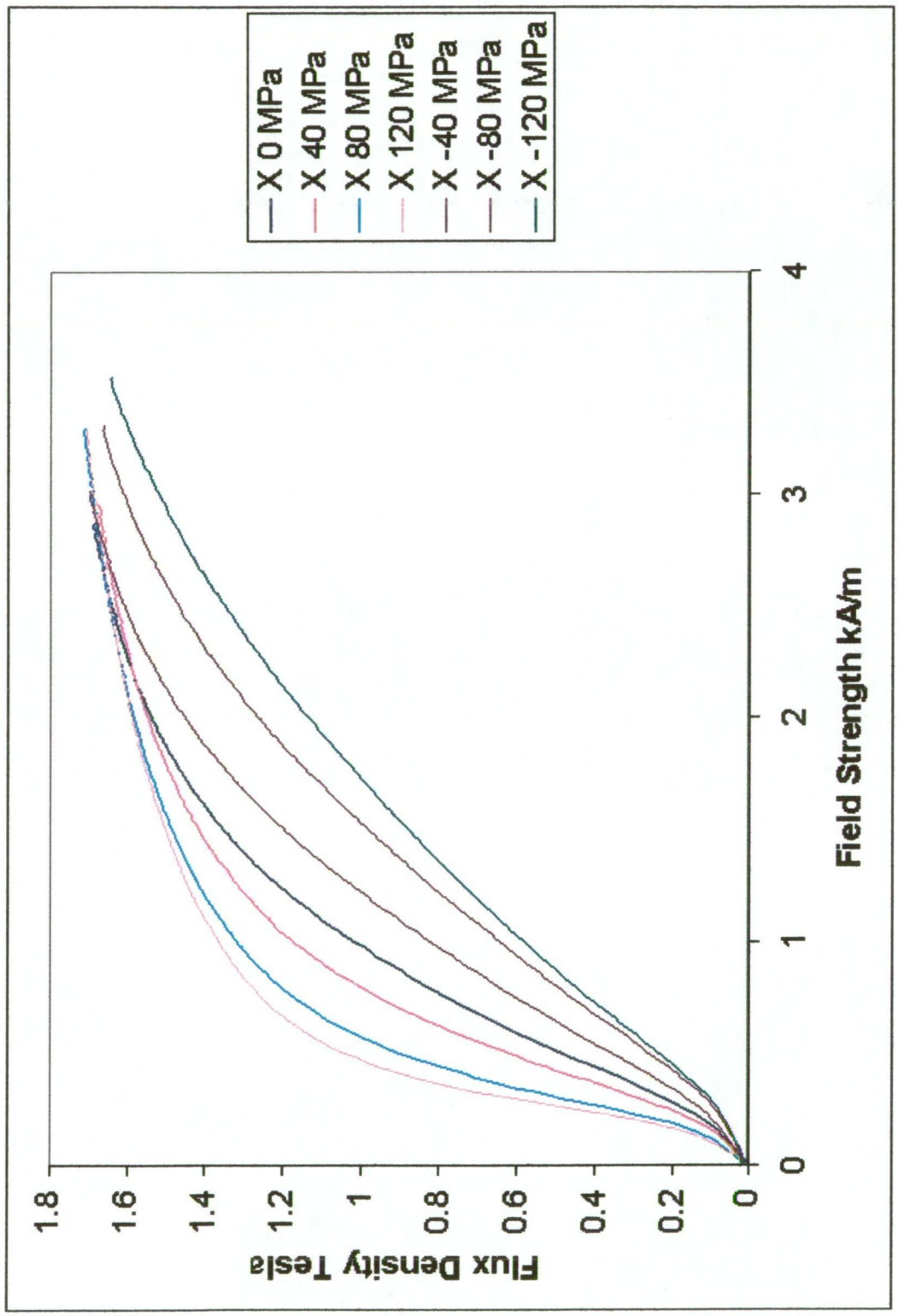

Figure B.10: Curves with 80 MPa in the y axis.

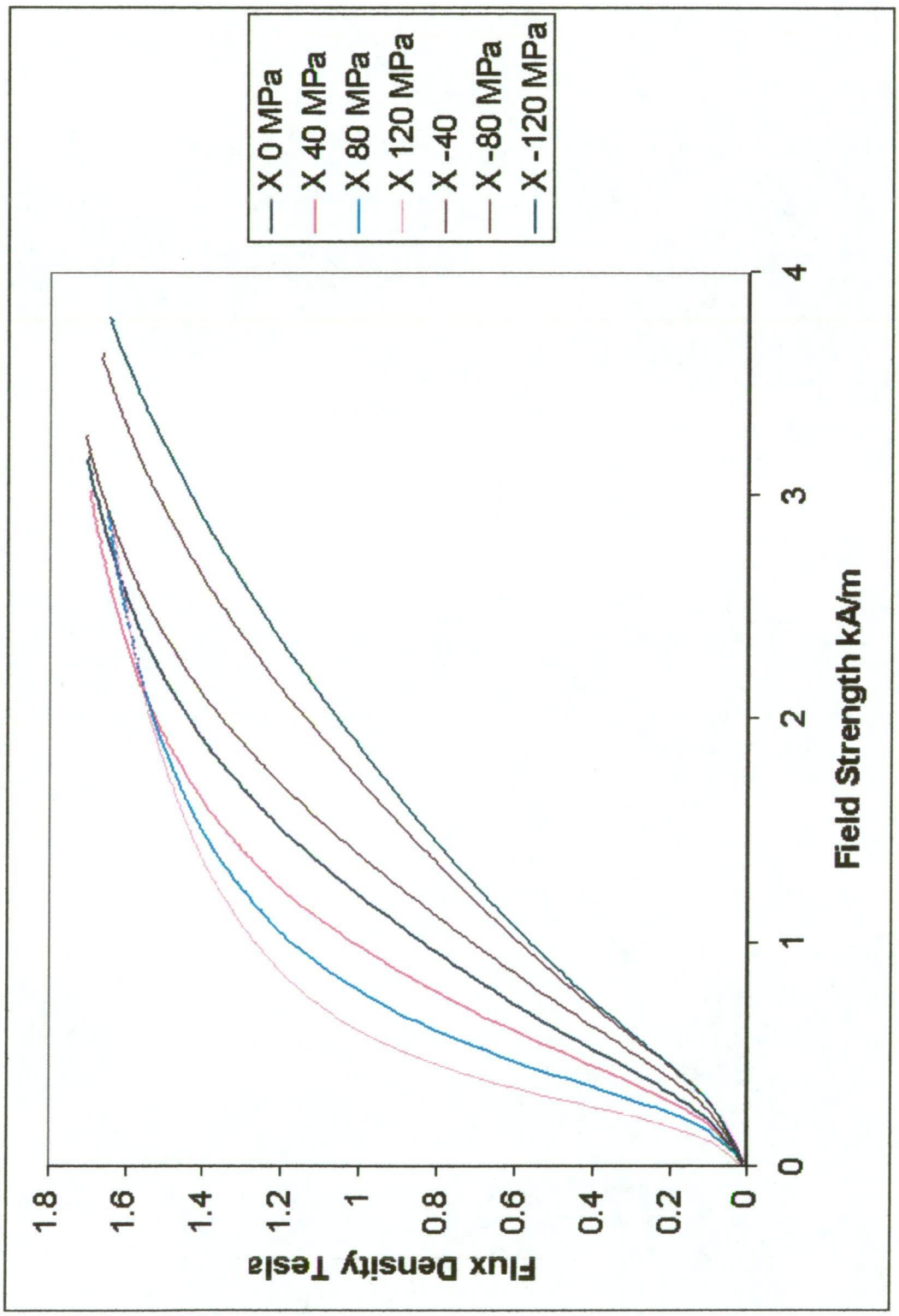

Figure B.11: Curves with 120 MPa in the y axis.

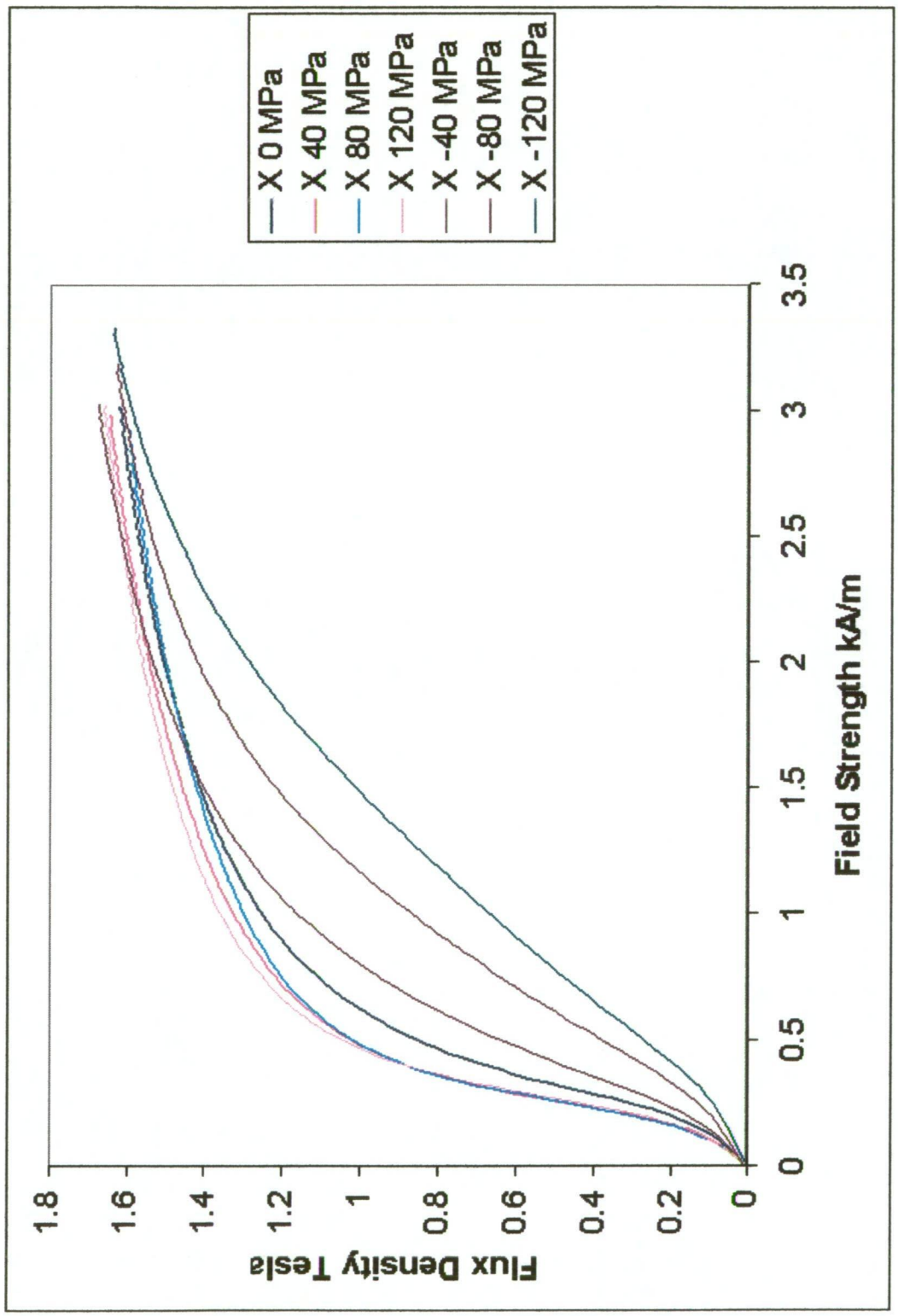

Figure B.12: Curves with -40 MPa in the y axis.

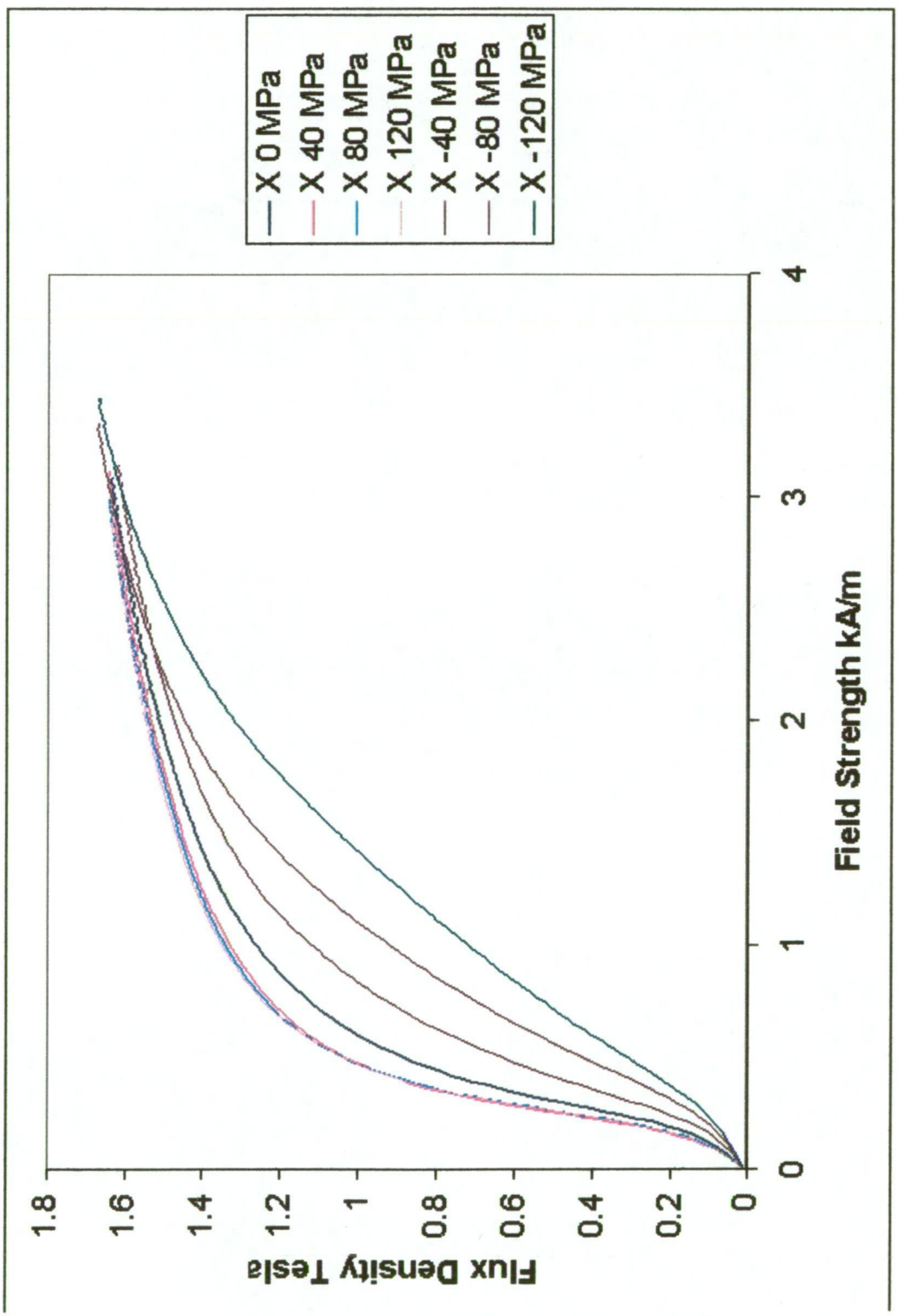

Figure B.13: Curves with -80 MPa in the y axis.

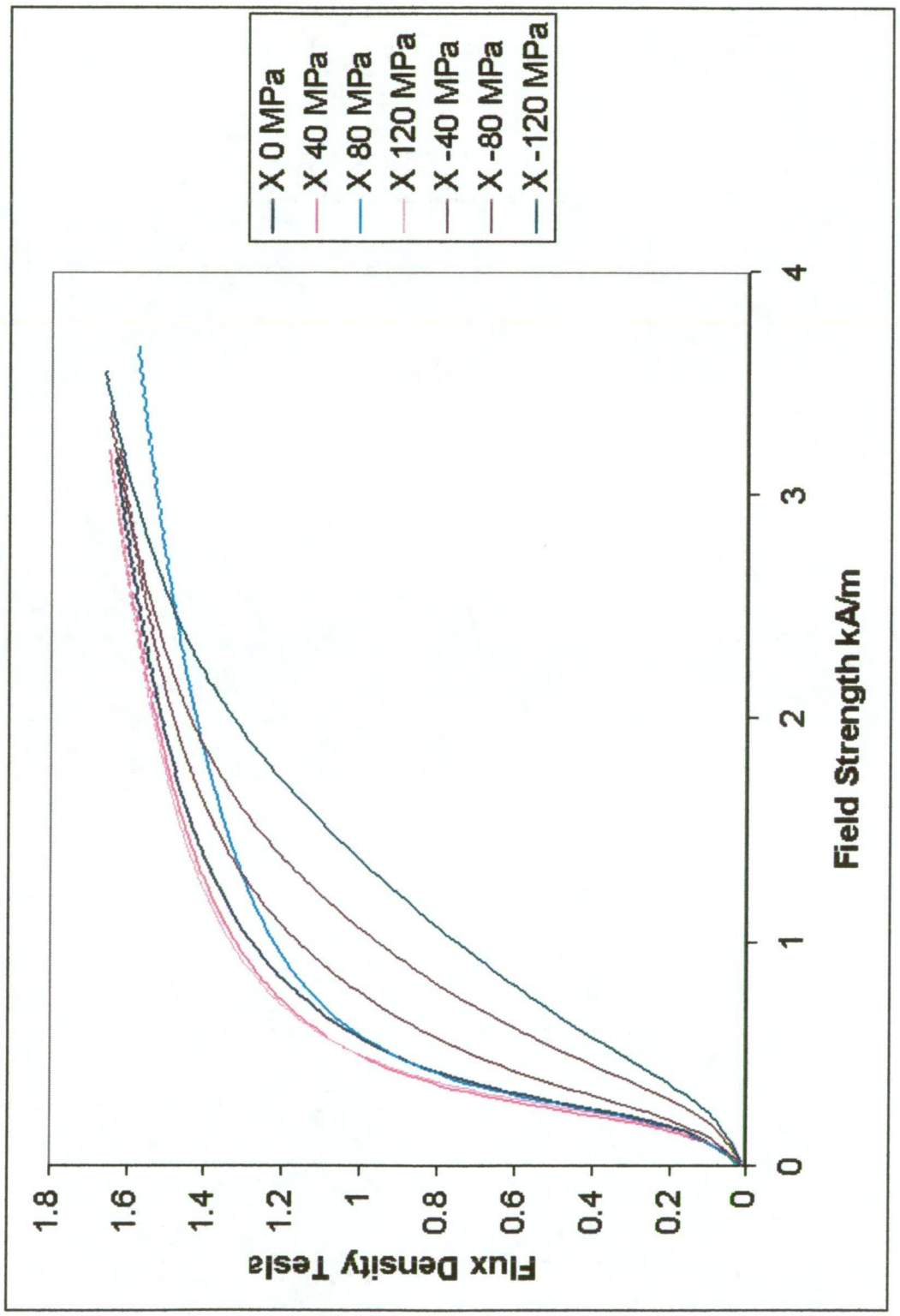

Figure B.14: Curves with -120 MPa in the y axis.

Bibliography

[1] A 341/A 341M-95. Standard test method for direct current magnetic properties of materials using d-c permeameters and the ballistic test methods. 1998 Annual Book of ASTM Standards, Volume 03.04.

[2] N.W. Ashcroft and N.D. Mermin. *Solid State Physics.* Saunders College, Philadelphia, 1976.

[3] P.J. Banks. On the influence of normal stresses on magnetostriction in (110)[001] silicon-iron sheet. *IEEE Trans Mag.*, Mag-13:1000–1005, 1977.

[4] R. Becker and W. Döring. *Ferromagnetismus.* Verlag von Julius Springer, Berlin, 1939.

[5] P. Beckley. Continuous power loss measurement with and against the rolling direction of electrical steel strip using nonenwrapping magnetisers. *IEE Proc.*, 130:313–321, 1983.

[6] Sablik Kwun Berkhardt and Jiles. Model for the effect of tensile and compressive stress on ferromagnetic hysteresis. *J. Appl. Phys.*, 61:3799–3801, 1987.

[7] G. Bertotti. *Hysteresis in Magnetism.* Academic Press, San Diego, 1998.

[8] R.R. Birss. Magnetomechanical effects in the rayleigh region. *IEEE Trans. Mag.*, Mag-7:113–133, 1971.

[9] F. Bloch. Theory of the exchange problem and of residual ferromagnetism. *Z. Physik.*, 74:295–335, 1932.

[10] R. M. Bozorth. *Ferromagnetism.* D. Van Nostrand Company, inc., Princeton, 1951.

[11] F. Brailsford. Domain-wall and hysteresis loss in ferromagnetic material. *Proc. IEE*, 117:1052–1055, 1970.

[12] W.F. Brown. Irreversible magnetic effects of stress. *Phys. Rev.*, 75:147–154, 1949.

[13] L. Brugel and G. Rimet. Effects des tractions sur l'aimantation de quelques aciers. *C.R. Acad. Sci.*, 261:5342–5345, 1965.

[14] L. Brugel and G. Rimet. Interprétation des effets irréversibles des contraintes au moyen d'un modèle d'hystérésis dans l'espace. *J. Phys.*, 27:589–598, 1966.

[15] C.W. Burrows. On the best method of demagnetising iron in magnetic testing. *Bur. of Standards Sci. Paper*, 78, 1908.

[16] C.W. Burrows. The determination of the magnetic induction in straight bars. *Bull. Bur. Stand.*, 6:31–88, 1909.

[17] A. Campbell and D. Dye. The magnetic testing of bars of straight or curved form. *J. IEE*, 54:35–45, 1915.

[18] K. Caputa and M.A. Stuchly. Computer controlled system for producing uniform magnetic fields and its application in biomedical research. *IEEE Trans. Instrum. & Meas.*, 45:701–709, 1996.

[19] R. Carey and E. D. Isaac. *Magnetic Domains.* English Universities Press Ltd., London, 1966.

[20] S. Chikazumi. *Physics of Magnetism.* Robert E. Krieger Publishing Company, New York, 1978.

[21] D. Craik. *Magnetism, Principles and Applications.* Wiley, Chichester, 1995.

[22] D.J. Craik and M.J. Wood. Magnetization changes induced by stress in a constant applied field. *J.Phys. D: Appl. Phys.*, 3:1009–1016, 1970.

[23] B. D. Cullity. *Introduction to Magnetic Materials.* Addison-Wesley Publishing Compnay, Massachusetts, 1972.

[24] D.C. Jiles D.L. Atherton H.E. Lassen D. Noble J. deVette and T. Astle. Microcomputer-based system for control of applied uniaxial stress and magnetic field. *Rev. Sci. Instrum.*, 55:1843–1848, 1984.

[25] J. A. Ewing. *Magnetic Induction in Iron and Other Metals.* The Electrician Printing and Publishing Co., London, 1892.

[26] J.A. Ewing. Contributions to the molecular theory of induced magnetism. *Phil. Mag. S. 5*, 30:205–222, 1890.

[27] M.W. Garrett and S. Pissanetzky. Polygonal coil systems for magnetic fields with homogeneity of the fourth to the eighth order. *Rev. Sci. Instrum.*, 42:840–857, 1971.

[28] E.W. Golding. *The Electrical Measurements and Measuring Instruments.* Sir Isaac Pitman & Sons, ltd., London, 1938.

[29] R. Grisenti and A. Zecca. Design data for a triple square coil system. *Rev. Sci. Instrum.*, 52:1097–1099, 1981.

[30] H.J. Hartley and E.J. Bradbury. Bright annealing of nickel and its alloys. Contribution to symposium on equipment for the thermal treatment of non-ferrous metals and alloys, London, 1952.

[31] C. Heck. *Magnetic Materials and Their Applications.* Crane, Russak & Co., Inc., London, 1974.

[32] Hewlett-Packard. Model 8875a differential amplifier. Operating and Service manual 08875-91999, July 1968.

[33] G.S. Hollister. *Developments in Stress Analysis.* Applied Science Publishers Ltd., London, 1979.

[34] A. Hubert and R Schaefer. *Magnetic Domains.* Springer, Berlin, 1998.

[35] M.G. Maylin J. Pearson, P.T. Squire and J.G. Gore. Apparatus for magnetic measurements under biaxial stress. submitted to Intermag. 2000.

[36] D.C. Jiles. Review of magnetic methods for nondestructive evaluation. *NDT int.*, 21:311–319, 1988.

[37] D.C. Jiles. Theory of the magnetomechanical effect. *J.Phys. D: Appl. Phys.*, 28:1537–1546, 1995.

[38] D.C. Jiles. *Introduction to Magnetism and Magnetic Materials, Second Ed.* Chapman & Hall, New York, 1998.

[39] D.C. Jiles and D.L. Atherton. Ferromagnetic hysteresis. *IEEE Trans. Mag.*, MAG-19:2183–2185, 1983.

[40] D.C. Jiles and D.L. Atherton. Theory of the magnetisation process in ferromagnets and its application to the magnetomechanical effect. *J.Phys. D: Appl. Phys.*, 17:1265–1281, 1984.

[41] D.C. Jiles and D.L. Atherton. Theory of ferromagnetic hysteresis. *J. Mag. & Mag. Mat.*, 61:48–60, 1986.

[42] C. Kittel. *Introduction to Solid State Physics.* Wiley, New York, 1953.

[43] L. Landau and E. Lifshitz. On the theory of the dispersion or magnetic permeability in ferromagnetic bodies. *Physik. Z. Sowjetunion*, 8:153, 1935.

[44] P. Langevin. Magnétisme et théorie des electrons. *Ann. Chem. et Phys.*, 5:70–127, 1905.

[45] R. Langman. Measurement of reversible permeability using solid (nonlaminated) specimens. *PROC. IEE*, 117, 1970.

[46] R. Langman. Measurement of the mechanical stress in mild steel by means of rotation of magnetic field stength. *NDT Int.*, Oct:255–262, 1981.

[47] R. Langman. The effect of stress on the magnetization of mild steel at moderate field strengths. *IEEE Trans. Mag.*, MAG-21:1314–1320, 1985.

[48] R. Langman. *Magnetic Analysis of Structural Steel.* PhD thesis, University of Tasmania, 1986.

[49] R.A. Langman. Magnetic properties of mild steel under conditions of biaxial stress. *IEEE Trans. Mag.*, 26:1246–1251, 1990.

[50] E. W. Lee. Magnetostriction and magnetomechanical effects. *Rept. Prog. Phys.*, 18:184, 1955.

[51] L. Néel. *Ann. Univ. Grenoble*, 22:299, 1947.

[52] J. Pearson and P.T. Squire. Field and stress dependence of the irreversible magnetisation changes in pure iron. *J. Appl. Phys.*, 83:6572–6574, 1998.

[53] F. Liorzou B. Phelps and D.L. Atherton. Macroscopic models of magnetization. *IEEE Trans. Mag.*, 36:418–428, 2000.

[54] F. Preisach. Untersuchung über den Barkhauseneffekt. *Ann. Phys. Lpz.v*, 3:737–799, 1929.

[55] C. Purcell R. Merritt and G. Stroink. Uniform magnetic field produced by three, four, and five square coils. *Rev. Sci. Instrum.*, 54:879–857, 1983.

[56] I.M. Robertson. A review of investigations of the magnetization of steel due to the application of stress. *Mat. Forum*, 15:117–131, 1991.

[57] I.M. Robertson. Direction of change of magnetization of a ferromagnet subjected to stress. *IEEE Trans. Mag.*, 29:2077–2080, 1993.

[58] I.M. Robertson. Effect of steel metallurgy on its magneto-mechanical behaviour in weak magnetic fields. *Acta Metall. Mater.*, 42:661–665, 1994.

[59] H.A. Rowland. On magnetic permeability, and the maximum of magnetism of iron, steel, and nickel. *Phil. Mag. S. 4*, 46:140–159, 1873.

[60] C.A. Faunce R.R. Birss and E.D. Isaac. Magnetomechanical effects in iron and iron-carbon alloys. *J. Phys. D*, 4:1040–1048, 1971.

[61] M. J. Sablik. Modeling the effects of biaxial stress on magnetic properties of steels with application to biaxial stress nde. *Nondestr. Test. Eval.*, 12:87–102, 1995.

[62] C.S Schneider and M. Charlesworth. Magnetoelastic processes in steel. *J. Appl. Phys.*, 57:4198–4200, 1985.

[63] C.S. Schneider and E.A. Semcken. Vibration induced magnetisation. *J.Appl. Phys.*, 52:2425–2427, 1981.

[64] J. Smit. *Magnetic properties of materials.* McGraw-Hill, New York, 1971.

[65] J.L. Snoek. *New Developments in Ferromagnetic Materials.* Elsevier Publishig Co. Inc., 1949.

[66] T. Spooner. *Properties and Testing of Magnetic Materials.* McGraw-Hill Book Company, London, 1927.

[67] K.J. Stevens. Stress dependence of ferromagnetic hysteresis loops for two grades of steel. *NDT & E int.*, 33:111–121, 2000.

[68] E. C. Stoner. *Magnetism and Matter.* Methuen & Co. Ltd., London, 1934.

[69] L.S. Pravdin K.B. Vlasov and V.G. Kuleyev. *Phys. Met. Metallogr.*, 47:60, 1980.

[70] J.N. Watson. The static m-h loops of stressed magnetic materials with intergranular interaction. *IEEE Trans. Mag.*, Mag-8:201–204, 1972.

[71] P. Weiss. L'hypothèse du champ moléculaire et de la propriété ferromagnétique. *J. de Physique*, 6:661–690, 1907.

[72] F.J. Wilkins and A.E. Drake. Instrument for measuring local power losses in uncut electrical sheet steel. *IEE Proc.*, 112:786–793, 1965.